DOCTOR OF MEDICINE

The Development & Application of Elastography to Ultrasound Guided Regional Anaesthesia

Munirama, Shilpa

Award date:
2019

THE DEVELOPMENT & APPLICATION OF ELASTOGRAPHY TO ULTRASOUND GUIDED REGIONAL ANAESTHESIA

DR SHILPA MUNIRAMA

Doctor of medicine(MD)

Date of graduation: 16 October 2019

Contents Page

ACKNOWLEDGEMENTS:

Malachy Columb

Statistics Advisor

Intensive care Unit, Wythenshawe Hospital,

South Manchester University Hospitals,

Manchester, UK

mlacolumb@doctors.org.uk

Mel McKendrick

Advisor to salience study

Assistant Professor in Psychology

School of Social Sciences

Heriot-Watt University

M.McKendrick@hw.ac.uk

Andreas Schwab

Wrote the Matlab algorithm for development of Fusion Elastography

BSc student Medical Physics, Ninewells Hospital

Biomedical Engineer

Institute of Medical Physics

Friedrich Alexander University-Erlangen-Nuremberg

andreas.schwab@imp.uni-erlangen.de

George A Corner Lead,

Medical Physics , Supervisor for Dr S Munirama and A Schwab

now Emeritus Professor of Bioengineering

University of Dundee

g.a.corner@dundee.ac.uk

Roos Eisma

Responsible officer for expert guidance, selection, maintenance of Thiel cadavers used for the studies

Centre for Anatomy and Human Identification,

University of Dundee

Joyce Joy and Anu Chandra

Helped with management of ultrasound equipment and maintenance used for imaging for the studies

PhD students in Bioengineering

University of Dundee

Professor Graeme McLeod MD FRCA FFPMRCA

Supervisor for Dr S Munirama and second rater, which was required in some studies for image analysis

Consultant Anaesthetist and Honorary Clinical Professor

Institute of Academic Anaesthesia, Division of Neuroscience

Medical Research Institute, Mailbox 8

University of Dundee, Dundee, DD1 9SY, UK Tel: +44 (0)1382 740525

Email: g.a.mcleod@dundee.ac.uk

DECLARATION

I, Shilpa Munirama, declare that I am the author of this thesis; all work recorded in the thesis has been done by the myself and I have acknowledged the contributions, support and supervision from various experts as required for the studies. I am very grateful to them for all their support and advice. This work has not been previously presented or accepted for a higher degree elsewhere

Dr Shilpa Munirama

Tables (Page)

Figures (Page)

Figures (Page)

CHAPTER 1 INTRODUCTION

Regional anaesthesia is an integral part of accelerated recovery after surgery (Carli et al 2014). Anaesthetists insert fine needles as close to, but not touching, the epineurium of peripheral nerves. Local anaesthetic is injected around target nerves in order that sodium channels are blocked and transmission of pain signal is halted. Typical examples of regional anaesthesia and its application include: interscalene block for shoulder arthroscopy or replacement, infraclavicular block of the cords of the brachial plexus for elbow replacement or combined femoral and sciatic block for lower limb amputation. Nerve block provides better and longer pain relief and fewer side effects than general anaesthesia (Luger et al 2010) and intravenous morphine analgesia (Richmann et al 2006). Because limbs are anaesthetised, sedation can be provided rather than general anaesthesia. However, many anaesthetists find regional anaesthesia difficult to perform, repeatedly fail to achieve good results, and are reluctant to incorporate nerve block into everyday practice. In order to understand why, it is first important to discuss the underlying mechanisms of nerve block, the attempts by manufacturers to improve the technical quality of equipment and the difficulties anaesthetists have interpreting ultrasound images.

1.1 Peripheral nerves and pain

Peripheral nerves lie enveloped within fascial planes between muscles, often accompanied by arteries and nerves. The relationship between anatomical structures varies both within and between each nerve block site. Nerves are classified according to the presence or absence of myelin and the conduction of different types of pain. For example, myelinated Aδ fibres transmit acute, sharp pain whereas C fibres transmit slow, noxious pain (Table 1).

Table 1. Classification of peripheral nerve fibres

Type	Subtype	Function		conduction
A	α	Motor	Myelinated, transmission	rapid
	β	Tactile sensation		
	δ	Sharp pain		
	γ	Motor, Proprioception		
B		Preganglionic autonomic		
C		Noxious pain Temperature	Unmyelinated, transmission	slow

Each nerve contains bundles of axons termed fascicles that are enveloped by a stiff layer of perineurium up to 20 µm thick (Fig 1). Fascicle size and distribution varies along the path of the nerve as axons interconnect within complex plexuses. The outer, more permeable membrane of the nerve is called the epineurium. Tissue between fascicles, termed the inner or interfascicular epineurium, contains a mix of adipose tissue, fibroblasts, mastocytes, blood vessels and lymphatics. The outer epineurium is bound to an extraneural layer described as the adventitia, paraneurium or gliding apparatus. This extraneural nerve sheath of loose connective tissue fills the space between the nerve and surrounding tissue, carries the segmental blood supply to the nerve, and fuses with the tunica adventitia of vessels in neurovascular bundles. The sheath protects against injury, and may serve as a conduit for injected local anaesthetic solution. Nerves have a binary blood supply: the external blood supply lies in the epineurium, and the internal blood supply runs within the fascicles.

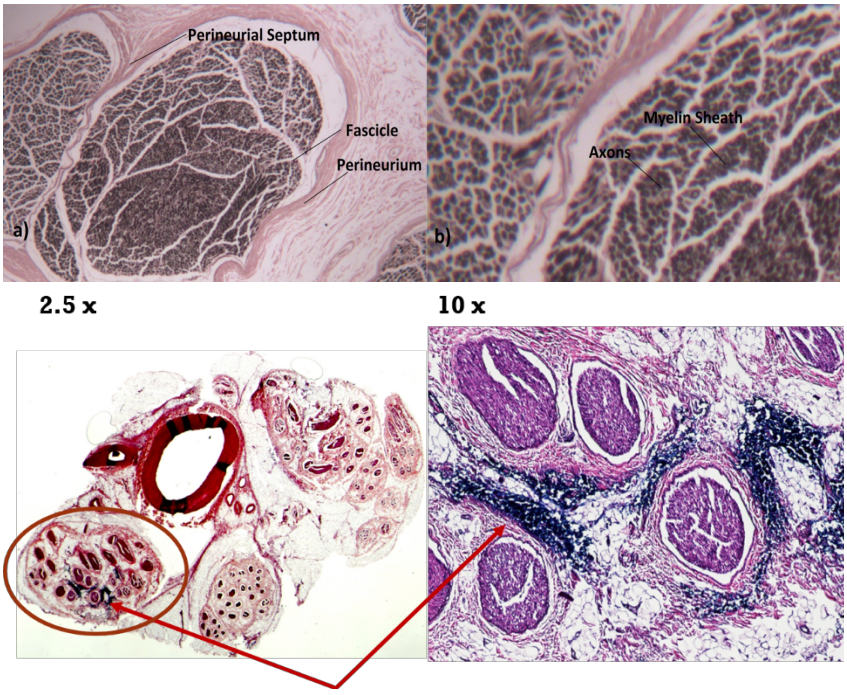

Fig 1. Peripheral nerve anatomy. Image courtesy of Ms Anu Chandra, Ultrasound department, University of Dundee. The example given above is the sciatic nerve. The paraneurium envelopes the smaller common peroneal nerve and larger tibial nerve. Each nerve has an outer epineurium and inner epineurium or stroma. Fascicles are protected by a stiff layer termed the perineurium indicated by the red arrows.

Pain sensation is transmitted to the central nervous system (CNS) by depolarisation of primary nerve afferents. Depolarization of the nerve is associated with influx of Na^+ ions. Change in the resting membrane potential from -70 mV to a threshold of approximately -45 mV generates an action potential and rapid depolarization to approximately 20 mV. Repolarization is associated with K^+ efflux and a refractory period to further depolarization.

The mode of action of local anaesthetics may be attributed to their amphipathic properties. The unionised fraction passes through the nerve and dissociates into an ionised moiety that blocks Na^+ channels and inhibits transmission of electrical impulses. The bioavailability of local anaesthetics is dependent on their protein binding and pKa, the pH at which the ratio of ionised to unionised drug is 50:50. For example levobupivacaine and ropivacaine have a slow onset of action and long duration of action because they are 85% ionised at physiological pH (pKa of 8.1) and highly protein bound (94% - 95%). In contrast lidocaine has a rapid onset of action because it is 65% ionised at physiological pH (pKa of 7.8) and less protein bound than levobupivacaine or ropivacaine (64%) (McLeod & Hales 2015).

1.2 The clinical problem

To the untrained, injection of of local anaesthetic around superficial nerves may appear straightforward. Yet regional block efficacy, defined as: "the proportion of participants receiving a nerve block who do not require rescue analgesia, sedation, general anaesthesia or spinal anaesthesia (Gelfand et al 2011, Walker et al 2009)" has been poor. Historical large observational studies (Fanelli et al 1999, Perris & Watt 2003) of regional anaesthesia outcomes in the 1990s and historical experience in Ninewells hospital (Cox et al 1998) suggest that before the introduction of ultrasound to clinical practice, block efficacy varied between 80% and 90%. In other words 10% to 20% of patients needed rescue medication, notwithstanding longer anaesthetic times, delays to surgical lists and poor patient experience. More recently a study of 1065 consecutive nerve blocks revealed that 1 out of 6 patients experienced technical problems, of whom half required several needle insertions. Block success in one study,

defined liberally as a pain score of <6 out of 10 in recovery, was only achieved in 86% of patients (Watts & Sharma 2007). Best efficacy recorded in a clinical trial using electrical peripheral nerve stimulation, the localization of peripheral nerves by eliciting muscle contraction, was reported as only 94% in 1999 by Fanelli et al. Overall, such results highlight the poor efficacy of regional anaesthesia, wide variability in block success, the widespread need for rescue intervention and explains the reluctance some anaesthetists to provide this mode of anaesthesia.

Ultrasound guided regional anaesthesia (UGRA) was introduced to clinical practice a decade ago. It has popularised the use of regional anaesthesia for upper and lower limb surgery because it allows visualisation of nerves, blood vessels and muscles, and real time imaging of local anaesthetic spread (Neal et al 2010). However, widespread clinical use of ultrasound has served to highlight its technical limitations. At increased depths peripheral nerves may be indistinguishable from surrounding tissue and needles difficult to see.

Uptake of regional anaesthesia has been tempered by the fear of accidental nerve damage (Selander et al 1977). Surveys (Barrington 2012, Barrington & Snyder 2011, Fredrickson & Kilfoyle 2009, Liu et al 2011), systematic reviews (Brull et al 2015) and meta-analyses (Abrahams et al 2009, Gelfand et al 2011) have all shown that neurological side effects occur secondary to unintentional intraneural injection. Poorly performed UGRA has serious consequences: increased risk of nerve damage with a reported incidence varying between 3 in 100 (Brull et al 2007) and 4 in 10,000 (Auroy et al 2002, Auroy et al 1997, Borgeat & Ekatodramis 2001), and risk of systemic local anaesthetic toxicity in up to 1 in 500 patients (Auroy et al 2002, Auroy et al 1997, Barrington & Kluger 2013).

Borgeat et al in 2001 using the nerve stimulation technique, described a 7 to 10 day postoperative incidence of neurological symptoms between 8% and 14%, reducing to less than 1% of patients six months after surgery. Early neurological symptoms followed by a gradual decrease in incidence over several months is well recognized pattern (Brull et al 2007). Fortunately, most nerve damage tends to be transient, in approximately 0.4% for interscalene blocks (Borgeat et al 2001).

Application of real-time ultrasonic imaging of needle/nerve interaction offered hope that nerve damage may be reduced. Unfortunately, this has not happened (Jeng et al 2010) and nerve damage still occurs. Reports of permanent nerve injury secondary to UGRA were reported in the literature in 2009 after ultrasound guided interscalene block (Cohen & Gray 2010) and supraclavicular block (Reiss et al 2010). Meta-analyses of RCTs comparing the efficacy and side effects of UGRA and electrical nerve stimulation showed no difference in the incidence of transient neuropraxia (Gelfand et al 2011). There was new evidence presented by Beigelssen et al (Bigeleisen 2006, Bigeleisen et al 2009) who purposefully injected between 2ml and 5ml local anaesthetic directly into the nerves of the brachial plexus, resulting in successful clinical anaesthesia yet with no residual neurological deficit reported at 6 months. Subsequent studies injecting between 4ml and 40ml of local anaesthetic directly into the sciatic nerve of patients (Rodriguez et al 2008, Sala Blanch et al 2009, Sala-Blanch et al 2011) and cadavers (Sala-Blanch et al 2009) confirmed his findings.

Indeed, intraneural injection may be more common than previously thought. Retrospective studies investigating anaesthetist interpretation of UGRA videos showed that novices accidently injected into nerves on approximately 1 out of 6 occasions, with no detriment to patients (Hara et al 2014, Liu et al 2011). Furthermore, a cadaveric study reported a 50% incidence of unintentional subepineural injection during simulated ultrasound-guided interscalene block (Orebaugh et al 2010). In order to explore this further, it is important to discuss the pathophysiology of peripheral nerve injury and the interventions used to recognise intraneural injection.

1.3 Pathophysiology of peripheral nerve injury

Nerve damage may be classified in increased grades of severity as neuropraxia, axonotmesis and neurotmesis (Hogan 2008). Neuropraxia describes damage to the myelin sheath typically associated with nerve stretching or compression while other structures remain intact. Recovery is often complete, although may take weeks to months. Axonotmesis is associated with fascicle damage and loss of axonal continuity. Recovery is poor and generally worse with more proximal injuries. Neurotmesis

describes transection of the nerve and requires surgical intervention.

The mechanisms of peripheral nerve injury (PNI) after surgery may be categorised as mechanical (trauma), vascular (ischaemia) and chemical (neurotoxicity).

1.3.1 Mechanical

Nerve trauma occurs secondary to needle insertion and forceful needle contact with the epineurium. Needle insertion into the substance of the nerve is associated with cellular change such as membrane channel expression, activation of signal transduction, neuropeptide production, and an increase in excitability at the dorsal horn neurons (Hogan 2008). Entry of the needle tip into a fascicle may result in inflammation and leakage/herniation of endoneural contents (Sugimoto et al 2002). Similarly, forceful needle nerve contact and application of needle pressure may lead to intraneural haematoma and neural inflammation (Steinfeldt et al 2011a). In contrast, intraneural injection into the interfascicular epineurium does not appear to result in nerve injury.

The structural organization, or internal architecture, of a peripheral nerve provides insight into the relative risk for mechanical injury among different nerves or different locations within the same nerve. Because epineurium is typically stiffer than surrounding tissues, nerves tend to be “pushed away” by an advancing needle, rather than penetrated, and the needle tip more likely to rest within interfascicular tissue. Fascicles tend to deflect the advancing needle although this protection may be undermined by abrupt needle advancement needle or forceful needle-nerve contact.

Nerve composition impacts on the incidence of nerve damage. Peripheral nerves with tightly packed fascicles as in the proximal brachial plexus, may be at greater risk of mechanical nerve injury compared to nerves with lower fascicular-to-connective tissue content (Moayeri et al 2008, Moayeri & Groen 2009) as in the lower limb.

The width and tip configuration shape of needles also dictate the extent of nerve damage. Small 24g needles are less likely to injure nerves compared to 19g needles (Steinfeldt et al 2010), and sharp long-beveled (12^{o}) needles are more likely to puncture the fascicle than short-bevel (45^{o}) needles (Selander et al 1977). However,

the type of needle appears not to make a difference. Nerve puncture with pencil-point or Tuohy needles causes a similar high degree of post-traumatic regional inflammation, myelin damage, and intraneural hematoma (Steinfeldt et al 2011b).

1.3.2 Chemical

Laboratory experiments have shown over several decades that local anaesthetics have myotoxic, neurotoxic (Gentili et al 1980, Radwan et al 2002), and cytotoxic properties (Lirk et al 2006, Perez-Castro et al 2009). Intrafascicular injection of small volumes of local anaesthetic < 1ml may result in axonal degeneration and permanent neural damage. Farber et al (Farber et al 2013) recently reported that intrafascicular local anaesthetic injury toxicity was in rank order bupivacaine >ropivacaine = lidocaine and local anesthetic toxicity was time and concentration dependent (Yang et al 2011) (Verlinde et al 2016).

Intraneural administration of local anaesthetics exposes axons to higher concentrations of local anaesthetic resulting in increased altered perineural permeability and fascicle oedema, leading to compression of the fascicle and reduced neural blood flow (Gentili et al 1980). Increased intra-fascicular pressure eventually results in axonal compression and perineural rupture. Proposed cellular mechanisms of toxicity include increases in intracellular calcium concentration, disturbed mitochondrial function, interference with membrane phospholipids, and cell apoptosis (Kitagawa et al 2004).

Simulation of intraneural needle insertion and fluid injection was achieved recently in an anaesthetised pig model (Kirchmair et al 2016). Intraneural needle insertion alone or with 2.5ml and 5ml intraneural volumes reduced compound muscle action potentials compared to extraneural injection control injections. However, no differentiation between subepineural or subperineural injection was made.

1.3.3 Vascular

Nerves are susceptible to ischaemia. External nerve compression secondary to large volumes of intraneural local anaesthetics, haematoma and tourniquets and surgical

positioning (Brull et al 2015) all contribute to ischaemic damage.

Local anaesthetics decrease neural blood flow. Lidocaine 2% reduced neural blood flow in rat sciatic nerves by 20% to 40%, and this difference persisted after washout of local anaesthetic (Myers & Heckman 1989, Partridge 1991). Laboratory experiments on human volunteers have shown a biphasic vascular response to several local anaesthetics over a wide range of concentrations (Newton et al 2005, Newton et al 2007, Newton et al 2003)

Epinephrine is a common adjuvant that is used to prolong the duration of blockade and to warn of intravascular injection/absorption. The recommended optimal concentration of adjuvant epinephrine for use with local infiltration anaesthesia is usually $5\mu g.ml^{-1}$. However, recent Doppler imaging studies injecting bupivacaine and levobupivacaine into the forearm skin of healthy volunteers showed equivalent vasoconstriction at $2.5\mu g.ml^{-1}$ $1.25\mu g.ml^{-1}$ concentrations. The clinical significance of this reduction in blood flow is unknown as many peripheral nerve blocks have been performed using a combination of local anaesthetic and epinephrine with no apparent neurologic consequences.

In summary, despite histological and EMG data in animals demonstrating that intraneural needle insertion and injection is associated with nerve inflammation, neurologic injury and impaired electrical transmission, clinical reports suggest that intraneural injections do not always lead to neurological impairment. The anatomical site of the intraneural needle tip placement is likely the most important factor of whether an overt neurologic injury will occur, but so far there is no technology available that differentiates between subperineural and subepineural injection. Thus, any intraneural injection must be regarded as presenting a higher risk of transient and permanent damage, and that practice should be restricted to extraneural injection.

1.4 Recognition of intraneural injection

Four methods are used in clinical practice to detect accidental intraneural injection – paraesthesia, electrical peripheral nerve stimulation, injection pressure monitoring

and ultrasound.

1.4.1 Paraesthesia

Paraesthesia in regional anaesthesia has been defined as a burning, shooting or electric sensation or pain usually radiating distally to arms or legs (Aldrete 2003, Pong et al 2009). For many years, nerve paraesthesia was the technique of choice for regional anaesthesia. Looking back, it is now acknowledged that many needle tips were placed within the substance of the nerve yet post operative neurological side effects remained uncommon or not reported. However, paraesthesia is not an accurate indicator of intraneural injection. A recent ultrasound study revealed that only 38% of patients experienced paresthesia during real-time visualisation of needle-nerve contact (Perlas et al 2006). Thus paraesthesia displays poor sensitivity (Selander et al 1979) for both needle tip location and postoperative neurological dysfunction and is no longer used in NHS Tayside.

1.4.2 Electrical Peripheral Nerve Stimulation

In 1962 Greenblatt and Denson introduced a portable nerve stimulator with variable current output and described its use for nerve location. The underlying physiological principle of the nerve stimulator is that the closer the needle tip to the nerve, the smaller the current needed to stimulate a muscle contraction (Urmey 2006, Urmey & Stanton 2002). Current flows from the positive skin anode to the negative needle tip cathode. Once an electrical threshold is reached, an action potential is generated. Depolarization of the nerve is dependent on the amount of electrical charge - the product of the current (milliamps) and the duration of the square wave electrical impulse (milliseconds). The curvilinear strength-duration curve (Fig 2) describes this relationship.

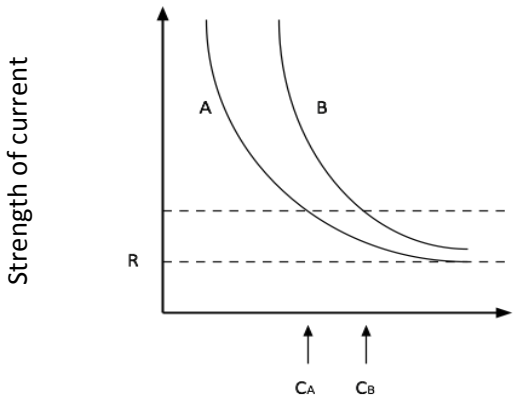

Fig 2. Schematic diagram of electrical strength-duration curve. The Rheobase (R) is the threshold intensity at longest pulse duration that stimulates nerves. Curve A represents a motor fibre and curve B represents a sensory fibre. Chronaxie is twice the rheobase. The chronaxie of the motor fiber A is less than the chronaxie of the sensory fibre B. Aα motor fibres have a much smaller chronaxie between 50 and 100 μs compared to Aδ delta (150 μs), or unmyelinated C fibres (400 μs).

The current needed to stimulate a peripheral nerve is dependent on the distance between the needle tip and target nerve, and is described mathematically by the inverse square law, $E = K (Q/r^2)$, where E = required current, K = constant; Q = minimum current; and r = distance from optimum position. Thus, by keeping the pulse duration fixed, less charge is needed the closer the tip is to the nerve. Conversely, as the needle moves away the amount of charge increases by the square of the distance.

The accuracy of peripheral nerve stimulation has been assessed by measuring threshold electrical stimulating current at three distinct regions of interest: (1) approximately 1 mm from the epineurium; (2) on the surface of the epineurium; and (3) subepineural, within the nerve.

Human study data reveal the following:

- There is a wide interindividual variability in the intensity of stimulating current required to evoke a motor response (Perlas et al 2006)
- Different nerves (e.g., radial and ulnar nerves at the elbow) in a given individual may have different stimulation thresholds (Sauter et al 2007)
- The same nerve in a given individual may have different stimulation thresholds at different body locations (e.g., median nerve in the axilla versus wrist) due to

different tissue-specific electrical impedances (Sauter et al 2009)

- Higher stimulation thresholds are observed in patients with neuropathy, such as diabetes (Bigeleisen et al 2009).

The ideal current threshold has not been established for electrical peripheral nerve stimulation because differentiation between extraneural, needle nerve contact and intraneural placement is difficult. For example, in a study of anaesthetized pigs, Tsai et al (Tsai et al 2008) showed that nerve stimulation below 0.2mA was associated only with intraneural injection (Fig 3). However, a threshold stimulating current >0.5 mA was associated with intraneural injection on 1 in 8 occassions.

Clinical studies confirm animal findings that stimulating current >0.5 mA does not exclude intraneural needle placement. Voelckel and colleagues (Voelckel et al 2005) were the first to describe the association between a low current and subsequent peripheral nerve injury. Histological nerve injury occurred in 50% of pigs after sciatic nerve block when injecting at stimulating currents < 0.2 mA compared to absence of histological changes at stimulating thresholds between 0.3mA and 0.5 mA. A recent study (Wiesmann et al 2014) in an open dissection pig model was unable to differentiate intraneural brachial plexus needle placement or needle-nerve contact using a stimulating current intensity <0.2 mA.

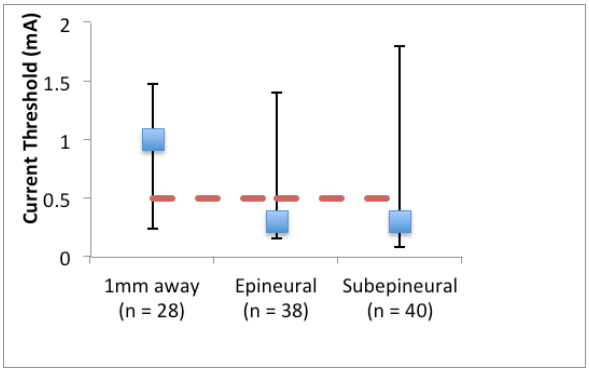

Fig 3. Relationship between current threshold and proximity to the nerve. Figure derived from Tsai et al (Tsai et al 2008) shows a range of measurements associated with thresholds obtained 1mm distant from the nerve, on the epineurium and within the nerve. The data distribution of electrical thresholds is non-parametric and the range of values from each modality overlap. The reduced number of measurements obtained 1mm from the nerve is indicative of a false negative rate of approximately 0.25 as seen in

clinical studies. Little difference is seen in the threshold profile obtained from needle tips abutting against or penetrating the epineurium.

The extraneural accuracy of the nerve stimulator was investigated in patients in a study conducted by Perlas et al (Perlas et al 2006) (Table 2). Needle tips were placed using ultrasound control close to but not touching the epineurium, nerve stimulation applied and muscle contractions sought. Despite close proximity to the nerve, electrical stimulation < 0.5mA failed to stimulate a muscle contraction in a quarter of cases, i.e. that sensitivity of nerve stimulation was 75%, but that the proportion of false negatives (otherwise termed β or type II error) was 25%. From a clinical perspective, this means that in one quarter of cases when a needle tip is positioned correctly, a muscle contraction is not elicited using electrical currents between 0.2mA and 0.5mA. Similarly, Robards et al (Robards et al 2009) studied 24 patients receiving sciatic nerve blocks in the popliteal fossa using both nerve stimulation and ultrasound guidance. The end-point for needle advancement was a motor response using a current intensity of 0.2 to 0.5 mA, or an apparent intraneural needle tip location, whichever came first. These investigators reported that in 5 out of 6 patients, a motor response could only be obtained on entry of the needle into the nerve and in the remaining 1 out of 6 patients, a motor response with a stimulating current of 1.5mA could not be obtained, even when the needle tip was deemed to be intraneural.

Taking these studies together, electrical peripheral nerve stimulation techniques offer very high specificity for the diagnosis of intraneural injection at stimulating currents <0.2mA but poor sensitivity. Moreover, when a motor response is elicited at low current intensity, needle-nerve contact and intraneural injection cannot be reliably detected (Wiesmann et al 2014).

Table 2. Sensitivity of needle tip placement. The study of Perlas et al measured the sensitivity of paraesthesia and nerve stimulation when the needle tip was placed close to the nerve. Other studies measured the sensitivity of intraneural/extraneural needle tip placement.

Mode	Sensitivity	β	Model	Study
Paraesthesia	0.30	0.70	Clinical	(Urmey & Stanton 2002)
	0.38	0.62	Clinical	(Perlas et al 2006)
	0.70	0.30	Pig	(Tsai et al 2008)
PNS	0.75	0.25	Clinical	(Perlas et al 2006)
	0.58	0.42	Clinical	(Sinha et al 2007)
Ultrasound	0.83	0.17	Clinical	(Liu et al 2011)

0.84	0.16	Clinical	(Hara et al 2014)

1.4.3 Injection pressure monitoring

The association between high injection pressures and intrafascicular injection was first described by Selander and Sjostrand (Selander & Sjostrand 1978). Evidence from animal models (Hadzic et al 2004, Kapur et al 2007) suggests that high subperineural pressure (>20psi to 25 psi or > 136kPa to 172kPa) is associated with histologic and functional nerve damage. In fresh human cadavers Orebaugh et al (Orebaugh et al 2012) reported that 100% of injections directly into the roots of the brachial plexus resulted in high injection pressures (>30 psi) with 1 occurrence of spread of the injectate into the epidural space.

Anaesthetists rely on subjective feedback from the needle tip during UGRA but perception of high injection pressure shows high inter-rater variability (Claudio et al 2004). A new disposable in-line pressure manometer has recently been introduced to practice (BSmart. B.Braun, Sheffield) that provides a visual, colour indication of injection pressure (white = 1-15 psi, yellow= 15-20 psi, orange > 20 psi.) In patients, Gadsden et al showed that placement of a needle tip within a nerve fascicle or direct contact against the epineurium is associated with mean tip pressure > 20psi (Claudio et al 2004, Kapur et al 2007, Orebaugh et al 2012) yet perineural injection close to but not touching the epineurium was associated with needle tip pressures 3-fold lower. Aborting the injection when opening injection pressure reached 15 psi reliably prevented commencement of injection in 97% cases of needle nerve contacts.

Criticism of the use of opening pressure is that peak pressure is not immediately achieved at the start of injection and is likely influenced by nerve size, nerve composition (connective tissue to nerve fascicle ratio), needle size, injection rate and volume. Moreover, low pressure has been observed during intrafascicular injection (<11 psi) in 42% (Hadzic et al 2004) to 60% (Kapur et al 2007) of cases. Nevertheless, current recommendations are that keeping the pressure below 15psi lowers the risk of fascicular injection. In all, opening pressure is a highly specific test (97%) of intraneural injection (all injections <15psi did not result in intraneural injection) but has poor

sensitivity (65%) because pressure >15psi does not differentiate between fascial, epineural or perineural needle tip placement. Expert groups recommend combined use of ultrasound, nerve stimulation and pressure monitoring, but no evidence exists to suggest that use of all three improves diagnostic accuracy.

1.4.4 Ultrasound

The primary benefit of ultrasound guidance for regional anaesthesia is visibility of the nerve location, anatomical variation, needle insertion and local anaesthetic spread.

Transducers have a linear array of ultrasound elements placed in a straight or curvilinear line, giving a cross-sectional or short-axis view of peripheral nerves. Long axis or longitudinal views are difficult to interpret although are useful when visualizing blood flow using colour Doppler. The use of ultrasound guidance has substantially facilitated the teaching and popularized the utilization of PNB while decreasing the incidence of systemic toxicity of local anaesthetics (Barrington & Kluger 2013, Sites et al 2012).

Ultrasound is sensitive enough to detect as little as 1ml of injectate (Chan et al 2007). Intraneural injection is visualized on ultrasound as nerve expansion and a reduction in nerve echogenicity (Fig 4). However, nerve swelling may be difficult to detect when conducting interscalene block as nerve roots appear less echogenic due to increased fascicular density. In a histological study Orebraugh demonstrated, using India Ink as injectate, that intraneural injection unknowingly occurred on 50% of occasions when conducting interscalene block on a cadaver (Orebaugh et al 2010). Two reasons may account for such a high incidence. Intraneural injection into fascicle-rich nerves is difficult to detect because of lack of contrast between dark fluid and dark fascicles, and anatomical description of the interscalene groove remains the subject of debate.

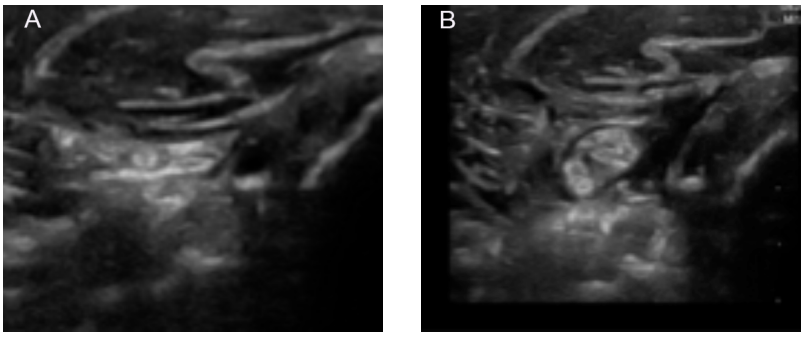

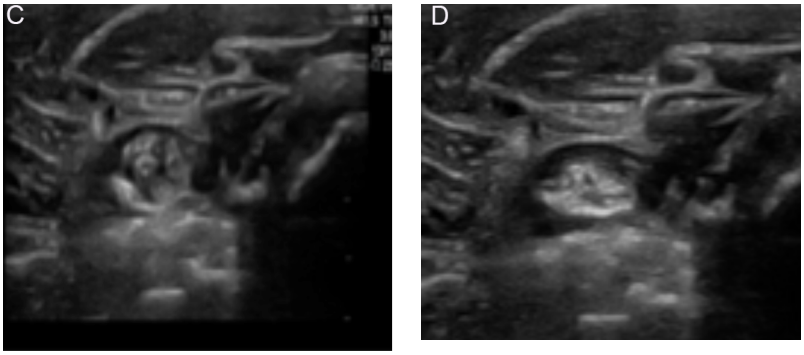

Fig 4. Accidental intraneural injection of median nerve. The upper left image shows the median nerve as a hyperechoic structure in the middle of the screen. The upper right image shows good perineural spread around the median nerve. The lower left image shows accidental intraneural injection of 1ml local anaesthetic. Note the considerable swelling and hypoechoic regions. An echogenic needle was used out-of-plane but was difficult to see. Image C shows median nerve centrally and return to normal dimensions within 30 seconds of intraneural injection

Current ultrasound technology does not have adequate resolution to discern between an interfascicular and intrafascicular injection (Lupu et al 2010) and adequate images of needle-nerve interface are not consistently obtained by all operators and in all patients (Sites et al 2007). Best outcome from UGRA follows from placement of the tip of the block needle as close to but not touching the nerve epineurium before injection of local anaesthetic (Neal et al 2015).

All in all, failure to accurately place the tip of the needle tip may be attributed to inaccurate and unreliable image presentation or erroneous image interpretation (Abdallah et al 2016), and is discussed in the following section.

1.5 Ultrasound image presentation & interpretation

B-Mode ultrasound images represent the reflection of acoustic waves from tissue boundaries - the greater the return of echoes, the brighter the tissue edge (Wells & Liang 2011). Interpretation of images may be difficult because adjacent tissues, such as nerve and adipose tissue, have similar acoustic impedance - the product of density and speed of sound through that tissue. For example, the femoral nerve is often difficult to visualise below the fascia iliaca and becomes apparent only after local anaesthetic is injected, heightening contrast between anechogenic fluid and nerve tissue.

Transducer frequencies between 5 MHz and 10 MHz transducer offer best resolution from 600µm to 300µm respectively, but fine anatomical detail, such as the adventitia of the interscalene nerve roots (Orebaugh et al 2012) is difficult to see and may account for untoward subepineural injection. The greater the distance between transducer and target nerve and the higher the transducer frequency (MHz), the more acoustic energy is dispersed as heat at a rate of approximately 0.5 to 1dB.cm^{-1}.MHz^{-1}. For example, imaging of a nerve lying at a depth of 3cm using a 10MHz transducer will lose 15 to 30dB of acoustic energy. Low frequency transducers, in contrast, lose less energy for a given depth and allow visibility of deeper structures, but with less detail.

Discrimination between fascicles and stromal tissue is difficult even using transducer frequencies up to 15MHz and is best demonstrated scanning the median nerve in the forearm; fascicles are dark and surrounding stromal tissue is white. Upper limb nerve roots appear almost anechogenic due to the higher ratio of nerve fascicle to stromal tissue, leading to the higher incidence of nerve damage at these sites.

Interpretation of B-Mode images is difficult. When conducting UGRA, anaesthetists and trainees failed to detect untoward intraneural injection on B-Mode images in 16% and 35% of patients respectively (Hara et al 2012, Krediet et al 2014, Liu et al 2011). Unfortunately, few anaesthesia studies have investigated the cognitive and perceptual mechanisms that account for such high false negative rates, and much research is needed in this area.

The inaccuracy and unreliability of needle tip positioning before local anaesthetic injection, secondary to poor technical image presentation and poor clinical interpretation, is likely the most important reason why differences in efficacy and side effects occur between patients. Needle tips may be placed unknowingly at several anatomical locations: (i) muscle; (ii) connective tissue; (iii) direct contact with the epineurium (needle nerve contact); (iv) within the inner epineurium (extra-fascicular); (v) direct contact with perineurium; (vi) within the endoneurium (intra-fascicular). Local anaesthetic injection within connective tissue, as close as possible but not touching the epineurium is likely to block nerve conduction. On the other hand, injection into muscle distant from the epineurium is less likely to block nerves because

the concentration of local anaesthetic reaching sodium channels is lower that the minimum necessary.

The clinical problem is compounded by changing patient characteristics. Patients are more obese, increasing the distance between skin and nerve; growing older; and more likely to have multiple chronic conditions such as diabetes that, along with age, change the pharmacodynamic profile of local anaesthetics. Therefore, the technical delivery of local anaesthetic, despite modern advances in technology and education, remains imprecise and unreliable and a need arises to improve both efficacy and side effects in order to cater for the anaesthetic needs of a changing population.

Before embarking on studies attempting to improve the accuracy and reliability of UGRA, I considered it important to review existing and novel technology with potential application to UGRA. Equipment currently being investigated includes: electro-magnetic needle guidance systems; 3D ultrasound imaging using electronic square arrays with beam steering; electrical impedance, optical coherence tomography (OCT) and micro-ultrasound.

1.6 Imaging technology

Imaging during the conduct of regional anaesthesia has several limitations: (i) anatomy must be inferred from knowledge and experience; (ii) once the transducer has moved, areas of interest are difficult to relocate; (iii) measurement of 2-D areas of interest do not necessarily correlate with 3-D volumes of interest; and (iv) needle shaft and tip visibility is only possible when the needle lies within the narrow line of the beam. Accordingly, experienced anaesthetists scan proximally and distally to the region of interest in order to create an imaginary 3D image of anatomybefore conducting regional anaesthesia.

Three dimensional ultrasound would conceptually seem to represent a natural progression from 2D imaging as it offers the opportunity to visualize coronal, sagittal and transverse planes. Two types of transducer are used in the creation of 3D images (Fenster et al 2011). Mechanical 3D transducers generate a series of 2-D images by sweeping a linear transducer around a pivot (like a fan) over the volume of interest. However, this mechanism has an in-built flaw. When acquiring images from greater

depths, increased physical separation occurs between images and resolution degrades. Newer matrix transducers, in contrast, have several thousand ultrasound elements arranged in a square configuration that projects ultrasound waves within a pyramid-like volume. Three dimensional images are visualized using two techniques. The first, multi-planar reformatting, presents images as a 3D crossed plane (Fig 5). With crossed planes, flat 2D planes are visualized in three orthogonal planes and each plane moved relative to the others in order to select the optimal image (Fig 5, bottom right image).

The second technique, termed volume rendering, projects 3D data onto a 2D surface by using ray-casting in order to optimize the projection effect, degree of translucency and surface shadowing of the image (Fig 5, bottom left image). Rendering works best in situations where fluid provides a contrast to tissue planes such as foetal imaging.

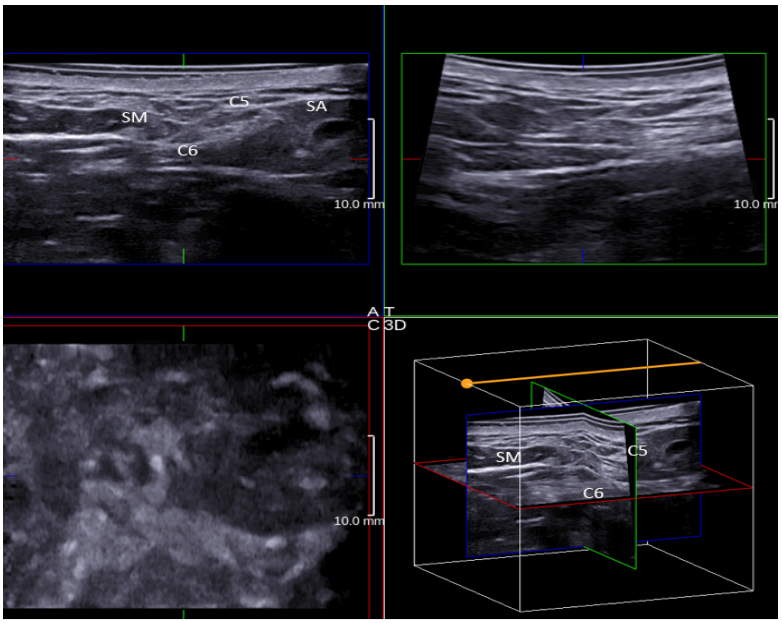

Fig 5. Three-dimensional ultrasound of neck of a volunteer. Image taken on volunteer in ultrasound laboratory, University of Dundee. The multiplanar image (white square) is constructed from a sagittal plane (blue square) and a coronal plane (green square). In the sagittal plane the interscalene groove and C5 and C6 nerve roots are visible, along with the scalenus medius (SM) and scalenus anterior (SA) muscles. The nerve roots are more difficult to see in the coronal plane. The multiplanar view offers little extra information and the rendered view (red square) is not interpretable.

Few studies have investigated the role of 3D or 4D imaging in regional anaesthesia. In volunteer studies, the 3D anatomy of the brachial plexus (Cash et al 2005), paravertebral region (Karmakar et al 2012b) and course of the sciatic nerve (Karmakar

et al 2012a) were described. In clinical studies, 3D ultrasound aided placement of popliteal (Feinglass et al 2007) and infraclavicular catheters (Clendenen et al 2010), visualise and measure local anaesthetic spread. The benefits and risks of three-dimensional US compared to a careful two-dimensional scan in both the short-axis and long-axis planes remain unresolved. At this time, 2D imaging offers better resolution than 3D ultrasound and it is hoped that future higher frequency phased arrays may offer better and more interpretable images and stimulate research into the role of 3D technology.

1.7 Needle technology

Needle tips and shafts are difficult to see during UGRA. Therefore, I also conducted a review of the properties of needles used in regional anaesthesia and those under development in order to inform me about the most appropriate needle to use during my experiments.

1.7.1 Textured needles

Regional anaesthesia needles are inserted in the plane of the ultrasound transducer, parallel to the linear array of elements, in order to visualise the needle shaft and tip. Poor coordination of hand and transducer movement may inadvertently place needles across the transducer midline, limiting visibility. Needle visibility is best with larger needles (Schafhalter-Zoppoth et al 2004) and when inserted parallel (0^o) to the ultrasound beam. Unfortunately, flat orientation of the needle to the transducer is rarely practical and steep angles or out-of-plane approaches are necessary, particularly for insertion of perineural catheters. In order to improve needle visibility, manufacturers have indented the surface of needles with angular depressions (Hebard & Hocking 2011) and claimed improved visibility compared to standard smooth needles due to better reflection of ultrasound waves.

1.7.2 Electromagnetic needle guidance systems

Electromagnetic needle guidance systems are available for clinical use. The SonixGPS consists of a transmitter/receiver unit that generates a weak magnetic field, a reuseable needle sensor element housed within a disposable stylet and a sensor embedded in a dedicated ultrasound transducer (Niazi et al 2014). Placement of the

needle within the magnetic field, and without breaching the skin, generates small voltages that calculate the position and orientation of the needle relative to the ultrasound transducer. A thin trajectory line is directed towards the target (Fig 6). In-plane alignment relative to transducer elements is represented on a schematic transducer. Optimal in-plane needle position is indicated by a change in colour of the schematic transducer surround from white to green. During out-of-plane needle insertion, the needle is framed by a red border and the target is indicated as an ”X”. Placement of the distal red tip on the “X” indicates correct needle tip positioning.

Needle insertion using the SonixGPS improved medical student (McVicar et al 2015) and nurse anaesthetist (Tielens et al 2014) performance in a pork phantom model; in-plane visibility of needles improved, procedural time was shorter and fewer needles needed repositioned. Case reports have described interscalene, supraclavicular and infraclavicular brachial plexus blocks (Umbarje et al 2013) and paravertebral blocks (Kaur et al 2013) successfully performed using the out-of-plane approach (Umbarje et al 2013).

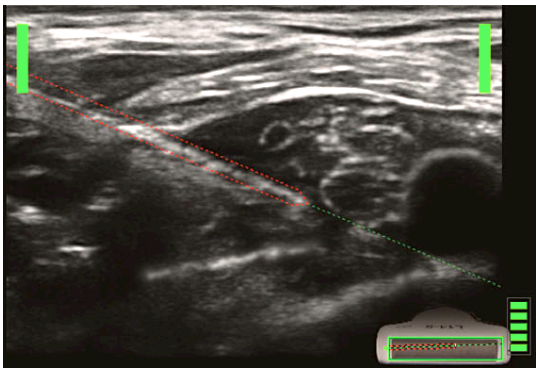

Fig 6. Real-time 3D needle tracking system. Image courtesy of Sonix GPS, Ultrasonix, Vancouver, Canada. The white trajectory plotted on the screen, aims for the target pre-block. During needle insertion, guidance is optimized with the aid of coloured orientation bars (where green represents good orientation and red represents poor orientation) and a schematic diagram of needle probe alignment

Two studies investigated the application of SonixGPS to spinal anaesthesia for knee arthroplasty. In both, a proprietary 17g SonixGPS needle was placed at the ligamentum

flavum-dura mater complex, the needle sensor removed and a Whitacre spinal needle passed through it. In the first study (Brinkmann et al 2013) CSF was obtained in 18 out of 20 patients, but required multiple attempts in 11 cases (55%). In a subsequent study (Niazi et al 2014) 20 low risk patients (body mass index < 35 $kg.m^{-2}$ and no history of spinal abnormalities) underwent spinal anaesthesia initially using an in-plane technique. However, 2 out of 4 insertions were unsuccessful and the remaining 16 patients received an out-of-plane technique. Even then, 4 insertions (75%) failed due to repeated bony contact. Combining the results of both studies, successful single shot spinal anaesthesia occurred in only 15 out of 40 patients, suggesting that application of GPS technology to spinal anaesthesia remains problematic.

An alternative electromagnetic tracking device has been developed by eZono (Gadsden et al 2015). Rather than use needles with in-built sensors, standard needles are magnetized by insertion into a small, sterile plastic cup with two built-in magnets. The ultrasound transducer incorporates a needle tracking system that identifies the position of the magnetized needle and measures the signal strength of the reflected soundwaves. Like the SonixGPS, a schematic transducer footprint on the screen indicates the position of the needle before skin penetration and a dashed line represents the predicted needle trajectory. A red box indicates the target and solid lines on either side of the needle trajectory line represent the actual depth of the needle. As the needle approaches and overlays the target, the colour of the box changes from red to green. The advantage of the eZono 4000 needle guidance system is that it it can be inserted in any angle or direction but does not require heavy transmitters or specific needles. In contrast, the SonixGPS is limited by the need to use proprietary needles and the magnetic field may be distorted by ferromagnetic materials. Uptake of either guidance system within the anaesthetic community has been negligible because both are regarded as teaching tool for novice anaesthetists.

1.7.3 Smart Needles

Awareness of the limited accuracy and reliably of ultrasound for UGRA has shifted the focus of technology away from transducer development towards smart needle technology. Smart needle technology may be categorized into two groups: (i) needles that measure tissue properties such as needle spectroscopy, impedance or force and

provide a surrogate measure of needle tip position: and (ii) needles that image tissue in detail using high frequency microultrasound.

1.7.4 Tissue Impedance Needles

Electrical tissue impedance monitoring is a modality featured in new nerve stimulators. It is a measure of the opposition of the flow to alternating current (AC) similar to the resistance of a conductor to direct current (DC). It is extremely sensitive to changes in tissue composition, particularly water content. In a pig sciatic nerve model, Tsui and colleagues (Tsui et al 2008) demonstrated that nerves have greater electrical impedance than the surrounding muscle and interstitial fluid because of their low water and high lipid content. However, data so far show large variance and poor suitability for clinical use.

1.7.5 Spectroscopy Needles

The optical characteristics of tissues, measured using spectroscopy, have been investigated as a means of differentiating between different tissues and indicate the position of the needle tip. Integrated optical fibres transmit visible and near-infrared light from the tip of the needle and tissues absorb and reflect light depending on their physical properties. Spectroscopic analysis over a range of wavelengths measures the scatter and absorption of tissue of light by haemoglobin, oxygenated haemoglobin, water and adipose tissue. Each tissue has a characteristic narrow absorption peak; oxyhaemoglobin absorbs light in the visible spectrum, whereas lipid and water absorb light in the near-infrared spectrum.

Light spectroscopy experiments conducted in pigs identified the ligamentum flavum and epidural space (Desjardins et al 2011) (Rathmell et al 2010) and transition from muscle to nerve in the axillary region. Proximity to peripheral nerves was associated with higher lipid and lower haemoglobin values in pigs (Brynolf et al 2011) and patients (Balthasar et al 2012). Future benefits may include detection of tissue vascularity (Soto-Astorga et al 2013) and reduction in accidental intravascular injection.

Although clinically appealing, several issues need to be resolved before commercialization. Adipose tissue stores vary between patients and with age, sex and

BMI; spectral change from muscle to nerve is more acute than adipose tissue to nerve; and false positive results may arise from blood accumulation at the needle tip due to repeated injections. Spectral analysis may also be altered by transducer compression, reducing the distance between the skin and nerve target, and needle angulation. Nevertheless this technology can detect optical spectra from tissues at catheter tips (Soto-Astorga et al 2013) and has the potential to provide real-time detection of intravascular catheter placement.

1.7.6 Peizo-electric Needles

Electrical vibration of peizo-electric crystals attached to the hub of needles vibrates the shaft (Sadiq 2015) at frequencies up to 25MHz, but remains imperceptible to the human eye. Colour Doppler imaging presents the needle as a linear range of colours, at angles between 0^{o} and 60^{o} (Liao et al 2016). Electrical driving of the needle offers dual functionality. Not only can it be seen throughout its length but the electrical properties such as peizo impedance and resonant frequency, as well as force from an in-line load cell, are measured in real-time (Sadiq 2015) (Fig 7). Epidural studies on pork lumbar specimens has demonstrated characteristic changes in peizo-electric impedance, resonant frequency and force (Liao et al 2016). The mechanism of action of this needle may be conceptualised as akin to that of a pneumatic drill; contact with hard bone reduces resonant frequency whereas contact with fascial planes increases resonant frequency. Force and impedance increase in the following rank order: bone > ligamentum flavum > interspinous ligament > epidural space. Multi-modal needles such as this provide both visual confirmation of needle tip position and accurate recognition of tissues. This needle remains under development and human trials are awaited, initially for cancer biopsy.

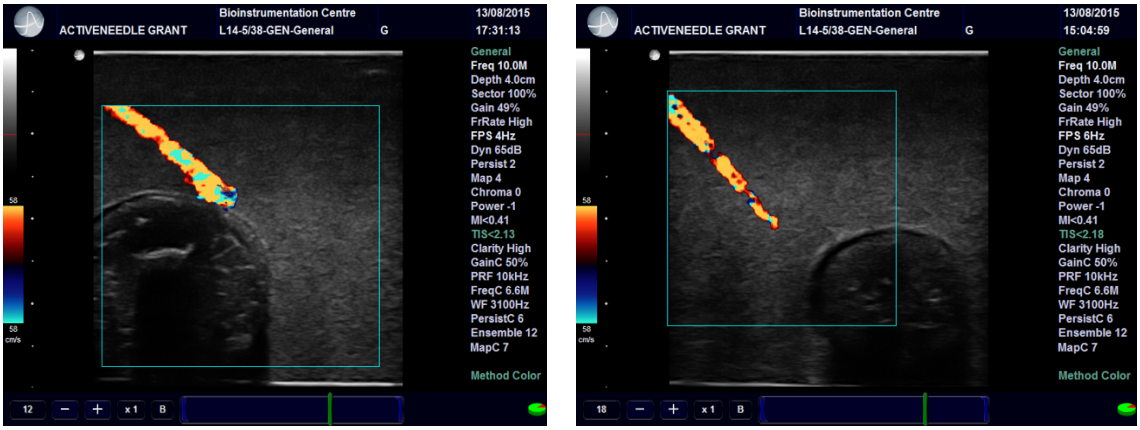

Fig 7. Peizo-electric needle. Injection into phantom with grape inclusion. The left image shows insertion of an actuated needle inserted at 30^0 using colour Doppler imaging. The right image shows insertion of the same needle at 45^O.

1.7.7 Optical coherence tomography needles

Optical coherence tomography (OCT) is a laser based imaging technology already used to image retinal disease. Incorporation of OCT into an epidural needle (Tang et al 2014) (Kuo et al 2015, Scolaro et al 2012), (Tang et al 2015) has the potential to image anatomy in deep spaces with very high resolution between 5 and 15 µm and reconstruct images in 3-D. Such resolution is similar to that obtained with histology. Unlike ultrasound, imaging may be performed in air without direct contact with tissue, and does not complicate interpretation secondary to tissue compression. The disadvantage of OCT is that backscatter and absorption of light limits imaging to the first 2 - 3mm of tissue. An optical fibre has been recently incorporated into the side of an 18g Tuohy needle and paramedian epidural block conducted in the lumbar and thoracic regions of five pigs (Kuo et al 2015). An anaesthetist rotated the transducer manually and built up a series of images. Identification of the epidural space had high sensitivity and specificity. Although this technology promises ultra-high resolution, it is expensive and needs incorporation into a needle guidance system. Pilot work in Ninewells hospital showed marked reflection from myelin of dissected human nerves and poor transmission of light into nerves.

1.7.8 Micro-ultrasound needles

The development of micro-ultrasound, using transducers with a frequency >30MHz and tissue resolution< 100µm was stimulated by the need to characterize the anatomy

of small animals in developmental biology, genomics and cancer (Foster et al 2011). Both CT and MRI provide high quality images but are expensive and cumbersome. In order to observe changes in tissue configuration, a high resolution of 20µm to 100µm is needed, corresponding to ultrasound frequencies between 150MHz and 30MHz. Mechanical single element transducers with a capacity to generate frequencies up to 100MHz have traditionally been used, but are now being replaced by linear transducer arrays with greater functionality.

Failure to reduce accidental intraneural injection despite ultrasound guidance suggests a potential role for micro-ultrasound in UGRA. The greater the distance between transducer and target, the greater the energy attenuation and the poorer image resolution. Experimentation with different shaped transducers using a wide range of frequencies is unlikely to resolve this clinical dilemma as obesity levels are rising within Western economies. One solution is to develop active ultrasound needles with peizo-electric crystals at the tip in order to more accurately identify relevant anatomy and target local anaesthetic injection. Microultrasound research for UGRA is within its infancy but, scanning fresh cadaver nerves using 30MHz frequencies, laboratory images (Chandra et al 2014) are already able to delineate the epineurium, the size of the nerve, the number and size of fascicles, as well as visualise needle insertion and intraneural tissue trauma. For clinical application we would propose using a combination of an active needle with a traditional ultrasound transducer and two images. The needle would be guided to, for example, within 1 to 1.5cm of the target nerve, then the micro-imageactivated, nerve and connective tissue identified and the needle tip guided precisely to its destination. Thus microultrasound holds out the promise of both improved efficacy and reduced nerve damage for UGRA but will be more complicated to use for many anaesthetists and probably confined to experts.

In summary, use of B-Mode ultrasound has made anaesthetists increasingly aware of the technological limitations of equipment. Resolution of anatomy is limited to a maximum of 200µm using 15MHz transducers, and detailed real-time visibility of intraneural and extraneural anatomy remains elusive. Research is focused increasingly on the development of smart needles that measure surrogate biological or physical tissue markers, or visualise tissue at very high resolution. It is likely, that in order to

improve accuracy and reliability of needle interventions, including cancer biopsy, different technologies are likely to be combined within disposable needles. However, none are as yet available to clinicians nor researchers. My literature review has indicated that before embarking on UGRA imaging studies on the soft embalmed cadaver, it will be necessary to standardise needle intervention. As only two needles are available commercially - smooth and textured needles – and are available in two sizes for single injection and catheter insertion, I shall need to conduct a randomised trial in order to determine the best type and size of needle to be used. The choice of needle will be determined by best visibility of the tip and shaft when both aligned in-plane and out-of-plane to the ultrasound transducer.

1.8 Tissue properties

In order to carry out translational studies on the soft embalmed cadaver and patients, I considered it important not only to consider the physical characteristics of the ultrasound transducer and needle but also their interaction with cadaver and human tissue. Within the ultrasound transducer, piezoelectric elements, such as lead zirconate titanate, expand and contract in response to electrical stimulation, generating high frequency ultrasound waves. Reflection and scattering of ultrasound waves occurs at the interface between tissues and is attributable to relative acoustic impedance, the product of density and speed of sound of acoustic waves. An 8-bit (2^8) grayscale image is formed, reflecting the relationship of underlying tissue with ultrasound waves. Acoustic energy is dissipated with increasing distance between transducer and target nerve and heat is absorbed. The higher the transducer frequency, the greater the energy attenuation, limiting high resolution to superficial anatomy. In contrast, low frequency transducers enable visibility of deeper structures, but with less resolution. Moreover, neighbouring anatomical structures such as nerve, muscle and adipose tissue have similar acoustic impedance – the product of tissue density and acoustic wave speed. The density (ρ) of adipose tissue is 916 $kg.m^{-3}$ and 1060 $kg.m^{-3}$ in muscle, whereas wave speed *(c)* ranges from 1629 $m.s^{-1}$ in adipose tissue to 1412 ms^{-1} in muscle.

Consideration of the product ($\rho.c$) indicates that relative reflection from borders is relatively small and prevents accurate differentiation between tissue layers.

Palpation, the examination of tissue elasticity (a material's resistance to deformation) is a time honoured clinical technique dating back to the ancient Egyptians and Chinese. For the purposes of modern medicine, however, palpation alone is an unreliable, subjective diagnostic tool, especially for the diagnosis of small and deep lesions. Elasticity is described mathematically as the application of force over a specified area (stress) with resultant displacement of tissue (strain). Stress (σ) is defined as Force per unit area with the units kPa or Nm^{-2} whereas strain(ϵ) is represented as: $\epsilon = (L_f - L_0) / L_0$ where L_f is the length after and L_0 is the length before tissue displacement. Thus strain is a unitless entity (Wells & Liang 2011). Definitions of tissue elasticity are given in Table 3.

Table 3. Definitions of terms used to describe tissue properties

Term	Definition
Stress	Force applied to tissue. (Not a property of the tissue itself)
Strain	Fractional change in tissue dimensions
Elasticity	A property of tissue; "continuum mechanics of bodies that deform under stress"
Stiffness	A property of tissue: the resistance of tissue to deformation under the influence of stress. The ratio of stress to strain

The mechanics of soft tissues are very complex and assumptions are made when measuring elastic properties Tissues are regarded as homogeneous, isotropic, incompressible solids that obey Hooke's law (i.e. low values of strain are directly proportional to stress), have a density ρ of 1000 $kg.m^{-3}$ and waveform velocity equivalent to the speed of sound, 1540$m.s^{-1}$. For incompressible tissue, Poisson's ratio is accepted as 0.5, shear wave speed $c_s = \left(\frac{G}{\rho}\right)^{1/2}$ and the relationship between Young's modulus and Shear modulus is fixed according to the equation: $E = 3.G$.

Table 4. Definition of tissue elasticity. Tissue elasticity (Pa) may be regarded as longitudinal, transverse and volume and described mathematically by Young's (E), Shear (G) and Bulk (K) moduli. The fourth important concept is Poissons's ratio (σ), the ratio of lateral contraction to longitudinal extension. All four terms are mathematically interrelated

Modulus			**Description**
Young's modulus (E)	Longitudinal	Tendency to deform along an axis when opposing forces are applied along that axis	$E = 2G(1 + \nu)$
Shear modulus or modulus of rigidity (G)	Transverse	Tendency to shear when acted upon by transvere opposing forces	$G = \frac{E}{(2(1 + \sigma)}$
Bulk modulus (K)	Volume	Tendency of an object to deform in all directions when uniformly loaded	$K = \frac{E}{(3(1 - 2\sigma)}$
Poisson's ratio (σ)		Lateral contraction per unit breadth divided by longitudinal extension per unit length	

1.9 Elastography

Elastography, invented in 1991 by Ophir (Ophir et al 1991), is the umbrella term used to describe several technologies that image elasticity, the resistance of tissue to deformation and described mathematically as the application of force over a specified area (stress) with resultant displacement of tissue (strain). Definitions of terms are given in Table 4. Stress may be applied mechanically using transducer compression (Treece et al 2011) or internally using an ultrasonic radiation force (Palmeri & Nightingale 2011) while measurement may be achieved using magnetic resonance imaging (MRI) or ultrasound. The latter is popular because it has a high spatial resolution, works in real time, and uses conventional ultrasound equipment.

Elastography is increasingly used for diagnosis of breast (Evans et al 2012, Evans et al 2010, Sim et al 2015) and prostate (Barr et al 2012) cancer because it provides a colour image representative of tissue stiffness.

1.9.1 Strain elastography

The elastic properties of tissue may be visualised using the qualitative method of strain elastography. Raw radiofrequency data (otherwise termed ultrasound A-lines), collected before and after transducer compression, is split into "windows" and compared using cross-correlation methods (Fig 8). The difference between waveforms equates to tissue displacement or shift. The rate of change in tissue displacement as a

function of the distance from the transducer, is computed and displayed as a colour elastogram.

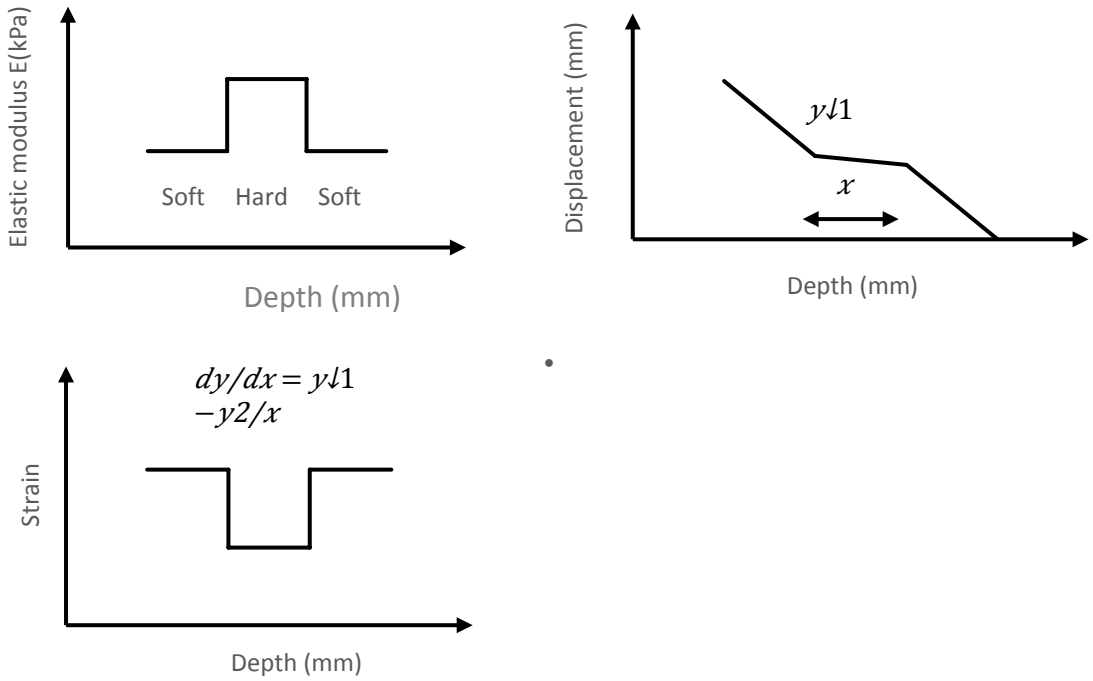

Fig 8. Mechanism of strain elastography. Transducer pressure results in displacement y_1 and y_2 (mm) at depth *x*. Strain is obtained by differentiation of displacement, that is, the ratio of the difference in displacement between two points to their pre-compression distance.

The difference between waveforms equates to tissue displacement or shift. The rate of change in tissue displacement as a function of the distance from the transducer, is computed and displayed as an elastogram (Fig 8). Low strain or tissue displacement in response to transducer pressure is visualised as a blue background colour whereas injection of local anaesthetic is displayed as yellow, red and orange colour due to greater displacement (Munirama et al 2012) (Fig 9). Application of elastography in

clinical practice has so far focused on diagnostic accuracy, for example discriminating between benign and malignant breast lumps (Evans et al 2010). In this case of a gel phantom containing an inclusion, the hardness of the object appears as a dark blue hue whereas the relative pliability of surrounding agar appears as a yellow / orange colour.

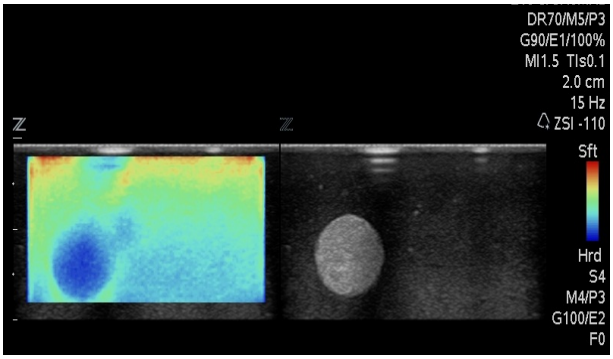

Fig 9. Strain elastography in agar phantom. Low strain or tissue displacement in response to transducer pressure is visualised as a blue background colour whereas injection of local anaesthetic is displayed as the yellow, red and orange colours, indicative of greater strain due to formation of a hydrospace. An example of strain elastography is shown in a breast phantom.

However, the application of strain elastography to UGRA has several potential limitations. Interpretation is qualitative because strain (relative displacement) is a unitless entity and subject to operator variability; the size and shape of the strain pattern does not equate to the size and shape of the hydrospace area because both fluid and tissue are displaced according to their intrinsic stiffness; and further, structures beyond 4cm are poorly compressible from skin pressure and needles, and even when moving, are indistinct with a wide strain pattern.

1.9.2 Shear wave elastography

Conventional ultrasound imaging processes one line at a time. A typical 2D image is made of 64 to 256 lines. The frame rate is the reciprocal of the time taken to transmit a beam, receive and process the backscattered echoes and repeat that for all the lines of the image.

For a conventional 2D image, The maximum frame rate is:

$$r \backsimeq \frac{1}{t}$$

where *t* = the time taken to build an image

$$t = \frac{N_{lines} * 2 * d}{c}$$

where N = number of lines, *d* = depth of image and *c* = speed of sound of ultrasound through tissue (water = 1540m.s^{-1}). For example, the maximum frame rate of a 128 element transducer imaging over a 3cm depth is 200Hz.

A novel technology termed ultrafast imaging has revolutionised cancer imaging. An entire ultrasound image is computed rapidly from a single broad insonification, allowing imaging frame rates up to 20,000Hz. Shear Wave Elastography has been developed from ultrafast imaging. Unlike strain elastography it provides quantitative visco-elastic analysis of tissues by capturing transient shear waves hitherto not seen on commercial ultrasound images.

The characteristics of shear waves differ markedly from compressional mechanical waves in soft tissue. Whereas compressional waves travel at approximately 1500m.s^{-1} depending on the nature of tissue, shear waves travel much slower around 10m.s^{-1}

Shear elastic modulus (kPa) is a function of tissue density and longitudinal ultrasound wave speed according to the formula (Wells & Liang 2011):

$$K = \rho . c_s^2$$

where $K = \text{shear modulus}$, c_s = shearwave speed and ρ = tissue density

Thus, the denser the tissue, the faster shear wave speed. Longitudonal or Young's modulus is approximately three times the the magnitude of shear modulus. There are three different types of source of transient shear waves in the body. The first type is natural body vibrations such as the arterial pulse, external vibrators or movement of tissue at the focus of a very high speed ultrasound beam, otherwise termed acoustic radiation force.

In 2004, a new imaging mode was introduced coupling radiation force induced transient shear waves and ultrafast imaging called Supersonic Shear Imaging (Bercoff 2011). In order to generate shear waves, ultrasound beams (Aixplorer, Supersonic

Imagine, Aix-en-Provence) are transmitted at high speed and focused in a cone-like shape, transferring energy to tissues and inducing shear waves at multiple tissue levels, not unlike the ripples generated by a stone thrown into water (Fig 10). Shear wave speeds vary between 1 and 10 $m.s^{-1}$, and are considerably slower than mean ultrasound (1540 $m.s^{-1}$) speed passing through tissue, and are picked up by trackers in the ultrasound transducer. The advantages of shear wave elastography (SWE) are that no manual compression is required, and that data is repeatable and reproducible. However, application of the transducer requires a light touch as any pressure will show as a surface tissue strain. Shear waves cannot pass through fluid pockets, and thus injectate appears as dark shadows, accurately mapping the size of the hydrospace.

1.10 Conclusion

1.10.1 Summary

My background studies revealed deficiencies in the technical presentation and the clinical interpretation of ultrasound images. The salient problems I identified are:

- The position of the needle tip relative to the epineurium is difficult to discern before injection, even in the hands of experts.
- The margin of the epineurium is indistinct on B-Mode images
- Increased distance between the skin and nerve target reduces tissue resolution and changes in acoustic impedance alter reflectivity at tissue margins.
- Changes in tissue morphology with increased age and vascular diseases such as diabetes are associated with poorer ultrasound images.
- B-Mode ultrasound does not offer sufficient resolution to identify intraneural or perineural anatomy. For example a standard 10MHz transducer has maximum resolution of only 300μm.
- Trainees and experts have difficulty recognising accidental intraneural injection.
- The needle shaft and tip are difficult to see at wide angles. Advanced needle technology is not yet commercially available.
- Elastography is a generic term for technologies that mimic traditional palpation.
- Strain elastography visualises tissue strain and shear wave elastography quantifies tissue elasticity.

Thus, I endeavoured to investigate the translation of elastography to UGRA by conducting a series of soft embalmed cadaver and patient studies in order to investigate the accuracy and reliability of image presentation and the accuracy and reliability of image interpretation using strain and shear wave elastography.

1.10.2 Hypotheses

I hypothesised that:

- Soft embalmed Theil cadavers can be used to visualise nerves, muscles and arteries on B-Mode ultrasound images at sites commonly used for UGRA.
- Textured needles had better visibility during UGRA than smooth surfaced needles, needle visibility improved during in-plane imaging and needle gauge had no further effect on visibility.
- Elastography was able to capture tissue displacement in colour using small volumes of embalming fluid, representative of test doses of local anaesthetics in patients.
- Software conversion of the elastography image had the potential to provide an objective measure of hydrolocation.
- Strain elastography might be able to differentiate between intraneural injection and extraneural injection.
- Shear wave elastography would allow presentation of peripheral nerves images in colour map, which indicated the density of the tissues being imaged.
- Shear wave elastography might be able to quantify the stiffness of nerves and surrounding tissue in cadavers and humans.
- The soft embalmed Thiel cadaver has physical properties and functional alignment such that it provides good simulation conditions for training ultrasound guided regional anaesthesia.

1.10.3 Thesis plan

Therefore, my thesis plan was as follows:

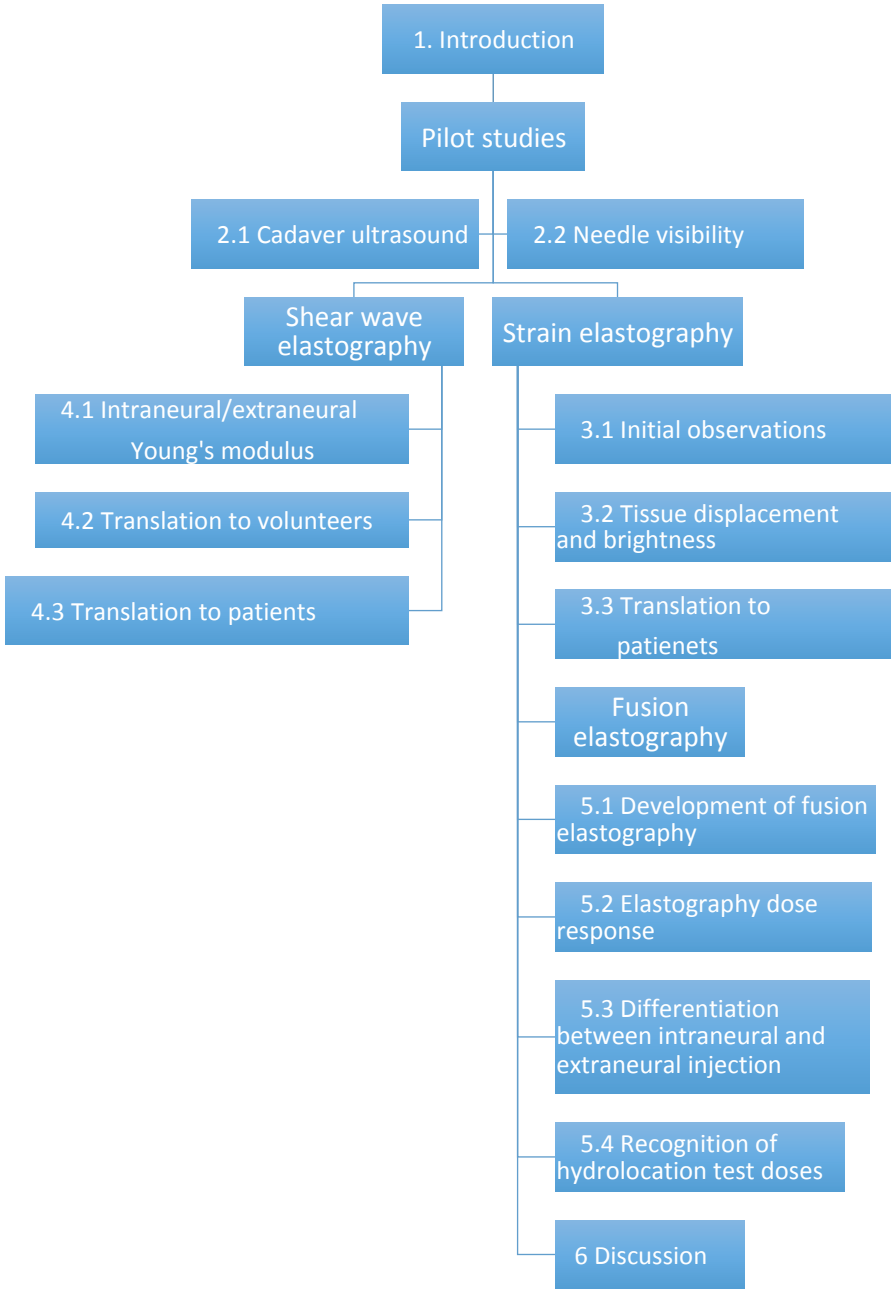

1.11 Statistical analysis

Before analysis, the nature, distribution and dependency of data was established. The nature of data was either qualitative (nominal or ordinal) or quantitative (ratio or interval). The distribution of data was tested using the Shapiro-Wilk test and normality plots in order to determine whether data followed the parametric distribution or not. If so parametric analysis was used. Otherwise, non parametric analysis was used. The dependency of data was assumed when experiments were carried out repeatedly on one to three cadavers, because cadaver availability was restricted at the time.

Categorical and Ordinal data

- Categorical data frequency was tested using 2x2 tables.
- Correct diagnosis was modelled using stratified logistic regression model (NCSS, Utah) and (Logxact, Cytel, Cambridge, MA) which controlled for repeated measures.
- Ordinal, dependant, paired data comparing secondary outcomes such as rater visibility of anatomy and spread of solution used the Wilcoxon signed-ranks test (Ch 5.2.3).
- Agreement between raters (Ch 2.2.3) was assessed using the Cohen weighted kappa (κ) statistic (95 % CI) and the observed weighted proportional agreement (Landis & Koch 1977). (Ch 2.2.3; Ch 5.2.3).
- Agreement was plotted using Bland–Altman plots (GraphPad Prism 5, GraphPad, CA) with mean area on the x-axis and differences between rater means on the y-axis and set the 95% confidence limits of agreement or smallest detectable change as bias ± 1.96 multiplied by the repeatability coefficient, defined as the product of √2 and within subject standard deviation(Bartlett & Frost 2008, Carstensen et al 2008). Within subjects standard deviation was calculated using R Studio, Version 0.98.978 according to the recommendations of Myles(Myles & Cui 2007).
- Comparison of visibility scores and proportions of needle tip visibilities (Ch 2.2.3) used Friedman analysis of randomised blocks and Exact Hodges-Lehmann estimates of median (95%CI) differences between groups.

- Recognition of intraneural or extraneural injection on paired B-Mode and fused elastography images was analysed using McNemar's test and presented as differences in paired proportions.
- The diagnostic accuracy of intraneural/extraneural was calculated using 2x2 tables to categorise rater diagnosis according to actual diagnosis. From this data the sensitivity and specificity of each modality, positive likelihood ratio and diagnostic odds ratio were calculated according to the following table:

	Outcome	
	+	**-**
Test	**a**	**b**
	c	**d**

Fig 10 : 2x2 table of Outcome vs Test

- **Prevalence** (pre-test likelihood of disease) = (a + c)/(a + b + c + d)
- **Predictive value of +ve test** (post-test likelihood of disease) = a/(a + b)
- **Predictive values of -ve test** (post-test likelihood of no disease) = d/(c + d)
- **Sensitivity** (true positive rate) = a/(a + b)
- **Specificity** (true negative rate) = d/(c + d)
- **Likelihood Ratio** LR (positive test) = [a /(a + c) / b/(b + d)]
  LR (negative test) = [c /(a + c) / d (b + d)]
- **Diagnostic Odds Ratio** Odds ratio = LR+/LR-

Independent continuous interval data

- The relationship between fixed covariates such as volume and type of block and continuous independant data such as area under the curve (AUC) of local anaesthetic spread was examined using analysis of variance (ANOVA). ANOVA is a form of the general linear model (GLM), characterised by the equation Y = A + B +AB + error where AB = interaction of the fixed effects A and B.

- For example (Ch 5.2.3) ANOVA and post-hoc Bonferroni tests, with volume injected and block performed as fixed covariates, were used to analyse the

AUC. Within subject standard deviation was used as an estimate of measurement error.

Dependant continuous interval data

- Elastogram strain or relative displacement is a unit-less entity. Therefore, the area of the coloured strain pattern was measured during injection. Colour elastograms were converted to grayscale images, scaled in pixels cm^{-1}, then further transformed to a binary image. The area of tissue displacement was visualised in black and demarcated from a white background on every 5^{th} image using a yellow tracing tool. Brightness of the area of displacement within the grayscale image using a 256 point scale between 0 (black) and 255 (white). Time to peak area and brightness followed a non-parametric distribution and was expressed as median [IQR].

- Change in area and brightness data used the geometric mean. Geometric mean is used to evaluate data covering several orders of magnitude and for evaluating ratios or percentage changes. The geometric mean "normalizes" the ranges being averaged, so that a given percentage change in any physical property has the same effect on the geometric mean. For example a 20% change in from 8 to 10 on one scale would have a similar effect on the

  geometric mean as a 20% change in another scale say from 64 to 80. In order to calculate geometric mean, I logged data using the formula:

  $$y = Ln\, x \; or \;\; y = Log_e\, x$$

  then anti-logged for presentation according to the formula:

  $$x = e^y.$$

  Difference between groups was expressed as geometric ratio. Mean Difference was calculated using Tukey-Kramer's All Pairs Simultaneous Confidence Intervals
- Mixed linear model analysis was used to investigate complex relationships between dependant continuous data. Mixed effects models are increasingly

used in place of classical statistical techniques such as the t-test, one-way ANOVA, general linear model (GLM) and repeated-measures GLM because they can cope with different group variances, time points and missing data. Mixed models extend linear models by allowing for the addition of random effects (e.g. between individuals) and can be used to test pair-wise comparisons and repeated measurements of subjects.

For example:

Let us assume that

$$\text{Shear speed} \sim \text{nerve type} + \varepsilon$$

where nerve type is affixed effect, "shear speed ~ nerve type" = systematic error and ε = random error

However, multiple measures taken from each cadaver violates the independence assumption. Therefore a random effect is added for each subject, and resolves non-independence by assuming a different "baseline" pitch and random intercept on the y-axis value for each subject depicted as 1|cadaver.

The mixture of fixed and random effects creates a mixed model

$$\text{Shear wave speed} \sim \text{nerve type} + \text{gender} + (1|\text{cadaver}) + \varepsilon$$

For example:

- Young's modulus at extraneural and intraneural sites of three nerves by two raters (4.1.3)

- Area and brightness (5.4.3) of intraneural and extraneural injection. Covariates included cadaver number, right or left sided injection, injection sequence, type of block (interscalene and femoral), volume (0.25, 0.5 and 1.0ml) and imaging region of interest (perineural fluid spread, area of fusion strain pattern).

- A stratified logistic regression model was used to analyse binary outcomes and take account of repeated measures. Trend analyses looked at the effects of volume.

Data were analysed using Number Cruncher Statistical Systems (NCSS) 11, NCSS Inc., Kaysville, UT and LogXact 8, Cytel Inc., Cambridge, MA. Power analysis used PASS Sample Size Software NCSS.com.

Educational validity

The validity of a measurement tool is the degree to which observations match expectations

The Streiner and Norman (2003) categorization and definitions are:

- Content validity is a subjective assessment of the breadth and depth of the construct it intends to measure. Expert literature review is a typical example.
- Criterion related validity is the degree to which an objective assessment using a tool compares to the best measure of that construct. There are two types of criterion related validity.
  - *Concurrent validity:* Is when a newly developed tool is compared to another test, which is considered to be the "gold standard," to measure the construct in question.
  - *Predictive validity:* Refers to the degree to which a test can predict a behaviour that will occur in the future.
- Construct validity compares a tool to another test that measures a similar construct, but that is not a "gold standard".

2 PILOT STUDIES IN THE SOFT EMBLAMED THIEL CADAVER

2.1 Cadaver ultrasound imaging

The experimental model for my studies was the soft embalmed Thiel cadaver, introduced into the UK in 2009 by the Centre for Anatomy and Human Identification, University of Dundee. The tissue preservation process is named after Professor Walter Thiel, University of Graz, Austria. Cadavers are soaked in tanks for between 4 and 6 months in a water-based solution of 4-chloro-3-methylenphenol, salts for fixation, boric acid for disinfection, ethylene glycol for preservation of tissue, chlorocresol and ethanol, and a very small amount of formaldehyde. This combination has anti-infective properties and limits carcinogen exposure, unlike traditional formaldehyde preserved cadavers. Skin is well preserved and joints are flexible. Thereafter, cadavers are kept within sealed bags. This preservation is effective in the long term, with estimated viability of 36 months, which potentially allows multiple uses of the cadavers, increasing availability and reducing costs. The Centre for Anatomy and Human Identification is governed according to the Anatomy Act (Scotland 2006). An example of dissection of the posterior triangle of the neck is shown in Fig 11.

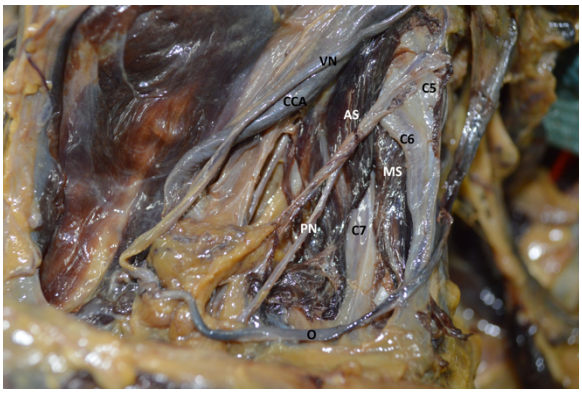

Fig 11. Dissected posterior triangle in soft embalmed Thiel cadaver. Note realistic shape and colour of tissues. Nomenclature: C5, C6 and C7 nerve roots; AS, anterior scalene muscle; MS, middle scalene nerve; PN, phrenic nerve; CCA, common carotid artery

2.1.1 Hypothesis and objectives

I hypothesised that the soft embalmed Theil cadavers can be used to visualise nerves, muscles and arteries on B-Mode ultrasound images at sites commonly used for UGRA. Evidence of good tissue visibility during and after embalming would allow me to

undertake a series of translational studies investigating the application of elastography to regional anaesthesia.

Therefore, the primary objective of this study was to assess the visibility of nerves, muscles and blood vessels in the interscalene groove, within the axilla, below the inguinal ligament and in the popliteal fossa over a 28 week period after death and embalming. My secondary objectives were to compare visibility between anatomical structures, between block sites and between raters.

2.1.2 Methods

I scanned the left interscalene, axillary, femoral and popliteal regions of a single soft embalmed Thiel cadaver 2, 3, 5, 8, 11, 14 and 28 weeks after death using a 5 to 10 MHz linear B-Mode ultrasound transducer (Zonare, Palo Alto, CA) or, in the case of the sciatic nerve, a 3 to 9 MHz curvilinear ultrasound transducer. The cadaver was soaked in Thiels embalming solution for 28 weeks, removed using a winch for our experiment then re-soaked after scanning.

Using ultrasound, I identified:

Nerves: C6 nerve root, axillary, radial, femoral and sciatic popliteal nerve.

Muscles: Anterior scalene, coracobrachialis, iliacus and biceps femoris muscles

Arteries: Carotid, axillary, femoral and popliteal arteries

Once the appropriate nerve, muscle and artery was identified on interscalene, axillary, femoral and popliteal scans, images were recorded and stored onto the hard drive of a Zonare Z-one ultrasound machine. Two independent raters using a seven point ordinal scale whereby 1 represented extremely poor visibility and 7 represented extremely good visibility assessed images. The geometric mean is useful for calculating central tendency for observations that show proportional growth. In this case the proportional change of visibility scores from the initial values. Also, since Likert's 7-point scale was used, I felt this would be more useful due to the ordinal nature of the values being analysed. The results being analysed were also relatively a small data set and it would not to ignore data extremes or outliers, which would happen with median.

Results will then be more usefully interpreted to see if that level of visibility score is acceptable to use it as an experimental model to carry out further studies

The geometric mean is useful for calculating central tendency for observations that show proportional growth. In this case the proportional change of visibility scores from the initial values. Also, since Likert's 7-point scale was used, I felt this would be more useful due to the ordinal nature of the values being analysed. The results being analysed were also relatively a small data set and it would not to ignore data extremes or outliers, which would happen with median.

Results will then be more usefully interpreted to see if that level of visibility score is acceptable to use Thiel cadaver as an experimental model to carry out further studies

2.1.3 Results

The cadaver remained soft and flexible throughout the 28 week study period and had full movement of limb joints and spine without impediment to use of ultrasound. Characteristic anatomical features were readily discernible. For example, the reduced echogenicity of interscalene nerve roots in patients secondary to the high ratio of fascicles to stromal tissue and the mixed echogenicity of the femoral and median nerves were similar in cadavers to that seen when imaging patients. Blood vessels were visible but not compressible.

Visibility data followed a normal distribution. A total of 168 measurements of visibility were made at 4 nerve sites (interscalene, axillary, femoral, sciatic) on 3 anatomical structures (nerve, artery, muscle) by 2 raters on 7 occasions (2, 3, 5, 8, 11, 14, 28 weeks) after embalming. Visibility of blood vessels, muscles and arteries differed, $p<0.001$ (Fig 14). However, visibility of anatomical structures did not differ over time, $p = 0.17$, nor between nerve site, $p= 0.57$ or between rater, $p = 0.09$. Geometric mean nerve visibility was 5.4 (95%CI: 4.3 - 6.9) at 2 weeks and 4.9 (95%CI: 3.8 - 6.2) at 28 weeks, geometric ratio 1.1 (95%CI: 0.8 - 1.7) P = 1.0. Geometric mean muscle visibility was 5.2 (95%CI: 4.2 - 6.5) at 2 weeks and 4.1 (95%CI: 3.3 - 5.0) at 28 weeks, geometric ratio 1.4 (95%CI: 0.9 - 1.9), P = 1.0. Geometric mean artery visibility was 4.6 (95%CI: 3.7 - 5.7) at 2 weeks and 4.8 (95%CI: 3.8 - 5.9) at 28 weeks, geometric ratio 1.0 (95%CI: 0.7 - 1.4), P = 1.0. Thus, nerve, artery and muscle visibility did not change between 2 weeks and 28 weeks after embalming.

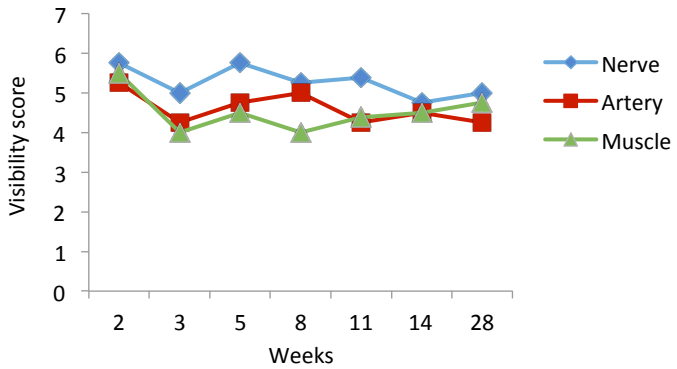

Fig 12. Mean nerve, artery and muscle visibility from 2 weeks to 28 weeks after embalming. Visibility measured on a 1 to 7 ordinal scale.

2.1.4 Conclusion

My exploratory ultrasound work showed good face and content validity of the soft embalmed Thiel cadaver as a tool for simulated ultrasound guided regional anaesthesia. The cadaver looked and felt like a human being. Peripheral nerves retained the anatomical integrity of epineurium and perineurium of peripheral nerves.

2.2 Needle visibility

I now wished to standardise the type of needle to be used during studies on the application of elastography to UGRA. As well as using the common in-plane approach, some anaesthetists insert needles using the out-of-plane approach, particularly for insertion of perineural catheters.

2.2.1 Hypothesis and objectives

I hypothesised that textured needles were more visible than smooth surfaced needles, that visibility was not dependant on needle gauge and was improved in-plane and out-of-plane to the ultrasound transducer at specific angles.

Therefore, the primary objective of this study was to compare the physical properties of a textured Tuohy needle, a textured single injection needle and a smooth-surfaced Tuohy needle when inserted at 30^{o}, 45^{o}, 60^{o} and 75^{o} angles, both in-plane and out-of-plane to the ultrasound beam, in the soft embalmed Thiel cadaver.

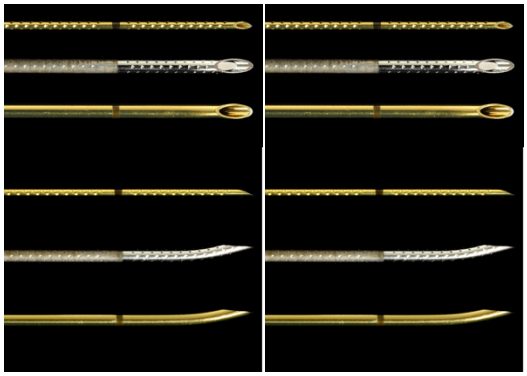

- **Figure 13.** Block needles: Top three needles, from above downwards: lateral views of single-shot textured needle, Tuohy textured needle and smooth Tuohy needle. Lower three needles: bevel views of same needles. All needles have a circumferential dark band that acts as a distance marker. In the textured needles, this lies in the centre of the non-reflective portion, between the two reflective regions.

2.2.2 Methods

Prior ethical approval for this randomised single-blind, controlled trial was obtained from the University of Dundee Thiel Advisory Group. A single soft embalmed Thiel human cadaver was selected by the Anatomy Scientific Officer (Centre for Anatomy and Human Identification at the University of Dundee). Block randomisation was

performed by random number generating computer software to 6 blocks, comprising a total of 24 combinations of angles (30^o, 45^o, 60^o, 75^o), needles (textured Tuohy, textured single injection and smooth-surfaced Tuohy), and ultrasound planes (in-plane and out-of-plane). Scanning of the left biceps and deltoid muscles used an L10-5 (5 to 10 MHz) linear ultrasound array (Zonare, Mountain View, CA) with integral video recorder. Needles (Pajunk, Newcastle, UK) were inserted 3cm over the biceps and deltoid muscles of a Thiel embalmed human cadaver on 3 occasions by an independent anaesthetist using a plastic guide, custom built in our university department of Medical Physics, with four surfaces angled at 30^o, 45^o, 60^o, 75^o incorporating smooth machined grooves for needle alignment (Guo et al 2012). All needle bevels directly faced the ultrasound beam and no fluid was injected at any time. All needles were 80mm in length.

A Bonferroni test is a type of multiple comparison test used in statistical analysis. The Bonferroni test is used to prevent data from incorrectly appearing to be statistically significant by lowering the alpha value. This multiple-comparison post-hoc correction is used when performing many independent or dependent statistical tests at the same time. The problem with running many simultaneous tests is that the probability of a significant result increases with each test run. Since I was making multiple comparision between different variables it was better to use this test to reduce the probability of significant results being calculated erroneously. This post-hoc test sets the significance cut off at α/n but it does suffer from a loss of power due to higher rate of Type 2 errors. I have increased the power of this study by a further 15% to compensate for this.

For the purposes of the study, 'in-plane' referred to needle insertion parallel to the transducer and ultrasound beam, whereas "out-of-plane" referred to needle insertion at right angles to (across) the transducer and ultrasound beam. Angle of needle trajectory was defined as the angle between the ultrasound beam and the surface of the needle. All procedures were performed and video recorded on a dedicated Zonare Z.one ultrasound machine used specifically for Thiel cadaver work. The research engineer collated and stored all images as DICOM files on a secure hard drive within the University. DICOM files were converted to TIFF format and uploaded to ImageJ (NLM, Washington DC) for analysis. Assessment of videos was performed by two independent raters using a 5-point Likert score for needle visibility (1 = very poor to 5 =

very good) and a binary outcome for needle tip visibility (0 = not visible, 1 = visible). The latter was used because clinical decisions about needle guidance in regional anesthesia are made on the presence or absence of the needle tip.

Based on a previous study investigating the visibility of regional block needles I assumed that the median visibility of the textured Tuohy, textured single shot and smooth Tuohy needles was 3, 3 and 2 respectively, and for angles 30^{o}, 45^{o}, 60^{o}, 75^{o}, median visibility was assumed to be 3, 3, 1.5 and 1.5 respectively. A randomized block ANOVA power analysis was performed using G*3 Power v3.1.3 (University of Kiel, Germany). The common effect size for needles and angles was assumed to be 0.5. Therefore, with $\alpha = 0.05$, $\beta = 0.8$, number of groups = 12 and df = 6, power analysis calculated that 62 injections were required for each ultrasound plane. Allowing an additional 15% injections to account for non-parametric data, I decided that 6 blocks of 12 combinations would be required, giving a total of 72 injections for each ultrasound plane and a total of Bonferroni corrections to p values and 95%CIs as appropriate for multiple comparisons. Results are presented as median (interquartiles [range]). Data were analysed using of 144 injections to account for in-plane and out-of-plane needle trajectories.

Randomized block design or RBD, splits up experimental units into groups or blocks of equal size, and then assigns a treatment to each group randomly. This makes sure that the data is not affected by outside situations

The Friedman test starts with ranking of observed values within blocks. The test statistic T suggested by Friedman is defined in terms of the sum of ranks for the ith comparison groups, R_i; the number of blocks, b; and the number of comparison groups, k, as follows:

$$T=12bk(k+1)\sum i=1kRi2-3b(k+1).$$

The Friedman test is often used for a randomized complete block design when the normality assumption is not satisfied or the data are ordinal. This method does not require the normality assumption, and can be used to analyze such designs. Friedman analysis of randomised blocks and Exact Hodges-Lehmann estimates of median (95%CI) was used for of visibility scores and proportions of needle tip visibilities differences between groups.

2.2.3 Results

Agreement between raters for visibility scores using weighted κ was good, 0.72 (95%CI: 0.61-0.83). The observed weighted proportional agreement was 0.92.

There were (*P*=0.015) differences in median (IQR [range]) needle shaft visibility for the textured Tuohy 4.04 (3.46 – 4.67 [3.00 – 4.92]), textured single shot 3.96 (3.75 – 4.46 [2.67 – 4.92]) and smooth Tuohy 3.00 (2.42 – 3.25 [2.25 – 3.50]) with the two textured Tuohy needles being more visible than the smooth in post-tests (Fig 14).

There were differences (*P*=0.0007) in the median (IQR [range]) proportion of visible needle tips for the textured Tuohy needle 0.83 (0.67 – 0.83 [0.50 – 1.00]), textured single shot needle 0.75 (0.67 – 0.83 [0.33 – 0.83]) and smooth surfaced Tuohy 0.33 (0.33 – 0.46 [0.00 – 0.50]) needles with the smooth surfaced Tuohy being significantly less visible than both in post-tests (Bonferroni *P*≤0.047 for both comparisons) compared to both textured needles (Fig 12).

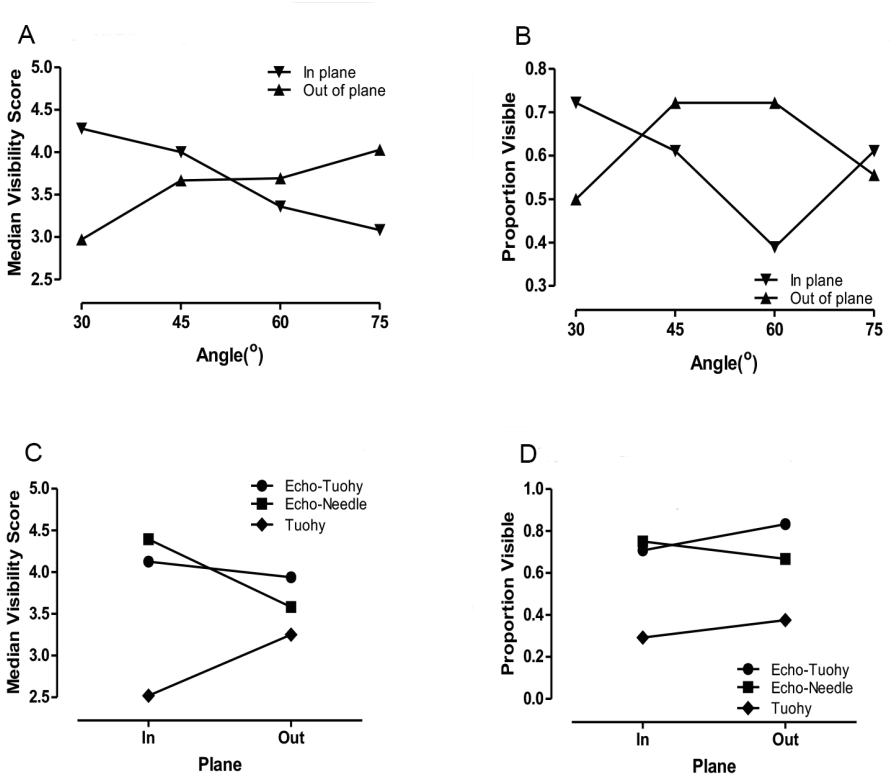

Fig 14. Needle shaft and tip visibility. Median visibility of needle shafts (A and C) and proportion of visible needle tips (B and D) presented according to angle and plane. Image A: Both textured needles are more visible than the smooth surfaced Tuohy needle when inserted in-plane and out-of-plane to the ultrasound transducer. Image B: Proportion of visible tips reduced at wider angles in-plane and more

shallow angles out-of-plane Image C: Shaft visibility reduced out-of-plane. Image D: Tip visibility poor for smooth needles both in-plane and out-of-plane

2.2.5 Conclusion

Textured Tuohy and textured single injection needles demonstrated better needle tip and shaft visibility in the soft embalmed human Thiel cadaver. Smaller, single injection textured needles were more visible than larger smooth surfaced Tuohy needles, and had similar visibility to larger textured Tuohy needles, suggesting that this new design has negated the relationship between needle gauge and visibility. However, the physical interaction between transducer orientation and angle of insertion, conventionally seen with smooth-surfaced needles, still existed. In both planes, one in four needle tips were not visible using textured needles, and out-of-plane needle visibility was no better than with the smooth-surfaced Tuohy needle.

Improved needle visibility can be explained by the design of textured needles (Fig 11). Multiple large, smooth reflectors positioned circumferentially reflect ultrasound beams back to the transducer, whereas smooth needles tend to scatter beams widely. An additional benefit is that the 10mm gap between reflector regions acts as a depth marker when visualised on ultrasound, preventing unintentional deep insertion.

Nevertheless, textured needles represent an advance, but still only a partial solution; even when using textured needles, tip visibility is not guaranteed because transducer and angle of insertion still interact. On the basis of my findings, I decided to use the single injection, textured needle for all my experiments on the soft embalmed cadaver.

3 STRAIN ELASTOGRAPHY

3.1 Initial observations

Having established that: (i) I was able to visualise nerves, muscles and blood vessels in the soft embalmed cadaver without any evidence of tissue deterioration over a 28 week period; and (ii) textured needles provided best needle shaft and tip visibility, I

wished to conduct regional anaesthesia on the soft embalmed cadaver using ultrasound and strain elastography.

3.1.1 Hypothesis and objectives

I hypothesised that elastography was able to capture tissue displacement in colour using 1ml volumes of injectate commonly used as test doses in patients. Therefore, the primary objective of this study was to interpret tissue changes in elastograms recorded alongside B-Mode ultrasound when used to conduct interscalene, axillary, femoral and popliteal nerve blocks.

3.1.2 Methods Regional blocks were performed as follows:

Interscalene block: The cadaver head was rotated laterally and a 5 to 10MHz linear transducer placed transversely at 90^{o} to the brachial plexus in an oblique plane. Scanning was performed from medial to lateral, identifying, in turn, the common carotid artery, internal jugular vein, scalenus anterior, the C5, C6 and C7 nerve roots and scalenus medius. A 50 mm B.Braun regional block needle was inserted out of plane and 1 ml of embalming fluid deposited between the C6 and C7 nerve roots.

Axillary block: The cadaver shoulder was abducted and externally rotated. A 5 to 10MHz linear transducer was placed transversely across the axillary plexus high in the axilla. In this position the musculocutaneous, median, radial and ulnar nerves were identified around the axillary artery together with triceps, biceps and coracobrachialis. Using a modified out of plane approach, a 50 mm B.Braun regional block needle was placed between the median nerve and axillary artery and 1 ml embalming fluid was injected at 10 o'clock to the radial nerve.

Femoral block: The cadaver was placed in the supine position with the groin exposed. A 5 to 10MHz linear transducer was placed transversely across the groin and structures were identified from medial to lateral as the femoral vein, femoral artery, femoral nerve, fascia lata and fascia iliaca. Using a 50mm B.Braun regional block needle, a 1 ml injection was placed approximately 1 cm lateral to the femoral artery below the fascia iliaca. The femoral artery was also used as a model for inadvertent intra-arterial injection by the purposeful injection of 1 ml embalming fluid into the femoral artery.

Sciatic block: The cadaver was placed on the right lateral side and a 3 to 8MHz linear transducer with wide array placed in the popliteal fossa. The tibial nerve, common

peroneal nerve, popliteal artery, long head of biceps and semitendinosus were identified, and the transducer moved proximally until the best view of the sciatic nerve was obtained. A 100 mm B.Braun regional block needle was inserted out-of-plane perpendicular to the skin. Two 1ml injections of embalming fluid were performed. The first was directed around the sciatic nerve; the second was placed within the substance of the sciatic nerve in order to mimic inadvertent intraneural block.

3.1.3 Results

Out-of-plane needle trajectory was identified by tissue distortion on B-Mode ultrasound and a linear, albeit indistinct strain pattern on the corresponding elastogram. Anatomy was not delineated well using elastography. Nerves were identified as a dark blue impression that was different in size to equivalent nerves on B-mode ultrasound. Fascial planes were seen as curvilinear dark blue lines.

Interscalene (Fig 15) and axillary injection were associated with circumferential neural spread, whereas femoral injection below the fascia iliaca revealed a sinusoidal pattern (Fig 16). Interscalene injection distended the space between the C6 and C7 nerve roots and a tissue strain pattern extending circumferentially around the C5, C6 and C7 nerve roots.

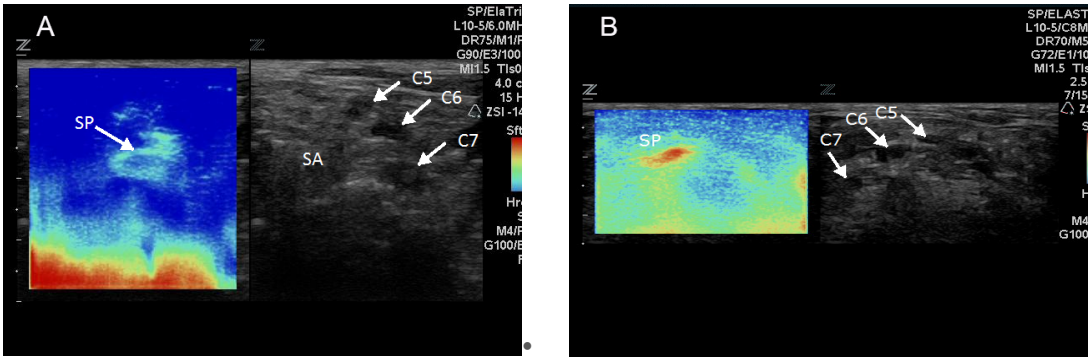

Fig 15. Strain elastography - Interscalene block. Nerve roots (C5, C6, C7) were apparent as hypoechoic structures lying between scalenus anterior (SA) and scalenus medius on the right side of the cadaver.

Injection between the median nerve and axillary artery unintentional spread inferiorly from the axillary artery, displacing the radial nerve medially (Fig 16B)

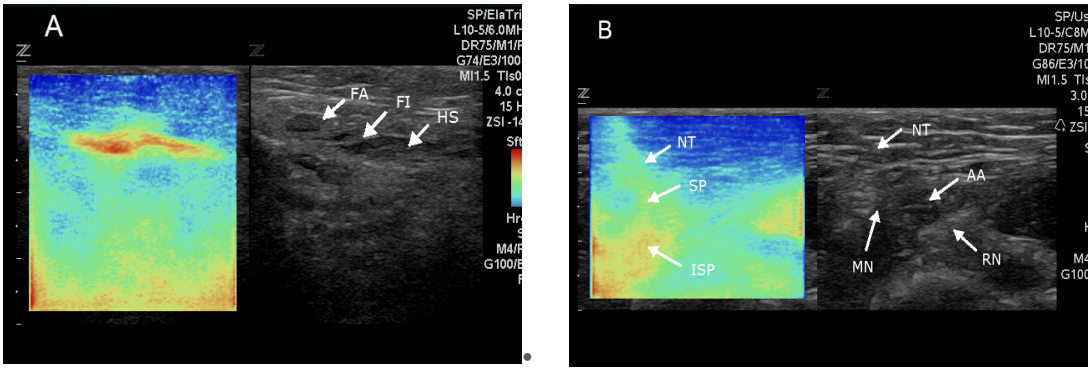

Fig 16. Strain elastography – femoral block. Femoral artery (FA), fascia iliaca (FI). Elastography (A) shows strain under the fascia iliaca as a coloured sinusoidal pattern. Aberrant spread (B). Elastography of axilla (B) shows needle trajectory (NT) and tissue strain infero-lateral to the median nerve (MN) and axillary artery (AA) with medial displacement of the radial nerve (RN).

Extraneural injection was seen as widespread circumferential coloured patterns, whereas intraneural injection was recognised by nerve swelling (Fig 17).

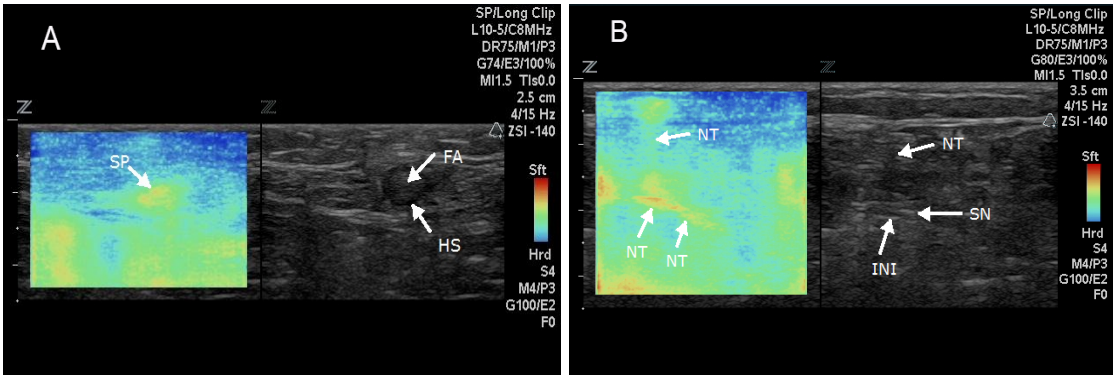

Fig 17. Strain elastography – [A] Intravascular injection into femoral artery (FA), SP-strain pattern. [B] Intraneural injection . Sciatic nerve (SN) visualised as round heterogenous structure . Intraneural injection visualised on B-Mode as a linear, horizontal spread and by a red linear and surrounding yellow tissue strain pattern with elastography. Further intraneural injection of 1ml resulted in disruption of the nerve membrane and extravasation of fluid inferolaterally.

3.1.4 Conclusion

This pilot work not only identified perineural spread of injectate but also readily identified tissue displacement that ordinarily is difficult to detect on B-Mode ultrasound such as distal spread and intraneural injection. A summary of the potential advantages and disadvantages of strain elastography is provided in Table 7.

Table 5. Potential strengths and weaknesses of elastography from pilot work

Parameter	Strengths	Weaknesses
Needle insertion	Enhanced visibility	Indistinct needle surface Noticeable only on movement
Perineural spread	Coloured Large, irregular pattern	Indicates strain on all tissue walls, Varies according to tissue elasticity. Nerve>muscle>fluid Does not equate with fluid spread
Inadvertent spread	Readily visible using small volumes. Potential for early detection of inadvertent spread	
Intraneural injection	Linear coloured streak within nerve Potential for early detection of intraneural injection	
Intravascular injection	Readily seen	
Overall	Supplements B-Mode ultrasound	Not possible to use alone

3.2 Tissue Displacement and Brightness

Having successfully identified tissue strain using 1ml injectate volumes, and identified the potential advantages and disadvantages of elastography, I now wished to: (i) evaluate the effect of a larger 5ml volume in order to replicate the effect of repeated injections given within a small time frame in clinical practice; and (ii) to gauge local fluid drainage in the soft embalmed cadaver.

3.2.1 Hypothesis and objectives

I hypothesised that coloured strain patterns were readily seen secondary to injection of 1ml and 5ml of embalming fluid during interscalene and femoral block and that fluid accumulation would not impair ultrasound visibility. My primary objective was to compare the displacement of 1ml and 5ml volumes. My secondary objectives were to compare the brightness of the elastogram image using 1ml and 5ml volumes, describe the dynamics of the strain pattern over time and evaluate any accumulation of perineural fluid after repeated nerve block. My primary end point was the time-weighted geometric mean area of the elastogram image. This was calculated by dividing the area under the curve of all geometric mean values and dividing by time (s). My secondary end point, the time-weighted geometric mean brightness elastogram image, was calculated in a similar way.

3.2.2 Methods

Therefore, in a second soft embalmed Thiel cadaver, I evaluated the mechanical and acoustic response to repeated injections of 1ml and 5ml volumes of injectate by measuring the area of displacement and brightness of tissues during interscalene and femoral nerve blocks. Block sites were chosen because patterns of spread secondary to local anaesthetic injection are distinct for each block. Injections were randomised to equal numbers of 1ml and 5ml volumes using a computer generated sequence of numbers. One ml volumes were injected on the first study day, and 5ml volumes injected on the following day in order to gauge any damage to the cadaver. I performed blocks using a 5 to 10 MHz linear B-Mode ultrasound transducer (Zonare, Palo Alto, CA). After identifying the nerve of interest, a 50mm bevelled regional block needle was inserted in-plane to the ultrasound transducer and Thiel embalming solution injected. Ultrasound images were recorded on a split display with the elastogram image on the left and the B-Mode image on the right of the screen. Blocks were repeated every 5 to 10 minutes. The operator was not blinded to the elastogram image, as it is not possible to guide needle tip position or identify nerve location using this colour modality. Videos were uploaded to Santesoft DICOM reader, converted to TIFF files and transferred to ImageJ (v1.47, NIH, Washington DC). In order to power the study using two blocks (interscalene, femoral) and two volumes (1ml and 5ml) and assuming $\alpha = 0.05$, $\beta = 0.80$, effect size = 0.6, and using ANOVA (G3Power, University of Dusseldorf) I calculated that 32 injections were needed to show a difference between blocks.

Change in area and brightness data used the geometric mean. Geometric mean is used to evaluate data covering several orders of magnitude and for evaluating ratios or percentage changes. The geometric mean "normalizes" the ranges being averaged, so that a given percentage change in any physical property has the same effect on the geometric mean. Difference between groups was expressed as geometric ratio. Mean Difference was calculated using Tukey-Kramer's All Pairs Simultaneous Confidence Intervals

3.2.3 Results

Mean (95%CI) Tissue displacement in cadavers (Table 6) was similar for femoral 2.39 (1.99 - 2.87) and interscalene blocks 2.34(1.96 - 2.79) (geometric mean ratio 1.02 (95%CI: 0.59 - 1.78), P=0.86) and for 1ml and 5ml injection volumes, 2.17 (1.80 - 2.62) vs 2.58 (2.17 - 3.07) (geometric mean ratio 0.84 (95%CI: 0.70 - 1.01), P=0.19. Displacement was similar between the first and eighth 1ml injection (geometric mean ratio 0.56 (95%CI: 0.30 - 1.43), P=0.67). Using 5ml volumes, displacement was greater with the first compared to the eighth injection (geometric mean ratio 1.50 (95%CI: 0.58 - 2.42), P<0.001).

Hydrolocation brightness in the cadaver was similar for femoral and interscalene blocks (geometric mean ratio 0.99(95%CI: 0.98 - 1.00), P=0.86) and 1ml and 5ml injection volumes (geometric mean ratio 0.84(95%CI: 0.83 - 0.85), P=0.19). Mean (95%CI:) brightness was similar between the first and eighth 1ml injection (geometric mean ratio 1.01(95%CI: 0.96 - 1.06), P=1.0). Using 5ml volumes, brightness was less with the first compared to the eighth injection (geometric mean ratio 0.94 (95%CI: 0.89 - 1.00), P<0.0010).

Table 6. Geometric mean B-Mode ultrasound displacement (cm^2) and brightness (0-255 scale) with regard to site, volume, injection sequence and the interaction of site: volume and sequence: volume. Mean (95%CI): displacement and brightness in cadavers was similar for femoral and interscalene blocks, 1ml and 5ml injection volumes. There was no sequential accumulation of fluid.

Fixed term	**Area (cm^2) mean (95%CI)**	**Brightness (0 – 255) mean (95%CI)**
Site		
Interscalene	2.34(1.96 - 2.79)	133.2 (132.0 - 133.2)
Femoral	2.39 (1.99 - 2.87)	132.1 (130.9 - 133.2)
Volume		
1ml	2.17 (1.80 - 2.62)	121.6 (120.5 - 122.7)
5ml	2.58 (2.17 - 3.07)	144.7 (143.4 - 145.9)
Injection sequence		
First	4.58 (3.34 – 6.29)	138.7 (136.6 - 140.9)
Second	1.70 (1.06 – 2.73)	124.2 (121.4 – 127.1)
Third	3.90 (2.62 – 5.81)	137.4 (134.7 - 140.1)

Fourth	2.63 (1.90 – 3.65)	133.2 (131.1 - 135.3)
Fifth	0.98 (0.67 – 1.44)	141.9 (139.4 - 144.4)
Sixth	2.89 (2.13 – 3.91)	120.1 (118.4 - 121.9)
Seventh	2.64 (1.93 – 3.61)	124.9 (123.0 - 126.8)
Eighth	1.63 (1.11 – 2.39)	142.5 (139.8 - 145.2)
Site*volume		
Interscalene: 1ml	2.03 (1.55 - 2.67)	127.3 (125.6 - 129.1)
Interscalene: 5ml	2.69 (2.16 - 3.36)	139.3 (137.8 - 140.8)
Femoral: 1ml	2.32 (1.79 - 3.01)	116.1 (114.6 - 117.5)
Femoral: 5ml	2.47 (1.88 - 3.24)	150.3 (148.3 - 152.3)
Sequence*volume		
1st injection: 1ml	3.97 (2.44 - 6.46)	128.4 (125.4 - 131.5)
8th injection: 1ml	2.26 (1.55 – 3.30)	127.5 (125.2 - 129.9)
1st injection: 5ml	5.28 (3.57 - 7.81)	149.8 (147.0 - 152.7)
8t injection: 5ml	1.17 (1.16 – 2.68)	159.2 (153.7 - 164.8)

The area and brightness of many colour elastogram patterns ebbed and flowed in a cyclical manner. Time to first and second peak was similar with femoral and interscalene block and using either 1ml or 5ml volumes (Table 7).

Table 7. Dynamics of elastography in the soft embalmed cadaver. Femoral and interscalene block.

	Femoral 1ml	**Femoral 5ml**	**Interscalene 1ml**	**Interscalene 5ml**
Duration (s)	12.5 [7.0 - 14.8]	18.0 [14.3 - 21.5]	12.0 [7.3 - 15.8]	12.5 [11.0 - 27.3]
Time to first maximal area (s)	5.0 [4.5 - 6.5]	5.5 [3.5 - 6.0]	5.0 [3.5 - 8.5]	7.0 [5 .0 - 8.8]
Time to second maximal area (s)	9.0 [9.0 - 12.0]	11.0 [9.8 - 13.3]	8.0 [7.0 - 10.5]	25.0 [18.0 - 28.0]
Second peak (n)	5	4	3	3
Time to max brightness (s(	7.0 [6.0 - 8.0]	10.0 [8.0 - 14.0]	7.5 [5.8 - 9.3]	8.5 [4.8 - 10.0]

3.2.4 Conclusion

Elastography provided a real-time image of strain and showed changes in the size, position, and shape of tissue specific to each block. Elastogram area did not change with sequential 1ml or 5ml injections, even when administered every 5 to 10 minutes. Elastogram area and brightness unexpectedly showed cyclical variation. This behaviour may reflect bulk movement of fluids within a confined space, displacement of soft tissue, and reflection of fluid from interfaces dependant on local tissue stiffness.

3.3 Translation of strain elastography to patients

Having successfully demonstrated intraneural and extraneural strain patterns while performing blocks on cadavers, I conducted interscalene and femoral blocks in two patients. I hypothesised that strain patterns in patients would be similar to those observed in soft embalmed cadavers.

3.3.1 Interscalene block

After obtaining written patient consent and Caldicott Guardian approval, an interscalene block was performed in a 59-year-old ASA 2, male patient scheduled for right shoulder rotator cuff repair. A 22g block needle was inserted under ultrasound-guidance (Zonare Ultra, Zonare, Mountain View, CA, USA) with B-Mode and strain elastography split imaging. The patient was monitored using ECG, SpO2 and non-invasive blood pressure to the patient, sedated with intravenous midazolam 2 mg and fentanyl 50 µg then placed supine with 30° head-up tilt and face turned towards the left side. Following aseptic preparation, a 5-10 MHz linear transducer was placed across the right interscalene grove and the C5 and C6 roots identified between the scalenus anterior and medius muscles. After subcutaneous infiltration of 1 ml of lidocaine 1%, a 5 cm short bevelled regional block needle (Stimuplex A, B.Braun, Sheffield, UK) was inserted in the plane of the ultrasound beam and passed it anteromedially through the scalenus medius muscle. With the needle tip placed within the fascial sheath and visualised underneath the C5 nerve root, a test dose of 1 ml of 0.375 % levobupivacaine was injected followed by a further three 5 ml increments. After confirming loss of sensation around the shoulder, general anaesthesia was administered.

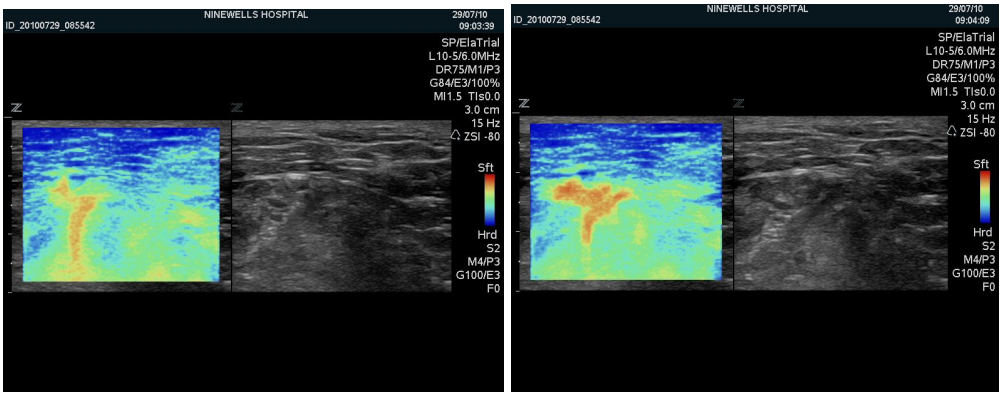

Fig 18. Clinical interscalene block. The left image shows the response to 1ml injection levobupivacaine 0.375% between the C5 and C6 nerve roots and the right image the response to subsequent 5ml injection. One ml injection passed between the C5 and C6 nerve roots but also passed distally down the interscalene groove. Five ml injection expanded the space between the nerve roots and passed distally. Tissue changes were difficult to follow on ultrasound images

3.3.2 Femoral block

A femoral block was performed in a 70-year-old ASA 2 patient scheduled for elective total knee replacement using ultrasound-guidance (Zonare Ultra, Zonare, Mountain View, CA), and before spinal anaesthesia. The patient was placed supine with slight hip abduction and the right groin cleaned with chlorhexidine and alcohol solution. I identified from medial to lateral, using a 5-10 MHz linear transducer, the femoral artery, femoral vein and femoral nerve, along with the fascia lata and fascia iliaca. A 50mm Tuohy-tipped block needle (Pajunk, Newcastle-upon-Tyne, UK) was inserted out-of-plane with respect to the transducer and advanced it under direct vision through both fascial layers to the medial aspect of the femoral nerve. A 19-g catheter was threaded proximally through the needle to lie 4cm alongside the femoral nerve. A test dose of 1 ml 0.024 % levobupivacaine was injected followed by four increments of 5 ml 0.024% levobupivacaine. When translated to patients, I visualised a dose dependent strain pattern using 1ml and 5 ml of local anaesthetic with high and low strain being shown as red and blue respectively.

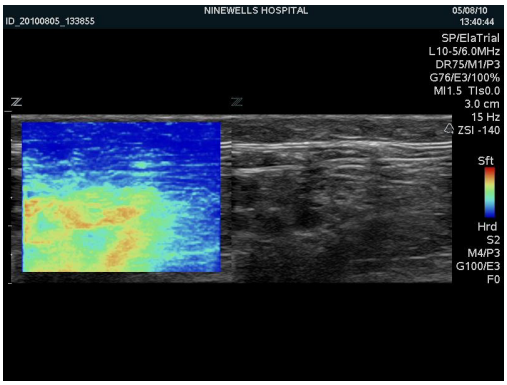

Fig 19. Clinical femoral block. The elastogram shows a characteristic sinusoidal strain pattern below the fascia iliaca and strain lateral to the femoral nerve

Perineural strain in patients (Table 7) exhibited similar characteristics to that seen in soft embalmed cadavers (Table 8). Elastograms showed peaks and troughs.

Table 8 Elastogram characteristics in patients receiving interscalene and femoral block

	Femoral 1ml	Femoral 5ml	Interscalene 1ml	Interscalene 5ml
Area (mm^2)	7.5	11.2	7.8	7.7
Brightness	187.4	181.3	201.7	195.7
Time to first peak (s)	1.6	1.0	1.0	2.0
No of peaks	2	2	1	1

3.2.3 Comparison of strain images in soft embalmed Thiel cadaver and patients

Fig 20 shows typical strain and brightness characteristics in soft embalmed Thiel cadaver and patients during interscalene and femoral nerve block. Fluid spread in both the soft embalmed cadaver and patients is smaller than the strain pattern. Strain shows displacement secondary to fluid and tissue compression. The degree of compression depends on the stiffness of different tissues and accounts for variability in the shape of the strain pattern.

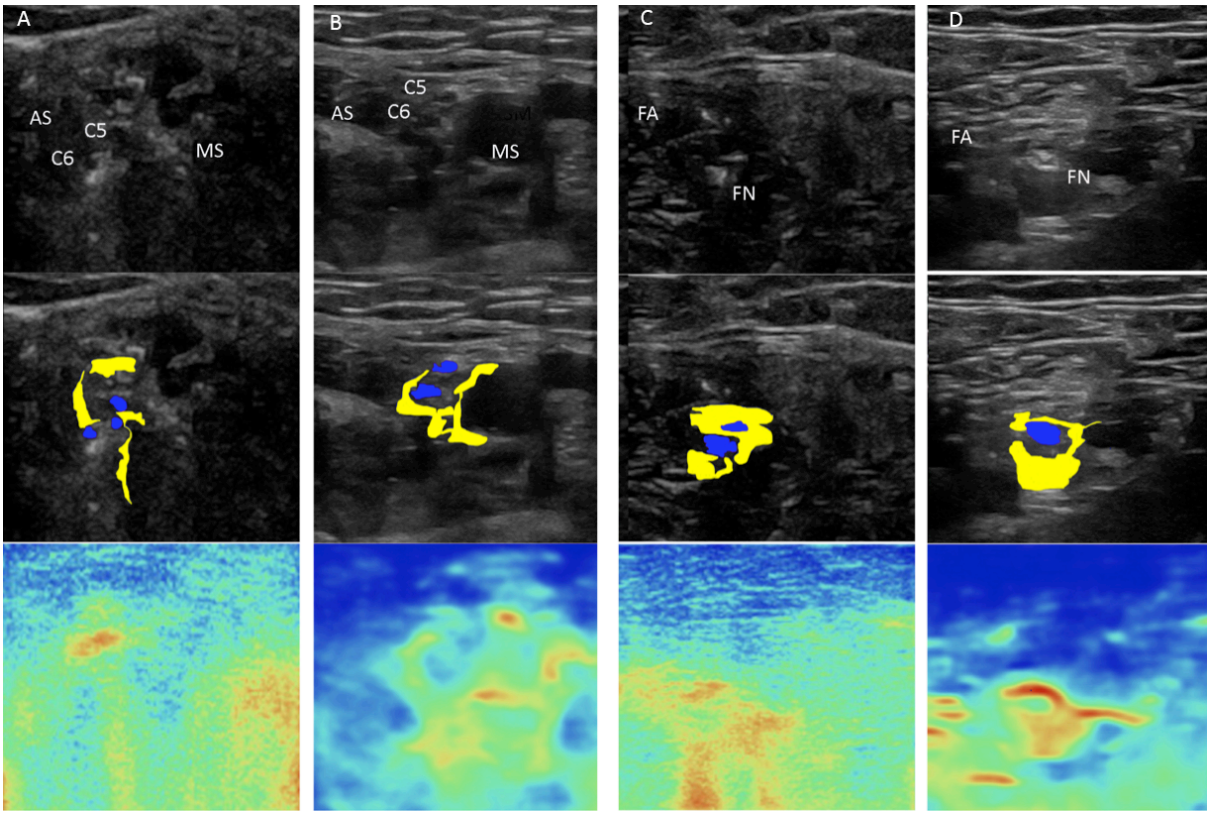

Fig 20. Strain and brightness characteristics in soft embalmed Thiel cadaver and patients during interscalene and femoral nerve block. Column A: interscalene block in the soft embalmed Thiel cadaver; column B: interscalene block in patient; column C: femoral block conducted in the soft embalmed Thiel cadaver; column D: femoral block conducted in patient. Upper images are the

standard B-Mode image with abbreviations: AS, anterior scalene; MS, middle scalene; FA, femoral artery; FN, femoral nerve. Middle images highlight the femoral nerve in blue and the spread of fluid in yellow. Lower coloured elastograms show tissue displacement associated with a 5ml bolus of injectate in both soft embalmed Thiel cadaver and patients. Fluid spread is smaller than strain.

4. SHEAR WAVE ELASTOGRAPHY

SWE is a quantitative, colour ultrasound mode used in Ninewells Hospital to diagnose breast and prostate cancer. Tissue elasticity (Young's modulus or *E*) is visualised as a colour map from blue to yellow to red whereby blue represents low tissue stiffness and red represents high tissue stiffness. The maximum value of Young's modulus used in the colour map varies between 28kPa to 180kPa and allows characterisation of different types of tumour and presentation according to stiffness.

4.1 Comparison of intraneural and extraneural Young's modulus using SWE

4.1.1 Hypothesis and objectives

I hypothesised that, because peripheral nerves during dissection felt stiffer than surrounding muscle, SWE had the potential to highlight peripheral nerves in colour and quantify the difference in stiffness between nerves and surrounding tissue.

Therefore, the primary objective of this study was to determine if SWE differentiated between nerve tissue and surrounding tissue tissue using visual colour maps and measures of Young's modulus in the soft embalmed cadaver.

4.1.2 Methods

The study was performed at three nerve locations – interscalene nerve root, median nerve and sciatic popliteal nerve. These nerves were chosen for the following reasons: (i) the interscalene nerve root has densely packed fascicles, less inter-fascicular stromal tissue and is associated with a greater incidence of nerve damage compared to the sciatic popliteal nerve; (ii) the median nerve at the mid-forearm shows the characteristic subepineural mixed echogenic pattern of fascicles and interstitial tissue; and (iii) the stiffness of upper limb muscles in flexion and extension has been recently defined (Eby et al 2015) using SWE in a large number of male and female volunteers, over a 70 year age span. Using computer generated

software, two anaesthetists scanned interscalene nerve roots, median and sciatic nerves of two soft embalmed Thiel cadavers after randomisation using the B-Mode facility of a 5 to 12MHz linear transducer and a 2 to 6MHz curvilinear transducer (Supersonic Imagine, Aix-en-Provence). The former transducer was used to image the interscalene nerve roots and median nerves, and the former to image the sciatic nerve roots. Block randomisation ensured equal allocation of anaesthetist to cadaver, location and operator. Anaesthetists were not blinded to location or block because a high level of knowledge and skill was required to perform the scan.

SWE superimposed a colour map of Young's elastic modulus onto an adjacent, identical B-Mode image, which was used for analysis. Each anaesthetist independently selected a circular region of interest (ROI) 3 mm in diameter corresponding to the centroid of each nerve or nerve root and to an area just outside but not touching the epineurium consisting of a mix of connective tissue and adjacent muscles. The extraneural placement of the ROI was standardised and overlapped either the anterior scalene, flexor digitorum superficialis or biceps femoris muscles outside the paraneural sheath of the sciatic nerve. Each intraneural and extraneural measurement was repeated 20 times.

The primary end point of the study was the geometric mean (95%CI:) Young's modulus (kPa) of paired intraneural and extraneural ROIs at interscalene, median and sciatic nerve sites. Secondary objectives were to determine the effect of neural pairs, cadaver, site, and anaesthetist on Young's modulus.

In order to power this study, I used measures of Young's modulus collected from a single soft embalmed Thiel cadaver. The geometric mean (95% CI:) intraneural Young's modulus was 44.2 kPa and extraneural Young's modulus 12.8 kPa. Powering the study at 90%, to find as significant at $P<0.05$ and doubling of log transformed elastic modulus, I required a minimum of N=17 paired measures per combination of anaesthetist and site. Therefore, a total of 240 images were taken (2 cadavers, 3 nerves, 2 anaesthetists and 20 repeated measures). Geometric mean was chosen to calculate central tendency, as elastic modulus was log transformed data.

4.1.3 Results

One cadaver was of a 35 years old and had been embalmed for 267 days; the other was of a 75 years old and had been embalmed for 141 days. Intraneural Young's modulus was greater than extraneural Young's modulus, geometric mean ratio 3.05(95%CI: 2.98 - 3.12), P < 0.001. Interscalene nerve root Young's modulus was less than the median nerve Young's modulus, geometric mean ratio 0.60(95%CI: 0.58-0.62), p < 0.001; and greater than sciatic nerve Young's modulus, geometric mean ratio 2.24(95%CI: 2.17- 2.31), P < 0.001. Median nerve Young's modulus was greater than sciatic nerve Young's modulus geometric mean ratio 3.71(95%CI: 3.59-3.84), P < 0.001.

Table 9. Geometric mean Young's modulus (kPa) in soft embalmed cadaver with regard to intraneural:extraneural pairs, anatomical p<0.001. The rank order (highest to lowest) of Young's modulus was median nerve > interscalene nerve root > sciatic nerve. Differences existed between all neural:site comparisons other than between median:extraneural and sciatic:intraneural combinations, P = 0.67.

Fixed term	**Estimated [adjusted] Mean (95%CI) shear wave speed (kPa)**	**Geometric mean ratio(95%CI) and p value**
Neural		
Extraneural	10.5 (6.5 - 17.0)	3.05(2.98 - 3.12), P < 0.001 (Extraneural vs Intraneural)
Intraneural	32.2 (20.0 - 52.1)	
Site		
Interscalene	18.5 (9.7 - 35.3)	0.60(0.58-0.62), p < 0.001 (Interscalene vs Median)
Median	31.9 (18.4 - 55.3)	2.24(2.17- 2.31), P < 0.001 (Interscalene vs Sciatic)
Sciatic	10.6 (5.6 - 20.1)	3.71(3.59-3.84), P < 0.001 (Median vs Sciatic)
Neural*Site		
Extraneural: Interscalene	12.7 (6.3 - 25.7)	

Extraneural: Median	18.8 (9.7 - 36.3)
Extraneural: Sciatic	4.8 (2.4 - 9.8)
Intraneural: Interscalene	26.9 (12.7 - 57.2)
Intraneural: Median	54.0 (27.7 - 105.3)
Intraneural: Sciatic	23.0 (10.9 - 48.9)

4.1.4 Conclusion

In the soft embalmed cadaver intraneural Young's modulus was three times greater than extraneural Young's modulus. There was a trend towards reduced nerve stiffness in the lower limbs.

4.2 Translation of shear wave elastography to volunteers

4.2.1 Hypothesis and objectives

Having demonstrated a 3-fold difference in tissue stiffness between intraneural and extraneural cadaver tissue, I hypothesised that a similar difference in Young's modulus occurred in humans.

4.2.2 Methods

Therefore, I scanned 11 healthy male and female volunteers in the Institute of Academic Anaesthesia using B-Mode ultrasound and SWE. A 5 to 10Mz ultrasound transducer was placed posterior to the sternocleidomastoid muscle over the interscalene groove. Once a good image of the C5 and C6 nerve roots was obtained, SWE was activated and a colour map generated.

A circular ROI was positioned over the C6 nerve root, adjacent to the C6 nerve root but not overlapping the interscalene sheath or paraneurium and over the anterior scalene muscle.

4.2.3 Results

Geometric mean (95%CI) Young's modulus was 22.8(18.8 - 26.8)kPa over the C6 nerve root; 7.0 (3.1 – 10.9)kPa over adjacent tissue.

4.2.4 Conclusion

Young's modulus over the C6 nerve root in humans was similar to that obtained in soft embalmed cadavers, and a difference in Young's modulus was present between neural and non-neural tissue. Although this volunteer study was small and failed to match for age and gender, the results confirmed my findings on the soft embalmed Thiel cadaver that, using SWE, it is possible to identify the C6 nerve root and differentiate between nerve and non-nerve tissue.

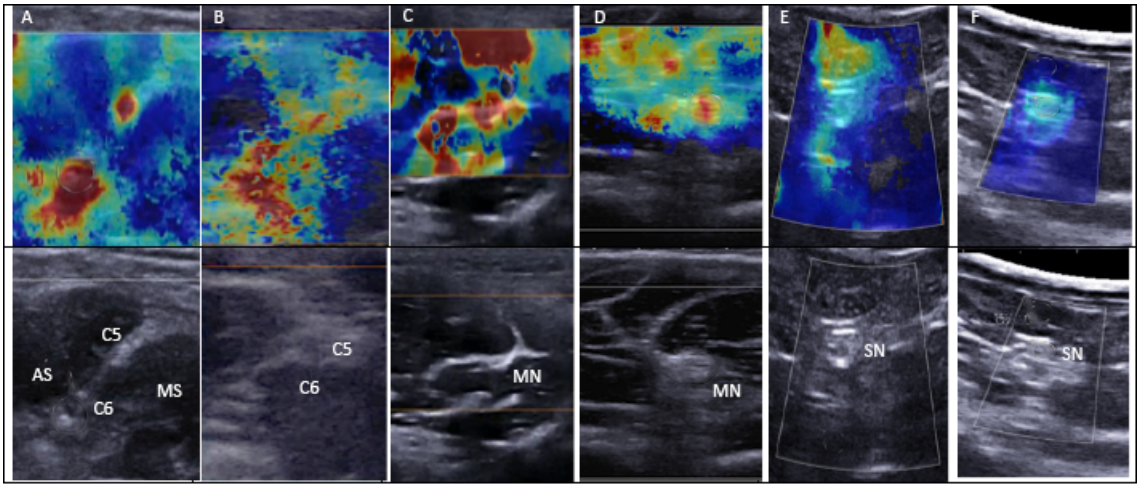

Fig. 21. B-Mode and SWE ultrasound images of interscalene nerve roots and median nerves in Thiel embalmed soft cadaver and humans. AS–anterior scalene muscle, MS–Medial scalene muscle, C5-cervical nerve root 5, C6–cervical nerve root 6, MN- Median nerve, SN- Sciatic nerve. Column A: interscalene nerve roots in the soft embalmed Thiel cadaver; column B: interscalene nerve roots in patient; column C: median nerve in the soft embalmed Thiel cadaver; column D: median nerve in volunteer; column E: sciatic nerve in the soft embalmed Thiel cadaver; column F: sciatic nerve in volunteer. Upper images are SWE and lower images are standard B-Mode ultrasound. Within the SWE images the coloured area gives a pictorial representation of Young's modulus. For both interscalene nerve roots and sciatic nerves Young's modulus gradient is represented by: dark blue, 0 - 7kPa; light blue, 7 - 14kPa; green, 14 -21kPa; yellow/orange 21 – 28kPa; red, 28 – 35kPa. For median nerve Young's modulus gradient is represented as: dark blue, 0 - 18kPa; light blue, 18 - 36kPa; green, 36 - 54kPa; yellow/orange 54 – 72kPa; red, 72 – 90kPa. Regions of interest (ROI) used to measure Young's modulus not shown. Coloured areas correspond to stiff interscalene nerve roots, median nerve, sciatic nerve and stiff connective tissue in both the soft embalmed Thiel cadaver and humans. Colour maps indicate stiffness of tissues within similar ranges in Thiel cadaver and humans. Note that order of stiffness in Thiel cadaver is the same as in human: median > interscalene > sciatic

4.3 Translation of shear wave elastography to patients

4.3.1 Hypothesis and objectives

I now wanted to further investigate the accuracy and reliability of SWE in a cohort of patients and hypothesised that the coloured ROI mapped by SWE was similar in size to the cross-sectional area of the underlying nerve.

My primary objective was to measure the accuracy of SWE in delineating peripheral nerve area by demonstrating agreement of cross sectional nerve area between B-Mode and SWE. My secondary objectives were to compare 2D local anaesthetic spread during local anaesthetic injection on B-Mode and SWE images, delineate the epineural border, assess the reliability of rater measurements and visualise neural anatomy in greater detail using a 3D surface array of shear wave speed.

4.3.2 Methods

B-Mode and shear wave videos were recorded simultaneously from 11 patients undergoing UGRA nerve blocks for elective orthopaedic limb surgery at Ninewells Hospital. The East of Scotland Medical Ethics committee stated in writing that no formal ethical approval process needed to be undertaken because data was being collected as part of normal practice and did not interfere with routine clinical care. Caldicott Guardian was obtained for elastography images, Data Protection Reg No Z8537226. In the UK, Caldicott Guardians are appointed to take responsibility for data governance and ensure patient confidentiality for all forms of data collection, particularly for studies not requiring full ethical approval but intending to be published. Study registration was not sought because we did not randomize to different groups and practice was unaltered.

UGRA was performed by the routine anaesthetist for the operating list using a linear SWE 5MHz to 12MHz ultrasound transducer and Aixplorer ultrasound machine (Supersonic Imagine, Aix-en-Provence, France). Anaesthetists used the B-Mode image alone for nerve recognition and needle alignment, and local anaesthetic concentration

and injection technique were completely at their discretion. No adjuvants were given. Routine medication such as analgesics, anti-emetics and anti-hyperalgesics were administered according to local guidelines on a pre-prescribed drug kardex. Each anaesthetist had no prior knowledge or training in SWE and was ignorant of image interpretation. Nerve blocks included: axillary radial (n =3); femoral (n=3); infraclavicular (n=2); interscalene (n=1); sciatic (n=1); and supraclavicular (n=1). Local anaesthetic was injected in 5ml aliquots up to a maximum of 20ml volumes at a rate of approximately 1ml. s^{-1}. During each block, two adjacent images were generated by the ultrasound machine; the first was a B-Mode image and the second the same B-Mode image with superimposed colour SWE. Video footage ran at a frame rate of 8 frames.s^{-1}. No additional information was available to each anaesthetist to guide practice.

DICOM videos were converted to individual Tagged Image File Format (TIFF) frames using Adobe Premier Pro video editing software (Adobe, CA). Each image was standardised for depth at 8.4 pixels cm^{-1}. Using the freehand drawing tool of ImageJ (v1.47, NLM, Washington), the cross sectional nerve area of the radial nerve (n =3); femoral nerve (n=3); infraclavicular posterior cord (n=2); interscalene C6 nerve root (n=1); and supraclavicular trunks (n=1) was measured on every 4^{th} frame (0.5 seconds) of B-mode and SWE videos by a single investigator. Local anaesthetic spread was also measured at these sites. For the purposes of measurement, the video frame immediately before local anaesthetic injection was designated time “0”.

The **Bland-Altman plot** is a graphical method to compare two measurement techniques. In this graphical method the differences (or alternatively the ratios) between the two techniques are plotted against the averages of the two techniques.

Horizontal lines are drawn at the mean difference, and at the limits of agreement, which are defined as the mean difference plus and minus 1.96 times the standard deviation of the differences.

The differences can be plotted against

- one of the two methods, if this is a reference or "gold standard" method
- against the geometric mean of both methods

- against the sample rank (where the samples are ranked by the average of the two methods) of the first or second method

I have chosen to plot the differences against the geometric means as this was more appropriate average for the measurements being analysed.

4.3.4 Results

In total 880 measurements of cross sectional nerve area and local anaesthetic spread were made divided equally between B-Mode and SWE. Distinct coloured ROIs were observed on the elastogram overlying peripheral nerves on the B-Mode image. Examples of paired SWE and B-Mode images during supraclavicular, interscalene and femoral block are demonstrated in Figs 31, 32 and 33.

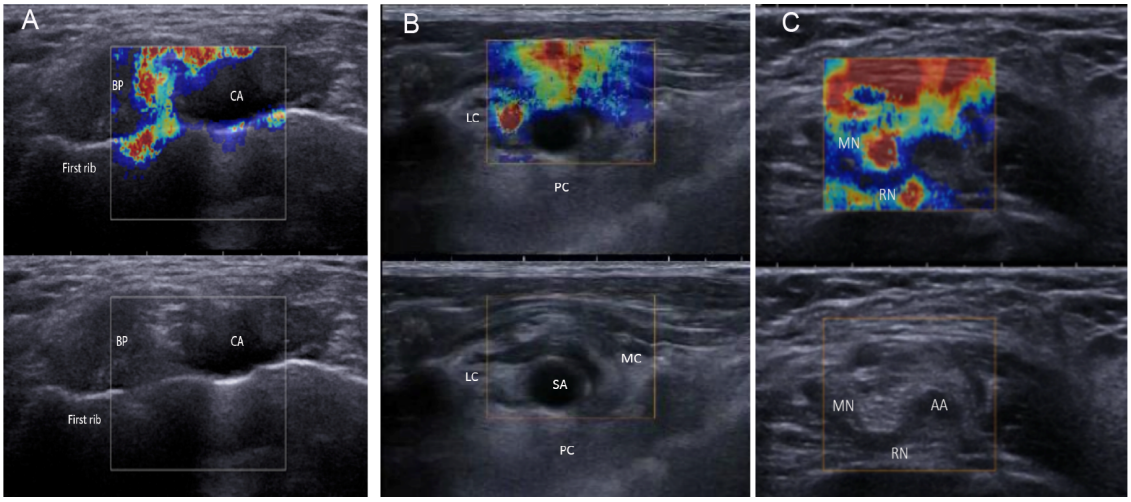

Fig 22. Supraclavicular SWE (above) and B-Mode (below) images. B-Mode image shows the characteristic "bunch of grapes" appearance of the trunks of the brachial plexus (BP), overlayed in the SWE image by a distinctive colour pattern. The surface of the first rib is highlighted in colour (upper image) and as a bright echogenic line in the lower image. The carotid artery (CA) is viewed as a black anechoic area in both images. Infraclavicular SWE (above) and B-Mode (below) images. A red, circular object is seen at 9 o'clock to the subclavian artery closely overlying the lateral cord (LC) of the brachial plexus (B-Mode image). The posterior cord (PC) and the medial cord (MC) are visualised on the B-Mode image. Axillary SWE (above) and B-Mode (below) images. The SWE image illustrates two red, circular areas at 9 o'clock and at 7 o'clock to the axillary artery (AA), consistent with the positions of the median nerve (MN) and radial nerves (RN) respectively in the B-Mode image below. Some superficial patterns were generated secondary to tissue strain.

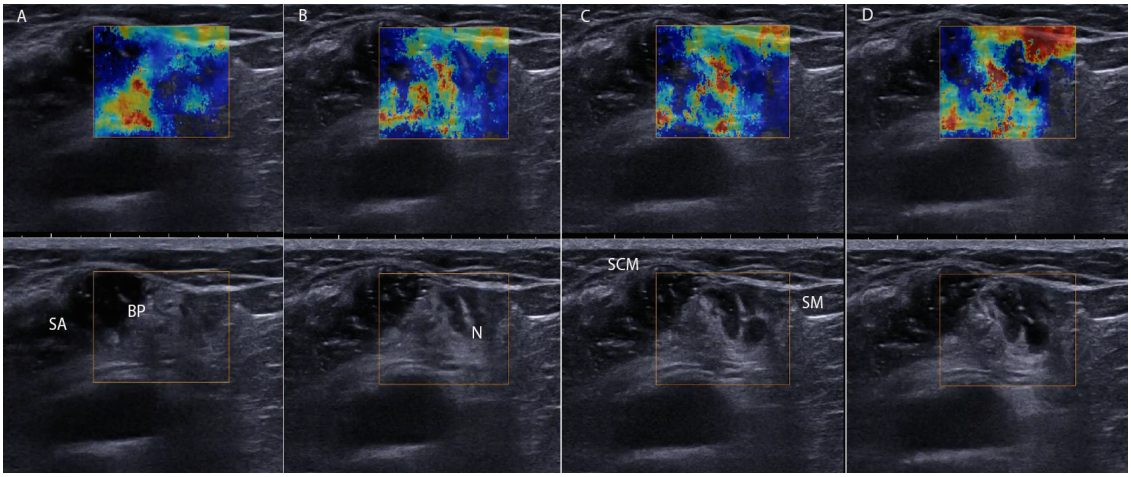

Fig 23. Interscalene SWE (above) and B-Mode (below) images. SA – subclavian artery, Brachial plexus, N-Needle SCM – Sternocliedomastoid muscle, SM- Scalenus medius muscle. On the B-Mode image the interscalene groove contains a mix of round, anechogenic nerve roots surrounded by echogenic connective tissue, whereas on SWE is seen as linear pattern of yellow/red colours on SWE. The block needle is seen posterior to the nerve roots in image B and image C. With increased injection of local anaesthetic, the interscalene groove on SWE becomes more intensely red and the hydrospace becomes better defined.

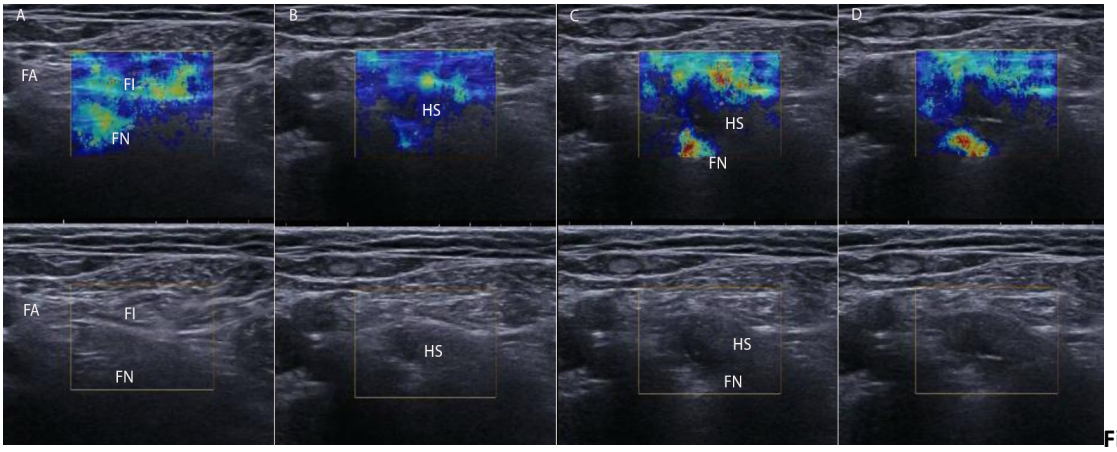

Fig

Fig 24. Femoral SWE (above) and B-Mode (below) images. On the B-Mode image (A), the femoral nerve is difficult to identify because the acoustic impedance of adjacent tissues is similar. The SWE image (A) identifies the femoral artery (FA), the sweep of the fascia iliaca (FI), and the femoral nerve (FN) as a separate coloured mass lateral to the femoral artery. Initial test dose injection of 1ml Hydrospace (HS) was associated with separation of the femoral nerve and fascia iliaca and reduction in colour intensity over the fascia iliaca and femoral nerve (B), albeit the epineurium remained discernible as a light blue colour with increased intensity inferiorly. With subsequent 5ml aliquots, nerve brightness intensified (C and D). On respective B-Mode images, the femoral nerve remained similar in appearance.

There was no difference between mean (95%CI) cross sectional nerve area on B-Mode

images 0.34 (95%CI: 0.20 - 0.60) cm^2 and mean (95%CI) cross sectional area on SWE images, versus 0.31 (95%CI: 0.18 - 0.55) cm^2, geometric mean ratio 0.09 (95%CI: 0.02 - 0.16) cm^2, P = 0.77 (Table 1). B-Mode local anaesthetic spread was similar to SWE local anaesthetic spread, 0.74 (95%CI: 0.42 - 1.31) cm^2 versus 0.80 (95%CI: 0.45 - 1.40) cm^2 respectively, geometric mean ratio 0.07 (95%CI: 0.00 - 0.14)cm^2, P = 0.82.

Table 10. Cross sectional nerve area and local anaesthetic spread using B-Mode ultrasound and shear wave elastography. There was no difference between mean (95%CI) cross sectional nerve area on B-Mode images and mean (95%CI) cross sectional area on SWE images, geometric mean ratio 0.09 (95%CI: 0.02 - 0.16) cm^2, P = 0.77. For cross-sectional area, there was no difference between blocks (P=0.51), or repeat data (P=0.42). Similarly, for fluid spread there was no difference between blocks (P=0.11) or repeat data (P=0.99).

	Mean (95%CI) cross-sectional nerve area (cm^2)	**Mean (95%CI) local anaesthetic spread (cm^2)**
Mode		
B-Mode	0.34 (95%CI:0.20 - 0.60)	0.74 (95%CI:0.42 - 1.31)
SWE	0.31 (95%CI:0.18 - 0.55)	0.80 (95%CI:0.45 - 1.40)
Nerve		
Femoral	0.33 (95%CI:0.17 - 0.66)	0.90 (95%CI:0.46 - 1.78)
Infraclavicular	0.19 (95%CI:0.08 - 0.45)	0.71 (95%CI:0.36 - 1.39)
Interscalene	0.24 (95%CI:0.07 - 0.78)	0.42 (95%CI:0.18 - 0.98)
Radial	0.32 (95%CI:0.16 - 0.51)	1.02 (95%CI:0.31 - 3.29)
Sciatic	0.33 (95%CI:0.21 - 0.53)	1.35 (95%CI:0.42 - 4.36)
Supraclavicular	0.45 (95%CI:0.14 - 1.46)	0.56 (95%CI:0.17 - 1.81)
Sequence		
1	0.27 (95%CI:0.17 - 0.43)	0.55 (95%CI:0.35 - 0.87)
5	0.33 (95%CI:0.21 - 0.53)	0.64 (95%CI:0.41 - 1.02)
10	0.36 (95%CI:0.23 - 0.56)	0.90 (95%CI:0.57 - 1.42)
15	0.31 (95%CI:0.19 - 0.48)	0.80 (95%CI:0.50 - 1.26)
20	0.28 (95%CI:0.18 - 0.44)	1.02 (95%CI:0.63 - 1.63)
Mode*Nerve		
B-Mode, Femoral	0.35 (95%CI:0.14 - 0.92)	0.75 (95%CI:0.29 - 1.75)
B-Mode, Infraclavicular	0.21 (95%CI:0.06 - 0.67)	0.39 (95%CI:0.12 - 1.27)
B-Mode, Interscalene	0.25 (95%CI:0.05 - 1.31)	1.03 (95%CI:0.20 - 5.43)
B-Mode, Radial	0.35 (95%CI:0.13 - 0.91)	0.83 (95%CI:0.32 - 2.17)
B-Mode, Sciatic	0.57 (95%CI:0.11 - 3.02)	1.25 (95%CI:0.24 - 6.55)
B-Mode, Supraclavicular	0.45 (95%CI:0.09 - 2.36)	0.54 (95%CI:0.10 - 2.84)
SWE, Femoral	0.31 (95%CI:0.12 - 0.82)	0.67 (95%CI:0.26 - 1.74)
SWE, Infraclavicular	0.18 (95%CI:0.06 - 0.59)	0.46 (95%CI:0.14 - 1.49)
SWE, Interscalene	0.23 (95%CI:0.04 - 1.22)	1.00 (95%CI:0.19 - 5.27)

SWE, Radial	0.30 (95%CI:0.12 - 0.79)	0.98 (95%CI:0.37 - 2.55)

4.3.4.1 Agreement between methods

A Bland-Altman plot demonstrated that measures of cross-sectional nerve area and local anaesthetic (injectate spread) lay within 95%CI limits of agreement (Fig 25).

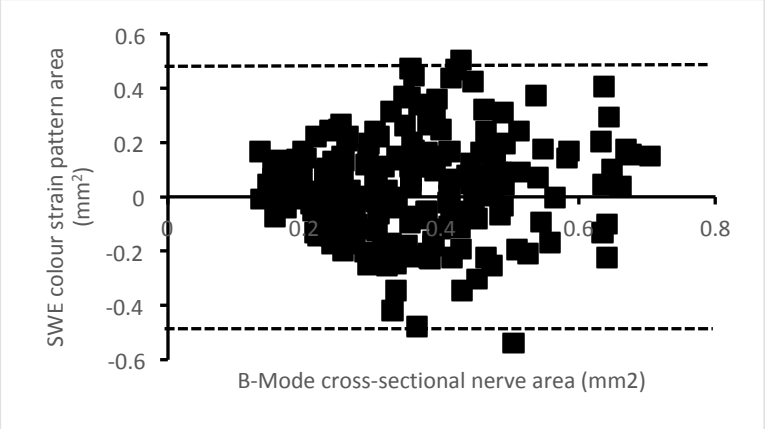

Fig 25. Bland-Altman plot showing agreement between measurement of nerve cross sectional area (A) and local anaesthetic spread (B) using SWE and B-Mode ultrasound.

For cross-sectional area, there was no difference between blocks (P=0.51), or repeat data (P=0.42). Similarly, for fluid spread there was no difference between blocks (P=0.11), or repeat data (P=0.99).

4.3.4.2 Resolution of epineurium

Using SWE, the shape and outline of the infraclavicular, axillary radial and femoral nerves were replicated. Nerves were characterized by a red colour surrounded by a thin yellow/green halo (Fig 25). Close inspection of the nerve surface area shows small lighter intraneural areas corresponding to nerve fascicles on the B-Mode image. However, not all fascicles were identifiable using SWE. In contrast, SWE identified intraneural stroma and the colour outline of interscalene nerve roots and supraclavicular trunks.

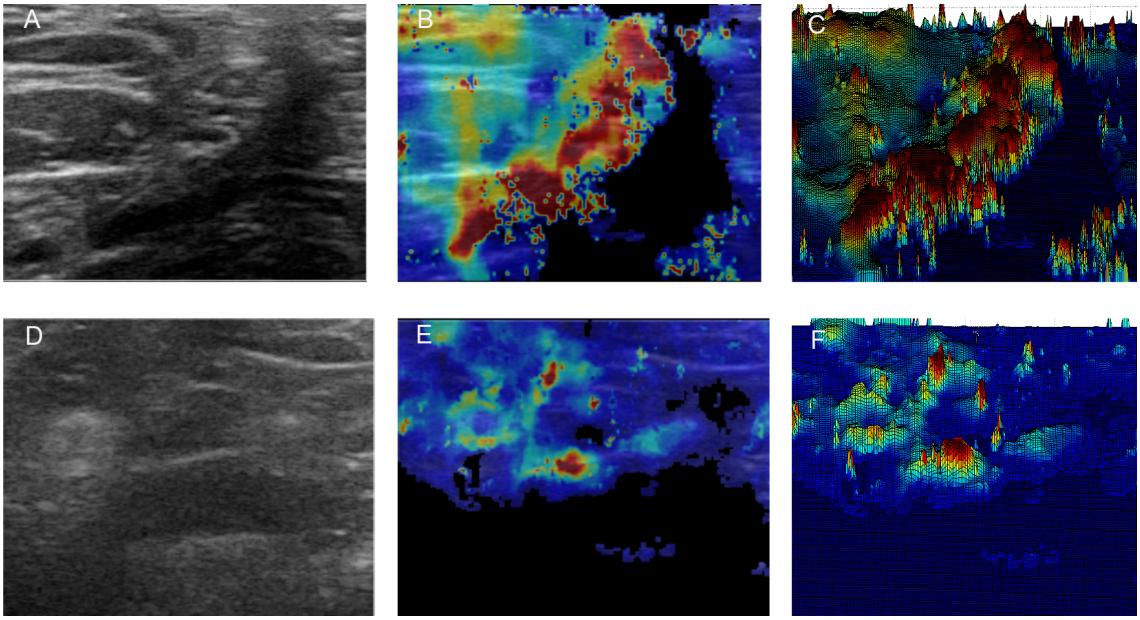

Fig 26. B-Mode, SWE and 3-D SWE map of interscalene block (A, B, C) and infraclavicular block (D, E, F). C5 and C6 nerve roots seen in image A with local anaesthetic spread over posterior border of nerve roots. Image B shows SWE colour map with areas of increased stiffness but poor correlation with anatomy on B-Mode ultrasound. Black area of hydrolocation provides distinct contrast and delineates posterior border of nerve roots. Interpretation of anatomy easier using 3D mapping of SWE. Highlights stiff epineurium and connective tissue between nerve roots.

4.3.5 Conclusion

The strengths of my SWE studies were that I was able to : (i) image cadaver with SWE and human nerves in a colour map which was coded for tissue shear modulus for the first time; (ii)demonstrate a 2 to 3-fold difference between intraneural and extraneural stiffness; and (iii) demonstrate a similar cross-sectional area of nerves and colour map overlay.

SWE readily identified stiff connective tissue planes and peripheral nerves. The femoral nerve is particularly difficult to see in practice and is often more lateral (2 to 3cm) to the femoral artery than novices anticipate. SWE highlighted the fascia iliac as a thin curvilinear edge and the femoral nerve lying on the iliopsoas muscle.

SWE kept track of peripheral nerves during local anaesthetic injection. This is important because the target nerve must be kept constantly in view in relation to the needle tip in order to avoid nerve puncture.

During block performance I made some interesting observations. First, with increasing local anaesthetic volume, the colour of the SWE map increased in intensity, indicating

an increase in nerve stiffness as local anaesthetic filled the sub fascial iliac tissue space. Second, with fluid expansion the anechoic perineural space closely mapped the border between tissue and local anaesthetic. This phenomenon occurred for all nerves. Third, despite injection of local anaesthetic I was counter-intuitively able to recognise nerves such as the radial nerve and posterior cord deep to fluid expansion. SWE waves are not generated within fluid and account for anechoic local anaesthetic spread. A possible explanation for this unexpected observation is that shear waves either passed straight through fluid and generated shear waves distally within the nerve, or passed from peripherally generated waves at an angle to tissue.

Maps of Young's modulus revealed marked differences in tissue stiffness at the nerve border, more so distally at the infraclavicular posterior cord, axillary radial and femoral nerves. Proximally in the brachial plexus the opposite was seen; stiffer connective tissue was identified circumferentially around the nerve roots and trunks but with limited colour identification within these structures.

Application of shear wave elastography to UGRA had some practical imitations. The transducer is bulkier than standard B-Mode ultrasound transducer and requires a very light touch in order to minimise artefact. Superficial colour changes are probably indicative of external compression but unsurprising given the complete lack of experience of operators using this mode of ultrasound. Although Young's Elastic Modulus is defined mathematically as stress (force applied over an area) divided by strain (relative displacement of tissue), I think it unlikely that superficial, longitudinal strain contributed to any error in measurement at nerve locations as Young's Elastic Modulus is derived from a 3-fold multiplication of transverse Shear Modulus, the product of tissue density and the square of transverse wave velocity.
Colour maps had sufficient resolution to identify epineurium but not intraneural structures and thus limits the application of this technology to UGRA.

However, the principal weaknesses that I perceived were a slight time delay in generation of colour SWE images. As such, the border of the SWE colour map did not lie exactly over the nerve. Close examination of images shows that the epineurium/connective tissue border was not exactly replicated. My results suggested

that that SWE technology was not accurate enough for dynamic needle intervention during regional anaesthesia and I decided not to pursue any further UGRA patient studies using SWE.

5. FUSION ELASTOGRAPHY

5.1 Development of fusion elastography

In light of the potential benefits of strain elastography, I hypothesised that it would be better to enhance strain elastography rather than shear wave elastography for clinical application. However, this would only be possible using an accurate measurement of change in strain area over time. In order to achieve this, I further hypothesised that software conversion of the elastography image had the potential to provide an objective measure of hydrolocation within each video frame.

Our engineer, Andreas Schwab wrote software using MATLAB 7.9 software (Mathworks, Natick, MA) with Image Acquisition and Image Processing Toolboxes in order to combine the B-Mode and elastography images. Colour elastogram videos were converted to 8-bit grayscale videos (Fig 27). Brightness thresholds between 0 and 255 on an 8-bit grayscale map were iteratively selected for each block in order to create a white image replicating the shape of the elastogram strain pattern onto a black background. The resultant pattern, visualised as a white, ebbing and flowing area, was termed enhanced elastography. The enhanced elastography image was then superimposed onto the B-Mode image as a translucent white “ghost” like shadow in order that the underlying nerve could be visualised. This image was termed fusion elastography (Fig 27). B Mode, elastography, enhanced elastography and fusion videos

were converted to constituent TIFF files and analysed using ImageJ*, (*NLM, Washington DC, Institutes of Health, Washington DC, http://rsb.info.nih.gov/ij/) and MATLAB, Mathworks, Cambridge, UK.

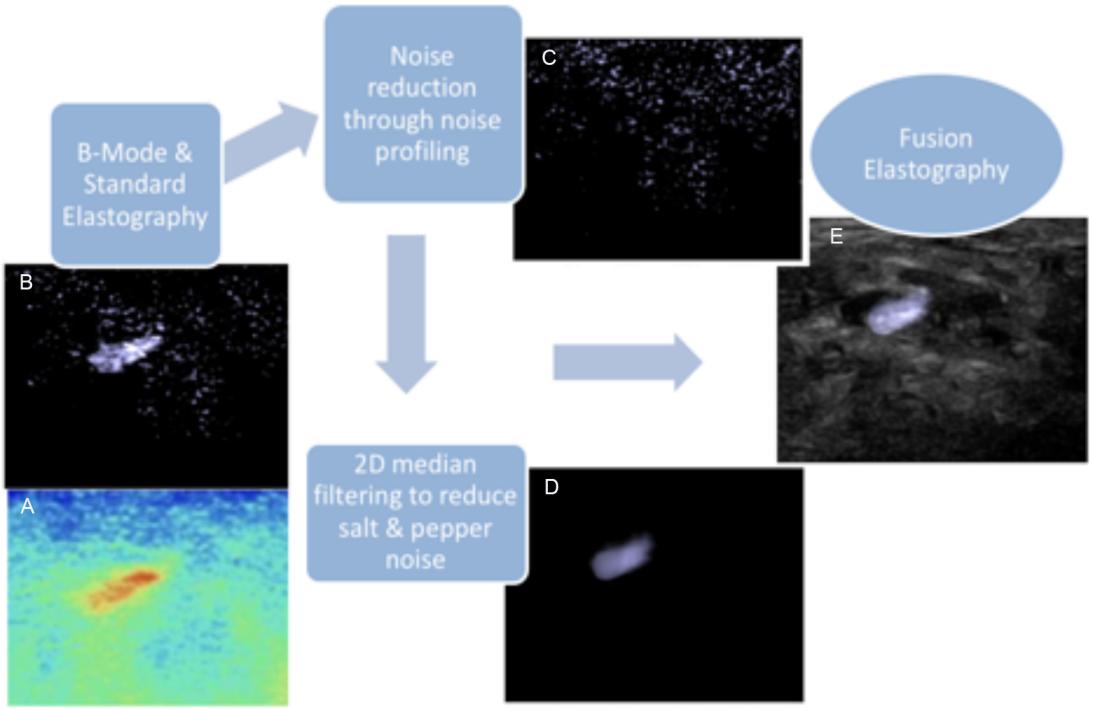

Fig 27. Software engineering of ultrasound guided regional anaesthesia videos. Image shows typical B-Mode image (A) and colour elastogram (B) on left. Images converted to 8-bit grayscale and ultrasound background "noise" reduced using noise profiling procedures (C) and 2D median filter. Brightness thresholds chosen between 0 and 255 on an 8-bit grayscale map for each block in order to create a white image replicating the shape of the elastogram strain pattern on a black background. White, ebbing and flowing area termed enhanced elastography (D). Superimposed onto B-Mode image (E). Visualised as a translucent white "ghost" like shadow in order that the underlying nerve could be visualised underneath. This image (E) was termed fusion elastography

Within each fusion frame a standardised square region of interest (ROI) of 25 by 25 pixels square (625). The number of pixels, up to a maximum of 625, representing tissue displacement, was multiplied by the mean grayscale brightness ($\mathbf{Ie}$) of the ROI where 0 = black and 255 = white. The hydrolocalisation index (*H*) can be regarded as measure of relative brightness of the ROI for each video frame. In order to account for change in

area and brightness over time I calculated the log area under the curve (log AUC) of *H* units weighted for time as the primary end-point (Fig 28).

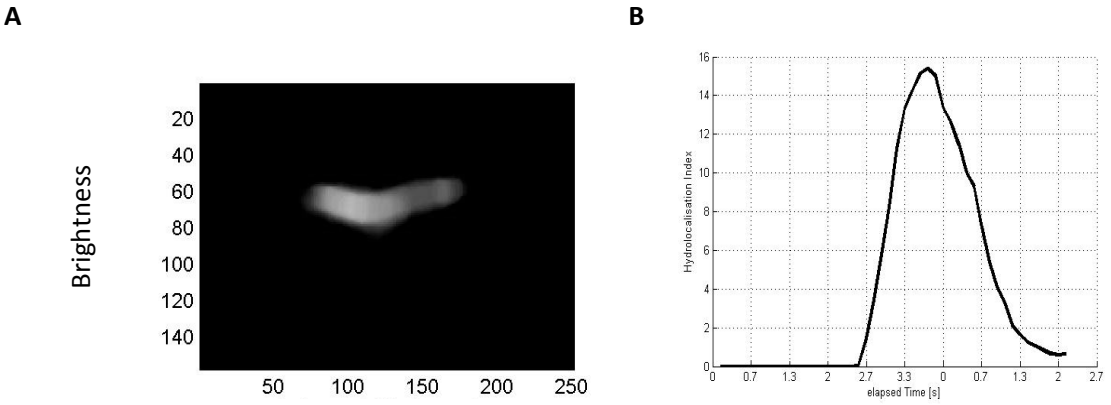

$$H = \frac{\sum_{n=1}^{nmax} \cdot \sum_{m=1}^{mmax} \mathbf{Ie}\,(n,m)}{nmax, mmax}$$

$$AUC = \int_{to}^{t0+t} H(t)dt$$

Fig 28. Enhanced elastography image. Colour elastogram converted to white shape on each video frame with black background (A). Graph (B) shows typical change in *H* with time. The area under the curve (AUC) is the integral of H over time.

5.2 Elastography dose response

Quantification of the strain image enabled me to investigate the strain dose response to perineural injection.

5.2.1 Hypothesis and objectives

I hypothesised that the displacement of tissues would be resisted by tissue with increasing volumes of injectate. The primary objective of this study was to measure the dose response of different volumes of embalming fluid (0.25, 0.5, 1, 2.5, 5 and 7.5 ml) for interscalene and femoral blocks in Thiel embalmed cadavers, by automatically measuring the area of the enhanced elastogram using ImageJ. Secondary outcomes were rater visibility of anatomy and spread of injectate.

5.2.2 Methods

I randomly performed 10 interscalene and 10 femoral blocks using volumes of 0.25, 0.5, 1, 2.5, 5 and 7.5 ml on five occasions, one to two weeks apart and divided equally

between left and right sides of a single female cadaver (age at death 85 years). Block randomisation was undertaken using a computer generated package according to type of regional block and side of the body. I felt confident from my previous work that separating injections by at least 45 minutes would prevent fluid accumulation.

Interscalene blocks were performed using an out-of-plane needle approach. The needle tip was placed adjacent to the C5 nerve root during interscalene block, and lateral to the femoral artery under the fascia iliaca during femoral block. Injections were recorded onto the Digital Imaging and Communications in Medicine (DICOM) standard for handling, storing, printing, and transmitting information. Video clips were scored using Likert and Vienna scores. Likert scores consisted of a 7-point scale: 1 being extremely poor; 2 - very poor; 3 – poor; 4 – fair; 5 – good; 6 - very good and 7 - excellent visibility. Vienna scores consisted of a 4-point scale:1 - internal structure of nerve visualised; 2 - nerve visualised as circular or oval-shaped bright halo (epineurium); 3 - nerve visualised as reflections determined by the anatomy of the surrounding tissue and 4 - anatomical position of nerve shows no response to ultrasound beam.

I assumed the log time weighted AUC to be 5 $U.s^{-1}$, and 6 $U.s^{-1}$ for femoral and interscalene blocks and 2, 4, 6, 6, 8 and 8 $U.s^{-1}$ for 0.25, 0.5, 1, 2.5, 5 and 7.5 ml volumes respectively with a common standard deviation of 1.2 $U.s^{-1}$. A factorial design with two factors (block and volume) and six variables gave 12 treatment combinations or cells. Thus a total of 96 injections were required to provide eight subjects per cell. This design achieves 90 % power when an F-test is used to test “block” and achieves 100 % power when an F-test is used to test “volume”, both at 5% significance. Considering the technical nature of the experiment I decided to perform 10 injections per cell.

Weighted Kappa was used to calculate the degree of agreement between the raters as this was important to ensure there high degree agreement to further use this for statistical analysis and comparison. All disagreement is treated equally as total disagreement and Kappa does not take into account the degree of disagreement between observers. Therefore when the categories are ordered, it is preferable to use Weighted Kappa (Cohen 1968), and assign different weights w_i to subjects for whom the raters

differ by *i* categories, so that different levels of agreement can contribute to the value of Kappa.

In the linear set, if there are k categories, the weights are calculated as follows:

$$w_i = 1 - \frac{i}{k-1}$$

The ***K*** value can be interpreted as follows (Altman, 1991):

Value of *K*	**Strength of agreement**
< 0.20	Poor
0.21 - 0.40	Fair
0.41 - 0.60	Moderate
0.61 - 0.80	Good
0.81 - 1.00	Very good

Analysis of variance was used to compare the groups, as there were atleast 2 groups or more for comparison. I confirmed that the dependent variable was continuous data, there were two or more independent groups / variables. There was no relationship between the observations and the study design ensured t.his with separate injection and video frame for each data point. I checked the data to rule out any outliers and establish that it was a normally distributed data. The data was also checked to confirm homogeneity of variances before ANOVA could be used for comparison of different groups.

As there were more than 2 groups for comparison for some variables, Bonferroni's post hoc analysis was used to pick out the two groups with most difference for different injectate volumes.

5.2.4 Results

Sixty 0.25, 0.5 and 1ml injections were performed, divided equally between interscalene and femoral blocks. High injection pressures and a desire to protect the Thiel cadavers from volume trauma restricted the number of injections in the larger

volume groups. For interscalene block, injections of 2.5, 5 and 7.5 ml volumes were restricted to seven, three and two occasions; and for femoral block, restricted to five, four, and two episodes. All were associated with high injection pressure and therefore, 18 interscalene and 19 femoral large volume blocks were not performed.

Probability plots showed a normal distribution pattern of spread. Concordance of visibility ratings was present between raters; linear weighted Kappa (95% CI) 0.66 (0.61 - 0.71). The characteristics of spread were similar with both interscalene and femoral blocks; spread increased with injectate volume up to 1 ml. Within-subject standard deviations were similar for both blocks (Table 2). Analysis of variance (ANOVA) showed differences in measured spread between injection volumes ($p = 0.009$), but not between regional blocks ($p = 0.05$). There was no interaction between injection volume and regional blocks ($p = 0.56$). Post-hoc Bonferroni analysis showed greater spread with 1 ml and 2.5 ml volumes compared to 0.25 ml (Table 11).

Table 11. Dose response. Area (SD) cm^2

Volume injected	**Interscalene block**	**Femoral block**
0.25	2.69 (1.34)	2.10 (1.40)
0.5	3.59 (1.34)	4.10 (1.82)
1.0	5.90 (1.13)	5.20 (1.58)
2.5	5.87 (2.51)	3.35 (1.20)
5.0	4.20 (1.58)	2.83 (1.97)
7.5	5.40 (0.46)	3.80 (0.60)

Secondary outcomes showed a non-parametric distribution. Spearman's correlation between Likert and Vienna score was $R^2 = 0.78$. Visibility of nerves (Likert and Vienna scales) and muscles before injection was better ($p=0.04$ and $p =0.02$ respectively) using B-mode ultrasound compared to strain elastography (Table 12). During injection, needle visibility was better ($p=0.02$) with B-mode ultrasound, but spread of solution better ($p=0.04$) with strain elastography .

Table 12. Secondary outcomes. Visibility of nerves, muscle, needles and fluid spread

	B-Mode	Sono-elastography	W	p
Nerve (Likert)	5 [2 – 7]	2 [1 – 3]	28	0.04
Nerve (Vienna)	1 [1 – 2]	4 [3 – 4]	36	0.02
Muscle	4 [2 – 6]	2.5 [2 – 4]	23	0.03
Needle insertion	4.5 [4 – 5]	2 [1 - 3]	36	0.02
Spread	5 [4 – 6]	6.5 [6 – 7]	28	0.04

5.2.5 Conclusion

Strain elastography showed similar spread for interscalene and femoral block with a maximal response using 1 ml and 2.5 ml of solution. Furthermore, repeated blocks did not accumulate perineural fluid. Reliance on the B-mode greyscale may not clearly show local anaesthetic spread at low volumes, especially when merged with a dark background and a colour scale has shown improved pattern recognition.

Strain elastography recognised rapid increases in tissue strain secondary to volume expansion of interstitial tissue and potentially offers three important advantages: recognition of (i) inadvertent interstitial spread of local anaesthetic; (ii) inadvertent intra-arterial and intra-neural injection; and (iii) real-time identification of strain with volumes as low as 0.25 ml. The extensive size of strain pattern in patients using only 1 ml suggested that strain elastography could possibly differentiate between intraneural and extraneural hydrolocation test doses.

5.3 Differentiation between intraneural and extraneural injection

Anaesthetists have difficulty diagnosing intraneural injection during ultrasound guided regional anaesthesia (UGRA); the incidence of intraneural injection using ultrasound varies between 16% in experts and up to 35% in trainees (Hara et al, 2012; Liu et al, 2012). Functional impairment such as temporary neuropraxia may occur in up to 1 in 8 patients and permanent nerve damage occurs in approximately 1 in 2,500 patients (Barrington et al 2011). More recently needle-epineurium contact was associated with intraneural haematoma, inflammation and myelin damage in over half of cases in animal studies (Steinfeld et al).

Inadequate regional anaesthesia training, patient factors, or technical imaging limitations may all account for the high incidence of intraneural injection amongst trainees. Inexperienced anaesthetists struggle to align the needle in the plane of the ultrasound transducer, and have difficulty visualising the tip of the needle relative to the epineurium at the point of injection. Obesity increases the distance between skin and the nerve target, dissipating acoustic energy into tissues as heat (Simons et al 2005). Nerves and adjacent tissue have similar acoustic impedance and are difficult to

differentiate, and optimal resolution of tissues is limited by transducer frequency(Nakashima 2013). There is a need for visual technology that offers novices the capacity to accurately, reliably and confidently recognise tissue displacement of test doses within peripheral nerves. The impact of such a technology would be rapid withdrawal of the needle from the nerve and injection repeated close to but not touching the epineurium.

During my cadaver work, I noticed that, using a 1ml test dose, intraneural injection was seen on elastography imaging as a distinct, small, bright, round flash over the nerve whereas extraneural injection was seen as a much larger, duller, asymmetrical pattern around the nerve. My rationale was that intraneural injection was restricted within the confines of a relatively stiff epineurium whereas extraneural injection diffused randomly according to the relative stiffness of tissues.

5.3.1 Hypothesis and objectives

My hypothesis was that the elastography visualisation of intraneural injection would differ from extraneural injection into connective tissue and muscle. USING FUSION In turn, visual and colour separation of local anaesthetic and tissue would be possible, allowing the development of a translational model differentiating between intraneural and extraneural injection. However, use of elastography in a routine clinical setting is difficult because the anaesthetist must visualise two screens in real-time, and this has restricted elastography in our practice to a *post-hoc* analysis tool.

Therefore, my primary objective was to use fusion elastography to test the ability of trainee anaesthetists to diagnose intraneural injection. My secondary objectives were to identify variables that predicted correct diagnosis, assess the reliability of assessment, gauge the level of trainee confidence for each diagnosis, measure changes in nerve cross-sectional area and brightness associated with extraneural and intraneural injection of 0.25ml. 0.5ml and 1ml volumes, and gain feedback from trainees at the end of the study.

5.3.2 Methods

5.3.2.1 Nerve blocks

I conducted 40 ultrasound guided median nerve blocks using 0.25ml, 0.5ml and 1ml

test doses in the soft embalmed Thiel cadaver to provide engineers with data to fuse elastography with B-Mode ultrasound. Injectate volumes of 0.5ml and 1ml were chosen because we routinely use these as test doses, and 0.25ml was chosen to to evaluate trainees' recognition of ultra-low volumes. Injections were administered at a rate of approximately 1ml every 2 seconds in order to mimic clinical practice. Using computer software, nerve blocks were randomly allocated to five sites, 2cm apart and intraneural/extraneural locations over the median nerve on both forearms of two soft embalmed Thiel cadavers on two occasions, one week apart. Nerve blocks were performed using B-Mode ultrasound and proprietary elastography using a Zonare (Mountain View, CA) Z.one ultrasound scan engine build release 4.2.

5.3.2.2 Image measurement

From B-Mode and elastogram block videos area and brightness measurements included: (i) the median nerve before and during nerve block; (ii) the coloured strain pattern on the elastogram and; (iii) the white strain pattern on the fused B-Mode and elastography image. Two independent raters, using the freehand drawing tool of ImageJ, circumscribed the cross sectional area of the median nerve and elastogram displacement on every 4^{th} video frame recorded at a frequency of $8.s^{-1}$. Each image was calibrated to a standard 7.28 pixels mm^{-2}. ImageJ automatically calculated tissue brightness as the sum of gray values between 0 (black) and 255 (white) of all pixels within outlined regions of interest divided by the number of pixels. In order to calculate the brightness of colour strain patterns each pixel was converted to grayscale using the weighted formula recommended by ImageJ whereby: gray = (0.299*red + 0.587*green + 0.114*blue).

5.3.2.3 Expert Assessment

Two UGRA experts met and agreed which injections were intraneural or extraneural by detailed analysis of B-Mode and fused B-Mode images. Experts judged intraneural injection as increase in the cross-sectional area of the nerve on B-mode images and overlay of the fused image on the nerve.

5.3.2.4 Anaesthetist training

This study received ethical approval from the University of Dundee non-clinical Ethics committee and the University of Dundee Thiel Advisory Committee. All trainees within the East of Scotland School of Anaesthesia were invited by e-mail to participate; twenty responded and voluntarily opted into the study. Before analysis of images, trainees were taught to recognise intraneural and extraneural injection on B-Mode, elastography and fusion elastography videos. Trainees were shown four training videos. The first showed an ultrasound guided median nerve block recorded in an anonymous patient showing circumferential spread of local anaesthetic, followed by nerve distention secondary to accidental intraneural injection. The second demonstrated a well-conducted interscalene block in a patient using B-Mode ultrasound and elastography, illustrating good perineural spread between the nerve roots of C5 and C6 on both modalities. The third highlighted an intentional sciatic intraneural injection in the soft embalmed cadaver demonstrating intraneural swelling on B-Mode ultrasound and intraneural colour enhancement using elastography. The fourth video showed examples of intraneural and extraneural injection using fusion elastography.

5.3.2.5 Rater assessment

The study was started when each rater was satisfied that they had gained sufficient knowledge to understand the patterns seen on B-Mode ultrasound and elastography during extraneural and intraneural injection. Assessment occurred on two separate occasions. Trainees were asked to interpret 40 B-Mode ultrasound videos, then the same B-Mode videos paired with adjacent elastography videos. One week later, raters were asked to interpret 40 fused elastography and B-Mode videos then repeat the assessment of the initial B-Mode ultrasound videos. The latter evaluation was termed test - retest. Because assessment of 80 videos in one sitting is arduous, the second half of the experiment was conducted one week later to reduce the effects of tiredness on trainee image interpretation and to lessen any effect of memory on performance.

Raters assessed the first static frame of each video over 5 seconds in order to identify anatomical structures. Each video was then run for 12 seconds and raters were asked to diagnose whether injection was extraneural or intraneural. The primary end point was the diagnosis of intraneural injection and secondary end point was diagnostic confidence for each video measured on a 3-point categorical scale (1 = low, 2 =

medium, 3 = high). In order to replicate clinical practice, no repeated viewings were permitted.

At the end of the study, trainees were asked overall how realistic B-Mode images were using a 1 to 5 categorical score where 1 = not very realistic and 5 = very realistic. Trainees were also asked how confident they were overall diagnosing intraneural and extraneural injection using each imaging modality using a 1 to 5 categorical scores where 1 = not very confident and 5 = very confident.

Likelihood ratio (LR) is used to assess how good a diagnostic test is and has advantage over sensitivity and specificity as LR is not prevalance dependent. iIt can be used to calculate post-test probability, which is particularly relevant to this study.

LR is very useful but there are limitations to using it in clinical practice. To use this measure a nomogram should be employed or pretest probabilities should be converted into Odds, then multiplied by LR, then converted back into post test probability (Post-test odds = pre-test odds* LR).

An LR equal to 1 represents a test that has no role in diagnosing a particular condition.

Positive likelihood ratio (LR+ve) and Negative Likelihood ratio (LR-ve) should be used

together, to understand how useful a diagnostic tool is in picking up the trait we are

interested in.

Positive likelihood ratio: ratio between the probability of a positive test result given the presence of the disease and the probability of a positive test result given the absence of the disease,

LR+ve = True positive rate / False positive rate = Sensitivity / (1-Specificity)

Negative likelihood ratio: ratio between the probability of a negative test result given the presence of the disease and the probability of a negative test result given the absence of the disease,

LR-ve = False negative rate / True negative rate = (1-Sensitivity) / Specificity

One suggested way to interpret LR is as follows (Ebell, 2005 Information Mastery AAFP Home Study):

> 10 large and often conclusive increase in likelihood of disease

5 – 10 moderate increase in likelihood of disease

2–5 small increase in likelihood of disease

1–2 minimal increase in likelihood of disease

1 no change in likelihood of disease

0.5 - 1.0 Minimal decrease in the likelihood of disease

0.2 - 0.5 Small decrease in the likelihood of disease

0.1 - 0.2 Moderate decrease in the likelihood of disease

< 0.1 Large and often conclusive decrease in the likelihood of disease

Logistic regression analysis was used, as the dependent variable (intraneural injection) being tested was a binary or dichotomous variable. It can be used to analyse the ralationship between a binary dependent variable and one or more independent variable which can be nominal, ordinal, interval or ratio- dependent variable. Hence, I felt it was suitable to use this test as I was comparing different types of independent variables and analysing their effect on correct diagnosis of intraneural injection

5.3.3 Results

Forty procedures randomised to 22 intraneural and 18 extraneural blocks were recorded. Experts agreed 18 blocks were extraneural, (6 - 0.25ml, 6 - 0.5ml and 6 - 1ml) and that 22 blocks were intraneural (7 - 0.25, 7 - 0.5ml and 8 - 1ml). A coloured strain pattern was seen with all injections. All fusion images were characterised by a white transparent, ghost-like strain pattern overlying the B-Mode image. Typical examples of intraneural and extraneural injection on B-Mode, elastography and fusion images are shown in Fig 29.

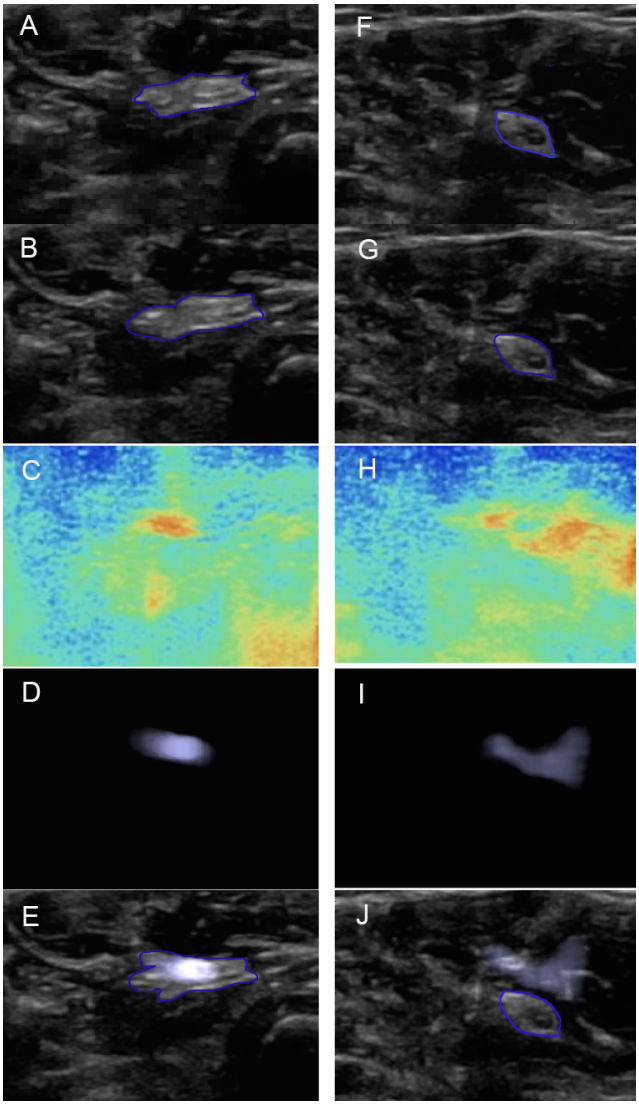

Fig 29. All image modes – median nerve. Pre-injection B-Mode, post-injection B-Mode, standard elastography, enhanced elastography and fusion elastography images captured from video of median nerve block within soft embalmed Thiel cadaver. The edge of the median nerve is highlighted in blue. Left hand column (A – E) shows typical response to intraneural injection. Image A shows a median nerve with typical mixed echogenicity. Image B shows expansion and reduced echogenicity of the same median nerve in response to 0.5ml injection. The elastogram, image C, shows a small, linear red and yellow pattern. The enhanced elastogram image D, is the black and white conversion of image C, and shows a round white object 5mm in diameter and the same, object transposed onto the median nerve onto the fusion elastogram, image E. Note the object is transparent and brighter on image E. The right hand column shows response to extraneural injection (F – J). The perineural elastogram displacement is greater in images H and I compared to the intraneural displacement in images C and D.

5.3.3.1 Diagnosis of intraneural injection

Mean (95%CI) diagnostic Odds Ratio for intraneural injection increased from 7.4 (5.2 – 10.6) using B-Mode ultrasound to 21.7 (14.5 - 33.3) using fusion elastography, P<0.001. However, there was no difference in diagnostic performance when comparing B-Mode ultrasound videos with combined B-Mode and Elastography or when re-testing B-Mode videos (Tables 13 and 14).

Table 13. Diagnosis of intraneural injection (a). B-Mode ultrasound, the combination of B-Mode and Elastography, Fusion elastography and B-Mode (re-test) ultrasound. Positive likelihood ratio (LR+) = sensitivity/(100-specificity) Negative likelihood ratio (LR-) = (100-sensitivity)/specificity.

	Sens(%)	**Spec(%)**	**LR (+) (95%CI)**	**LR (-) (95%CI)**
B-Mode	59.6 (54.8 - 64.2)	83.4 (79.2 - 87.1)	3.60 (2.83 – 4.60)	0.48 (0.43 – 0.55)
B-Mode + Elastography	55.1 (50.3 - 59.7)	81.1 (76.7 - 85.1)	2.92 (2.33 - 3.69)	0.55 (0.49 - 0.62)
B-Mode (re-test)	63.8 (59.1 - 68.3)	81.0 (76.6 - 84.9)	3.35 (2.70 - 4.21	0.45 (0.39 - 0.51)
Fusion Elastography	72.1 (67.7 - 76.3)	89.4 (85.8 - 92.4)	6.81 (5.04 - 9.28)	0.31 (0.27 - 0.36)

Table 14. Diagnosis of intraneural injection (b). Diagnostic Odds Ratio = LR+/LR-. Concordance between raters expressed as Kappa.

	Kappa (95%CI)	**Odds Ratio (95%CI)**	**Diagnostic Odds Ratio (95%CI)**	**P-value**
B-Mode	0.42 (0.36 - 0.48)	Reference	7.4 (5.2 – 10.6)	
B-Mode + Elastography	0.35 (0.29 - 0.41)	0.83 (0.67 - 1.04)	5.3 (3.8 - 7.4)	0.10
B-Mode (re-test)	0.45 (0.39 - 0.51)	1.07 (0.85 - 1.33)	7.5 (5.3 - 10.6)	0.57
Fusion Elastography	0.60 (0.55 - 0.66)	1.70 (1.35 - 2.15)	21.7 (14.5 - 33.3)	<0.001

5.3.3.2 Number of Correct Diagnosis

Compared to B-Mode ultrasound, diagnosis improved in 7 out of 20 trainees using combined B-Mode and elastography; in 9 out of 20 trainees on re-testing B-Mode ultrasound and in 17 out of 20 trainees using fusion elastography (Fig 30).

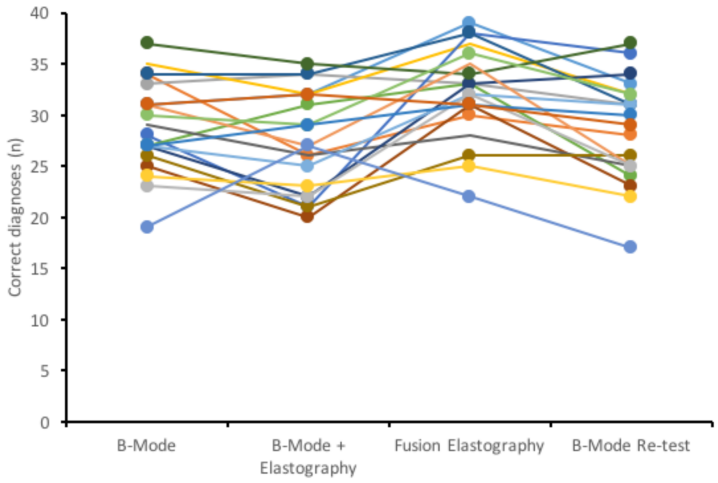

Fig 30. Number of correct diagnoses (intraneural and extraneural combined) for each trainee (colour coded) with regard to B-Mode videos, B-Mode and standard elastography videos, fusion elastography videos and re-testing of B-Mode videos.

Logistic regression analysis (Table 15) showed that independent predictors of correct diagnosis were fusion elastography OR (95%CI) 1.77 (1.39 – 2.25), P<0.001, right side of cadavers OR (95%CI) 1.37 (1.36 – 1.64), P<0.001, and choosing extraneural injection OR (95%CI) 3.15 (2.64 – 3.77), P<0.001.

Table 15. Univariate and multivariate analysis. Outcome = correct diagnosis. Independent predictors of correct diagnosis were fusion elastography, injection on the right side of the cadavers and choosing extraneural injection as the diagnosis.

	Univariate analysis Odd Ratio (95%CI)	p-value	Multivariate analysis Odd Ratio (95%CI)	P-value

Actual diagnosis				
Intraneural	----------			
Extraneural	3.17 (2.66 – 3.79)	<0.001	3.15 (2.64 – 3.77)	<0.001
Training year				
2	----------			
3	0.78 (0.50 – 1.20)	0.27		
4	0.74 (0.42 – 1.33)	0.35		
5	0.83 (0.36 – 1.90)	0.78		
6	0.96 (0.50 – 1.85)	1.00		
8	2.00 (0.57 – 7.21)	0.34		
Cadaver				
1	----------			
2	0.94 (0.89 – 0.99)	0.01		
Side				
Left	----------			
Right	1.50 (1.31 – 1.72)	<0.001	1.37 (1.36 – 1.64)	<0.001
Volume				
0.25 – 1ml	0.96 (0.74 – 1.23)	0.72		
Trainee confidence				
1 – 3	1.89 (1.69 – 2.11)	<0.001		
Imaging mode				
B-Mode	----------			
B-Mode + elastography	0.83 (0.67 – 1.04)	0.10	1.00 (0.69 – 1.46)	0.99
B-Mode re-test	1.07 (0.85 – 1.33)	0.57	1.05 (0.82 – 1.34)	0.70
Fusion	1.70 (1.35 – 2.15)	<0.001	1.77 (1.39 – 2.25)	<0.001

5.3.3.3 Cross-Sectional Area

Geometric mean cross-sectional area differed between modes of imaging (P<0.001). There was no difference in cross-sectional nerve area between extraneural and intraneural groups either before (geometric ratio 0.12 (95%CI: 0.35 – 0.58), P=0.99) or after nerve block (geometric ratio 0.35 (95%CI: 0.11 – 0.82), P=0.27, (Fig 23A). Intraneural injection was associated with a reduction in tissue displacement on the elastogram geometric ratio 0.48 (95%CI: 0.02 - 0.95), P=0.04, but not on the fusion elastogram, geometric ratio 0.27 (95%CI: 0.19 – 0.74), P=0.62, (Fig 23A). Cross-sectional nerve area did not change in response to intraneural injection of 0.25ml, 0.5ml or 1ml volumes, (1ml vs 0.25ml geometric ratio 0.01 (0.48 – 0.49), P=1.0), (Fig 23B). Extraneural injection of 0.25ml, 0.5ml and 1ml volumes showed a dose response (1ml vs 0.5ml geometric ratio 0.22 (0.36 – 0.81), P=0.84; 1ml vs 0.25ml geometric ratio 0.47 (0.11 – 1.06), P=0.17.

5.3.3.4 Brightness

Geometric mean brightness differed between modes of imaging, P<0.001, intraneural

and extraneural injection P<0.001 and volume, P=0.005. There was no difference in brightness between extraneural and intraneural groups either before (geometric ratio 0.07 (95%CI: 0.10 – 0.24), P=0.91) or after nerve block (geometric ratio 0.05 (95%CI: -0.10 – 0.21), P=0.96). Intraneural injection was associated with an increase in nerve brightness using fusion elastography geometric ratio 0.33 (95%CI: 0.16 - 0.49), P<0.001, Fig 31.

Fusion elastography was associated with an improvement in diagnostic reliability, Kappa value of 0.60. Expert concordance was Kappa 0.80 (95%CI: 0.68 – 0.92). Trainees had greater confidence diagnosing individual images using fusion elastography. OR (95%CI) 1.89, they felt the images provided information to make decisions about intraneural or exraneural positions. Reflecting overall on the study, trainees were more confident using fused elastography than B-Mode ultrasound, P<0.001.

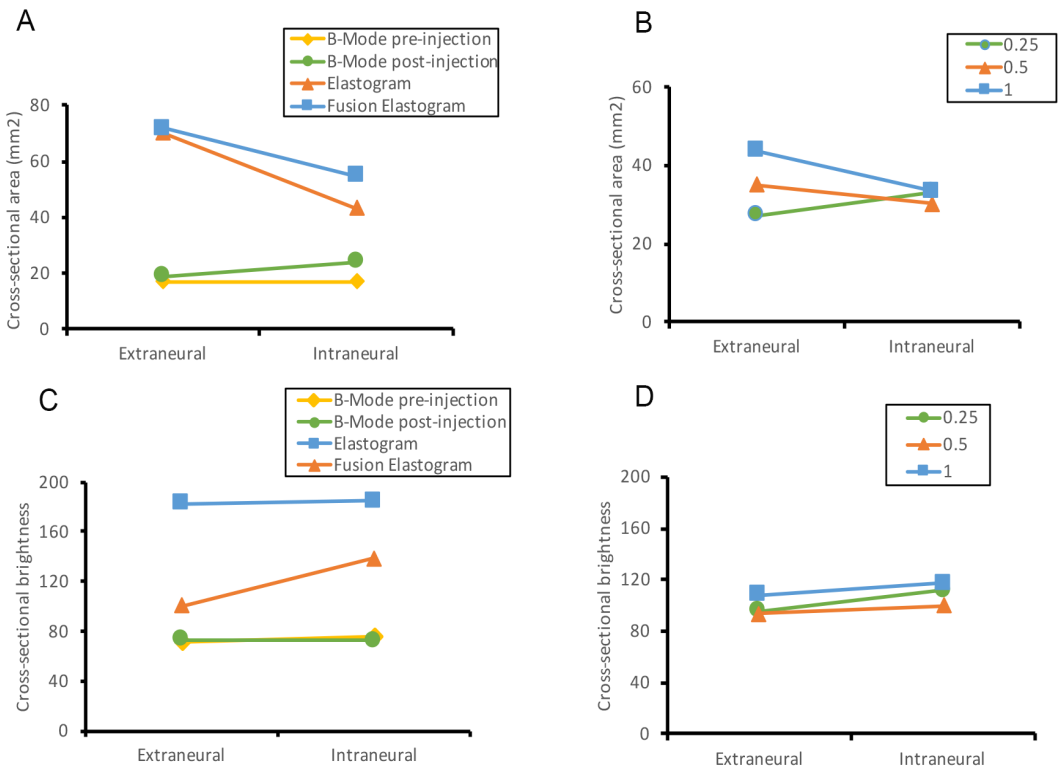

Fig 31. Area measurements with respect to mode of imaging and volume during intraneural and extraneural injection. Clockwise, upper right, image A shows convergence of nerve cross sectional areas

of nerve, strain pattern and fusion image with intraneural injection. Intraneural injection was associated with a reduction in tissue displacement on the elastogram, P=0.04. Image B, upper right, shows convergence of nerve cross sectional areas of 0.25ml, 0.5ml and 1ml volumes with intraneural injection and an extraneural dose response. Image C, bottom left, shows increase in brightness with fusion image with intraneural injection, P<0.001. Image D, bottom right, shows no difference in brightness using 0.25ml, 0.5ml and 1ml volumes.

5.3.4 Conclusion

This study showed that trainee diagnosis of intraneural injection was better using fused B-Mode and elastography videos compared to separate, adjacent B-Mode and elastography videos or B-Mode videos. The likelihood of correctly diagnosing intraneural injection using fusion elastography was almost twice that of other imaging modalities. Fusion elastography was associated with greater trainee confidence and improved diagnostic reliability. Diagnostic success was not improved by retesting trainees with B-Mode videos.

5.3.4.1 Strengths of study

The strength of this study was that the functionality of proprietary elastography was enhanced then translated as a simulator of intraneural injection. Early identification of intraneural injection allows anaesthetists to withdraw the needle, reposition it outwith the epineurium, reducing the potential for nerve damage. Although historical reports suggest no adverse clinical outcome secondary to subepineural injection(Bigeleisen 2006, Sala Blanch et al 2009), recent data (Steinfeld describe nerve inflammation, intraneural haematoma, fascicle damage and reduction in compound muscle action potential amplitudes secondary to needle trauma in animals. Thus, this teaching innovation also has the potential with development to improve patient safety by acting as an early warning system.

Trainee diagnosis was improved, notably, by both reducing the proportion of false negative and false positive results. Nevertheless, there remained a tendency, similar to the results of Krediet et al[27], for trainee anaesthetists to over-diagnose extraneural injection one third more often than intraneural injection when using B-Mode ultrasound. We have no indication from our results why this should be so as there was no disagreement between experts, and volume of injectate and grade of anaesthetist

had no effect on the results. One surprising result was the improved odds of obtaining the correct diagnosis when examining videos from the right side of the cadaver. I have difficulty accounting for this result as B-Mode images from the left and right arms were similar. The shape of extraneural strain patterns is much more variable than intraneural strain patterns and our result may reflect small differences in needle tip position and pathways of least resistance within local anatomy.

My previous work mentioned in chapters 23 and 24 demonstrated the feasibility of elastography as an adjunct to B-Mode ultrasound during UGRA by demonstrating distinctive, colour patterns around nerves. Exact needle tip position, volume and rate of injection, tissue elasticity, and transducer compression are all likely to alter the ebbing and flowing of fluid within connective tissue spaces and, thus, elastogram patterns tend to differ in size and shape between patients. This study confirmed this observation and showed that using 1ml test doses, extraneural fusion elastogram area was approximately 33% greater than intraneural fusion elastogram area, a difference readily perceived by anaesthetists routinely using 1ml test doses.

In marked contrast, intraneural injection was characterised by similar cross-sectional areas using B-Mode, elastography and fusion elastography imaging modalities and 0.25ml, 0.5ml and 1ml volumes, and a brighter focused targeting of intraneural injection using fusion elastography. Intraneural injection was brighter (Fig 24) because the brightness of the mixed echogenic nerve enhanced the brightness of the overlying strain pattern. In contrast, extraneural injection was duller because the strain pattern was superimposed on relatively hypoechoic muscle. Nerve expansion was limited by stiff epineurium, and local anaesthetic spread both radially and longitudinally within the nerve taking the path of least resistance.

5.3.5.2 Weaknesses of study

One criticism is that I failed to confirm intraneural injection using injection of dye and anatomical dissection. I am aware that consultants without elastography experience would not attain such accuracy and that a learning curve is necessary. Although diagnostic sensitivity of intraneural diagnosis improved by one fifth, this cannot be regarded as sufficient to apply as yet to clinical practice. Another criticism is that trainees were asked to interpret videos without the benefit of haptic feedback. The

sensation of touch conveyed from the tip of the needle aids interpretation and enhances learning during UGRA. I would recommend that simulation of intraneural injection is introduced into training courses using the soft embalmed cadaver in order that competency is achieved in both nerve block and the early recognition of intraneural injection.

Real-time detection of intraneural injection remains a challenge in clinical practice because ultrasound equipment and operators lack sufficient confidence and accuracy. Increase in clinical morbidity such as obesity, diabetes and ageing-related chronic illness will increase the need for UGRA but, as such, will be technically more difficult. I have shown that fusion elastography may be a valuable diagnostic training aid and, indicated that it has the potential for further development as a visible warning signal that may prevent further harm. Development of an accurate and reliable detector of intraneural injection will probably require a computing solution such as machine learning in order to extract and analyse image data. The advantage of using computers is that diagnosis would be instant, and visualised or heard as an alarm, and algorithms would automatically improve with increased use.

5.4 Recognition of hydrolocation test doses using fusion elastography

During my pilot studies I noted that after injecting a small 0.5ml to 1ml hydrolocation test dose that not only did a perineural strain pattern appear on the elastogram but that in many instances, an extra strain pattern would occur either at the same time or more commonly, a few seconds later. I categorised these additional or secondary strain patterns as:

Errors may occur during the visual search, recognition and decision making phases (Kundel et al, 1978) of ultrasound-guided regional anaesthesia (UGRA) nerve block. Search errors are attributable to failure to see lesions that are normally noticed by anaesthetists (Van der Gijp et al 2017). With recognition errors, lesions are seen but confusing; and decision errors occur when a lesion is fixated on for long periods but the anaesthetist either does not recognise features or dismisses them. (Krupinski et al 2011).

While conducting interscalene and femoral nerve block in cadavers (Munirama et al 2016) and patients (Munirama et al 2012) we noticed novel features on paired B-Mode and elastography ultrasound images in response to injection of test doses. Tissue strain intermittently presented as two patterns instead of one. Additional patterns, termed distractors, were distinguished from primary target displacement patterns by brightness, size, position or movement (Eckstein et al 2011). In contrast, test doses as low as 0.25ml were always seen on B-Mode images, but distractor patterns much less so. Our impression was that elastography exhibited greater saliency, the extent to which a location differs from its surroundings, than B-mode images because: (i) key regions differed in brightness, colour, orientation, and motion; and that (ii) anaesthetists' visual attention was attracted towards these features.

Visual salience describes the visual processing mechanism that enables the brain to select important features that stand out from other items or locations (Treue et al, 2012) (Table 1). Salience is associated with passive, automatic visual search or "bottom-up processing" rather than cognitive, goal driven "top-down processing" (Melloni et al, 2012). Consideration of both processes creates an saliency map, a topographic representation of relative stimulus strength and behavioural importance. This map is distributed throughout the visual cortex and linked via the oculomotor system to eye movement and eye gaze (Moore et al, 2017). Eye gaze characteristics such as fixations and saccades are quantified using eye-tracking technology and are used in many industries to measure technical performance.

Visual search and salience differ between experts and novices. Experts rely on bottom-up processes that facilitate efficient search, albeit mediated by prior knowledge when encountering novel stimuli (Melloni et al, 2009). Novices, in contrast, are primarily goal driven but can be salience led to very obvious targets.

5.4.1 Hypothesis and objectives

I hypothesised that improvements in novice visual perception were salience driven, and if so, would provide evidence for investigation of the role of eye gaze technology and augmented reality during simulator training. This approach could help train

anaesthetists better, target local anaesthetic more and improve patient safety.

Therefore, the primary objective was to test anaesthetists' perception of the number and proportion of targets and distractors on B-Mode and fused elastography videos collected during femoral and sciatic nerve block on soft embalmed cadavers.

Secondary objectives were to measure differences in perception between novices and experts, between test dose volumes, measure the area and brightness of spread and strain patterns over time, and propose underlying mechanisms for tissue displacement.

5.4.2 Methods

All trainee anaesthetists at basic, intermediate and higher levels of training working in Ninewells Hospital were invited to take part in this study along with two consultant subspecialists in regional anaesthesia. Our exclusion criterion for trainees was the prior use of elastography. The study was approved by the University of Dundee Committee on Non-Medical Ethics.

Elastography and its applicability to the diagnosis of intraneural injection is described in detail. In summary, our engineer converted colour elastography video frames to filtered and despeckled black and white images using MATLAB software (Natik, MA) and a grayscale threshold tool. Enhanced elastography patterns were fused onto corresponding B-Mode images. Tissue displacement in response to fluid injection was seen as a flowing translucent, white area, superimposed onto paired B Mode images. Fusion videos were converted to TIFF files and analysed using ImageJ (Wayne Rasband, Research Services Branch, National Institute of Mental Health, Bethesda, MD)

A single independent, experienced anaesthetist conducted 24 interscalene and 24 femoral ultrasound-guided nerve blocks, randomised equally using a software randomisation program to 0.25ml, 0.5ml and 1ml volumes to both sides of two soft embalmed cadavers. UGRA was performed on two occasions, one week apart as before. Blocks were recorded to DICOM.

Interscalene block was performed using a 100 mm needle (B.Braun, Sheffield, UK), in-plane to a 5 to 10MHz ultrasound transducer, and embalming fluid deposited between

the nerve roots of C5 and C6. Femoral block was performed using a 50mm needle at 90^{o} to the plane of the same ultrasound transducer and injected below the fascia iliaca and superficial to the femoral nerve. We recorded nerve blocks using a Zonare (Mountain View, CA) Z.one ultrasound scan engine build release 4.2 with B-Mode ultrasound and proprietary elastography. Blocks were recorded on DICOM imaging software.

Before starting the study, participants were shown videos of interscalene and femoral block using B-Mode and elastography ultrasound by one of two independent investigators. Participants deemed themselves ready for participation in the experiment. Each assessed 96 videos comprising 8 blocks performed at 2 sites on 2 nerves (interscalene and femoral), using 3 volumes (0.25ml, 0.5ml, 1.0ml) and 2 imaging modes (B-Mode ultrasound and fused B-Mode and elastography). Each video was played once to replicate practice. Patterns were rated according to whether perineural fluid spread or strain tissue had occurred in isolation or not. Distractors were defined as distinct patterns of spread or strain differing from target perineural spread or strain by size, movement or time. Our primary endpoint was therefore recorded as a “1” or “2” corresponding to the number of events observed. We did not ask trainees to refine their choice further because this study focused on the detection of events and not their interpretation or impact on decision-making. We did not know if sufficient homogeneity existed between patterns that would have allowed ready, simple classification by non-experts. For descriptive purposes, video examples of fluid spread and strain patterns were categorised by two researchers at the end of the study in order to minimise bias.

5.4.4.1 Area and Brightness Measurement

The cross-sectional area and brightness of B-Mode fluid spread and strain patterns were measured on every fourth video frame (every 0.5s) by a single rater using ImageJ. To test the reliability of our data, two raters independently measured the area of fusion elastograms using the yellow tracing tool available on ImageJ. Duration of fluid spread or strain was defined as the time from the first visible evidence of tissue distention to tissue relaxation. Each image was calibrated to a standard 7.28 $pixels.mm^{-2}$. Mean tissue brightness was calculated as the sum of the grey values between 0 (black) and 255 (white) of all the pixels within the region of interest divided

by the number of pixels. Area and brightness measurements were log converted for analysis. Our secondary end-points were measurements of area (mm^2) and brightness.

5.4.3 Results

Twenty anaesthesia trainees and 2 consultant UGRA experts examined 48 paired B-Mode and fusion elastography videos, giving 2112 observations. Median (IQR) trainee anaesthesia experience was 3 (1 – 4) years. All participants recognised perineural spread or strain at all volumes between 0.25ml and 1ml.

Distractors were recognised in 133 (12%) of B-Mode and 403 (38%) fusion elastography videos, differences in paired proportions, $P < 0.001$. Use of fusion elastography improved novice recognition from from 12% to 37% ($P < 0.001$) and consultant recognition from 24% to 53% ($P< 0.001$). Recognition of distractors improved from 8% to 31% using 0.25ml volumes ($P < 0.001$) and from 15% to 45% using 1ml volumes ($P < 0.001$).

Using stratified logistic regression, recognition of distractors was better with: fusion elastography Odds Ratio, OR (95%CI) 5.31 (3.14 – 8.96), $P < 0.001$; consultant anaesthetists OR 3.84 (2.29 - 6.45) $P < 0.001$; greater volumes of injectate OR 2.19 (1.11 – 4.31), $P = 0.02$; and worse with interscalene block OR 0.58 (0.35 – 0.94), $P = 0.03$ (Table 3). Area and brightness were greater with fusion elastography and with increased injectate volume.

Three distinct strain patterns were categorised retrospectively by two additional experts in response to injection: (i) Bilateral pattern - two areas of similar size, shape and brightness but spreading in opposite directions from the tip of the needle (Fig 32) ; (ii) Recurrent spread - initial tissue displacement followed by a sudden reversal in flow and secondary displacement at the initial site of injection (Fig 34) and (iii) Distal spread - tangential displacement away from the injection site (Fig 33). Pattern (i) was observed during 7 femoral blocks. Pattern (ii) occurred 13 times with interscalene and 5 times with femoral block, and pattern (iii) occurred once with each block.

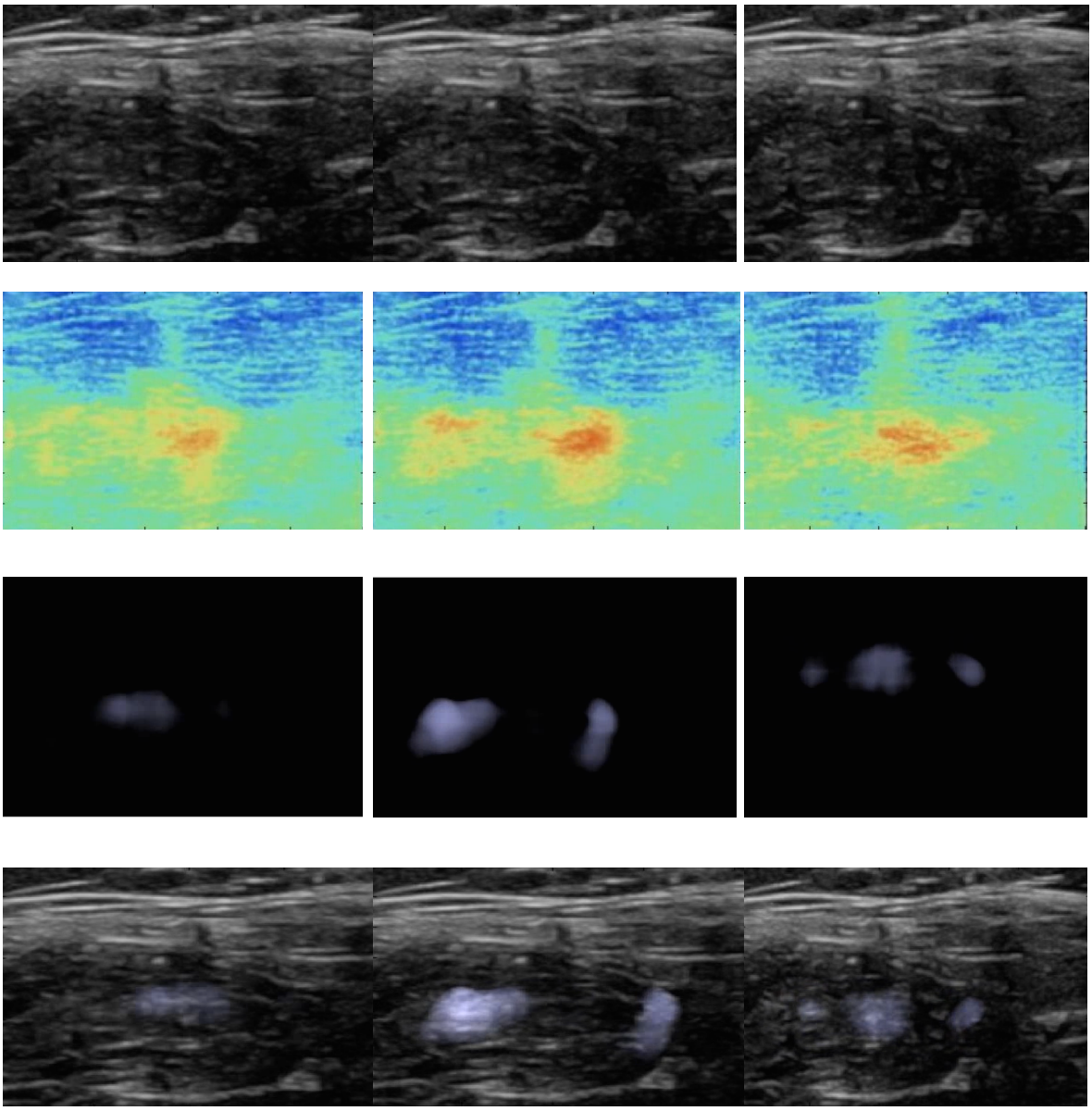

Fig 32. Bilateral displacement. Femoral block using out-of-plane needle insertion and injection of 0.5ml embalming fluid. Columns represent time immediately before injection and 0.5s, 1s and 1.5s afterwards. First row is B-Mode ultrasound image. Second row is proprietary colour elastogram. Third row is conversion of colour elastogram to black and white image. The latter is formed by iteratively choosing a brightness threshold between 0 and 255 that defines the cut-off between black and white pixels. B-Mode hydrolocation difficult to see. Femoral nerve and fascial iliaca highlighted. Colour elastogram shows needle distortion and distinct bifid pattern. Fusion pattern shows white strain pattern above the femoral nerve then bilateral displacement.

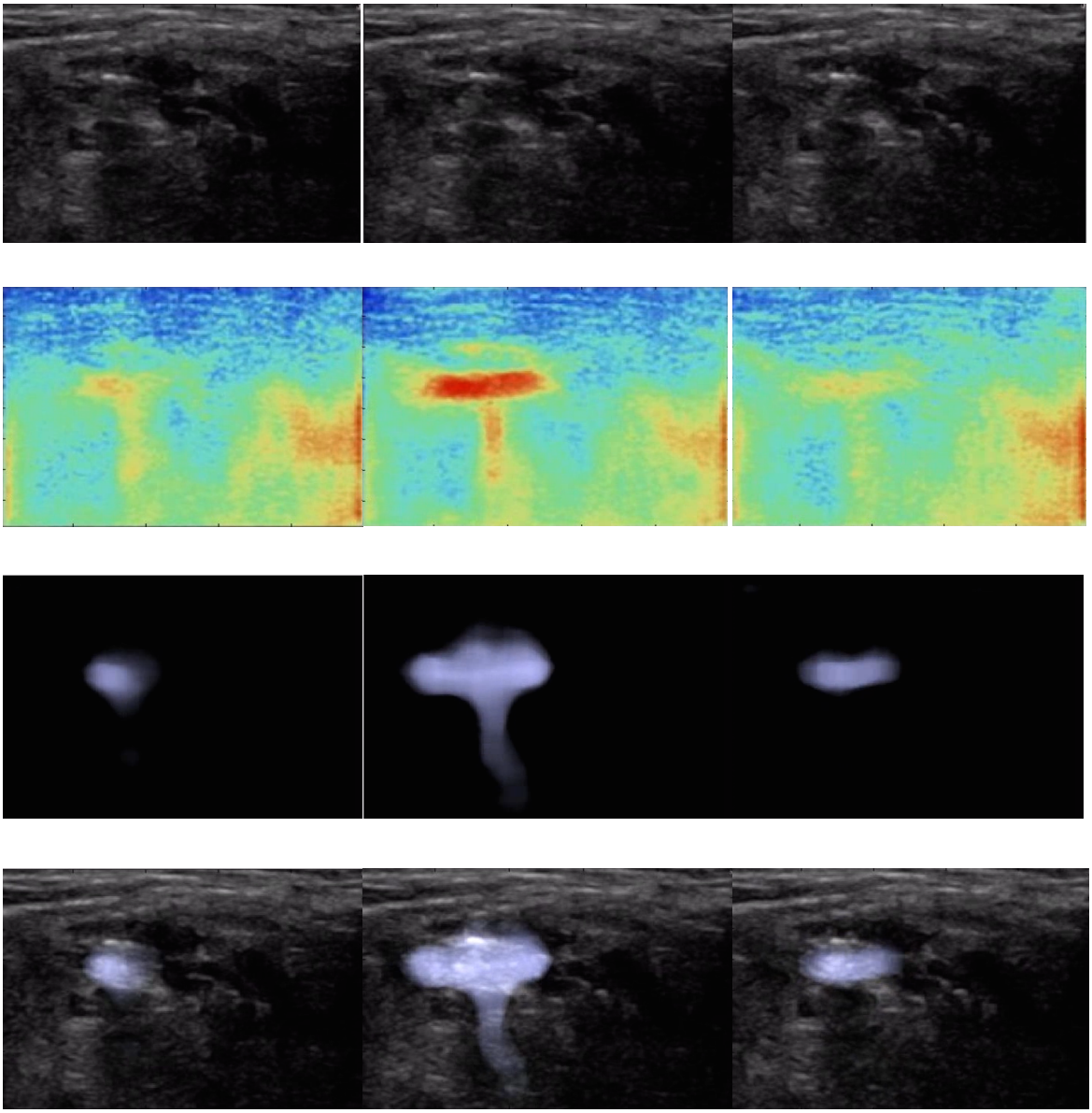

Fig 33. Distal spread. Interscalene block using in-plane needle insertion and injection of 1ml embalming fluid. Colour and fusion elastograms show distinct strain pattern flowing between C5 and C6 nerve root, and some posterior spread almost perpendicular to trajectory of needle. Continuous complex strain pattern with secondary, tangential displacement distal to injection site. Extension has different shape and size.

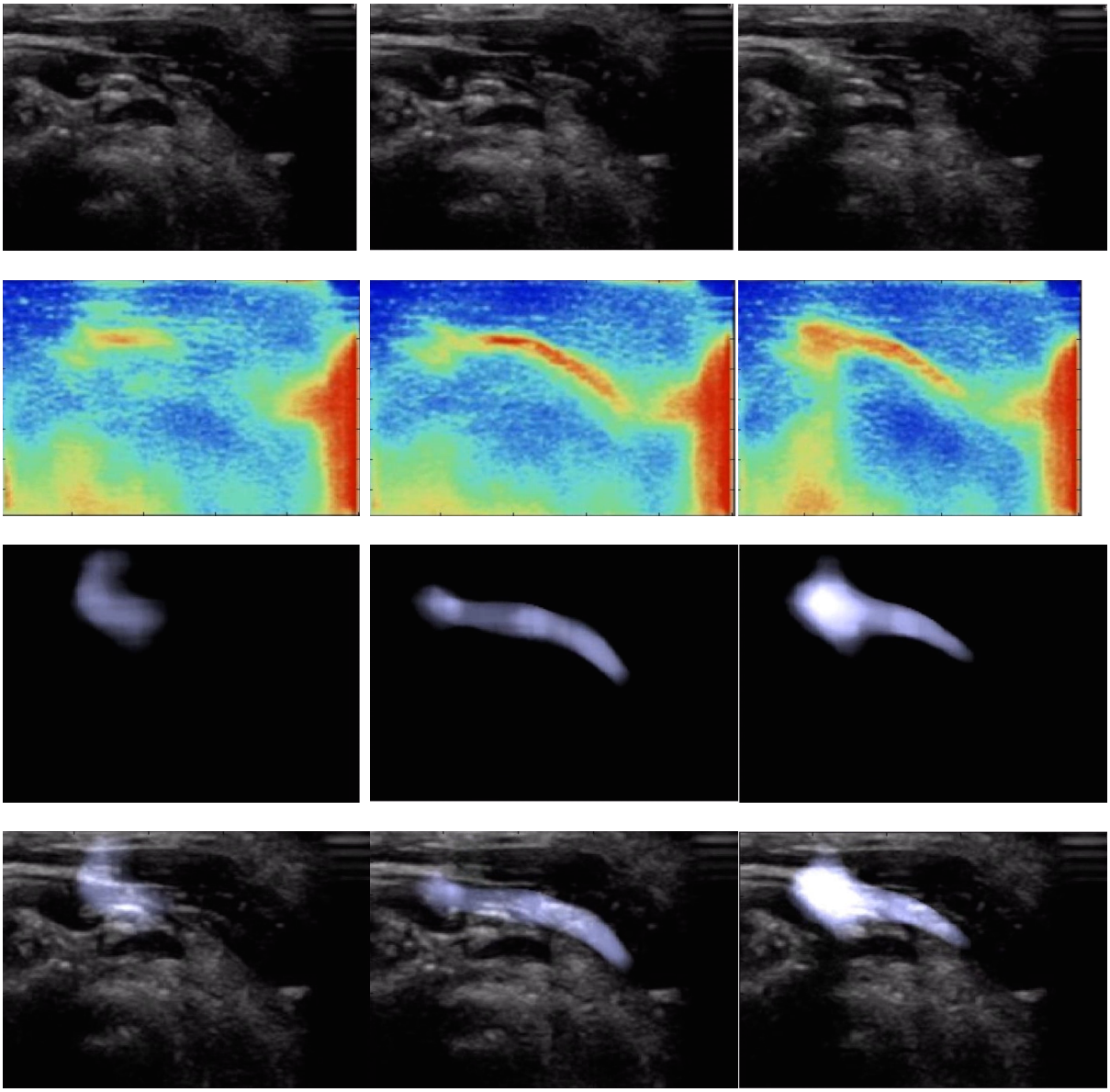

Fig 34. Recurrent displacement. Interscalene block using in-plane needle insertion and injection of 1ml embalming fluid. Columns represent time immediately before injection and 0.5s, 1s and 1.5s afterwards. First row is B-Mode ultrasound image. Second row is proprietary colour elastogram. Third row is conversion of colour elastogram to black and white image. C5 and C6 nerve roots and hydrolocation highlighted on B-Mode image. Colour and fusion elastograms show distinct strain pattern flowing from C5 nerve root posteriorly within the interscalene groove then returning and re-expanding above C5 as a brighter, more focused area.

Table 16. Number and proportion of outcomes identified by raters according to variable.

	Variable	Total (n)	Outcome	
			No. (%) 1	No. (%) 2
Rater	Consultant		192 (76%)	75 (24%)
	Trainee	1056	1920 (61%)	461(39%)
Nerve	Interscalene	1056	819 (78%)	237 (22%)
	Femoral		757 (72%)	299 (28%)
Volume	0.25	704	566 (80%)	138 (20%)
	0.5	704	521 (74%)	183 (26%)
	1.0	707	489 (69%)	215 (31%)
Block*B-Mode	Interscalene	528	463 (88%)	65 (12%)
	Femoral	528	460 (91%)	68 (9%)
Block*Elastography	Interscalene	528	356 (67%)	172 (33%)
	Femoral	528	297 (56%)	231 (44%)
Volume*B-Mode	0.25	352	322 (91%)	30 (9%)
	0.5	352	305 (87%)	47 (13%)
	1.0	352	296 (84%)	56 (16%)
Volume*Elastography	0.25	352	244 (69%)	108 (31%)
	0.5	352	216 (61%)	136 (39%)
	1.0	352	193 (55%)	159 (45%)
Volume*Interscalene	0.25	352	294 (84%)	58 (16%)
	0.5	352	272 (77%)	80 (23%)
	1.0	352	253 (72%)	99 (28%)
Volume*Femoral	0.25	352	272 (77%)	80 (23%)
	0.5	352	249 (71%)	103 (29%)
	1.0	352	236 (67%)	116 (33%)

Strain pattern area and brightness was greater than tissue displacement area and brightness on B-Mode images. Area and brightness increased from 0.25ml to 0.5ml (Table 17).

Table 17. Area and brightness of spread and fusion pattern

	Covariate	Cross-sectional area Geometric mean (95%CI)	Brightness Geometric mean (95%CI)
Mode	B Mode, perineural spread	18.5 (14.9 – 23.0)	27.5 (25.2 – 29.9)
	Elastogram, fusion	41.8 (33.7 – 51.9)	114.5 (105.1 -124.8)
Volume	0.25ml	19.7 (13.7 - 28.5)	52.3 (45.1 – 60.5)
	0.5ml	33.4 (23.1 – 48.2)	59.5 (51.4 – 68.9)
	1.0ml	32.6 (22.7 – 46.9)	56.7 (49.1 – 65.6)
Block	Interscalene	28.3 (21.0 – 38.0)	64.1 (56.9 – 72.2)
	Femoral	27.3 (20.2 – 36.9)	49.1 (43.5 – 55.3)
Mode: Volume	Fluid spread, 0.25ml	14.4 (9.9 – 21.0)	28.9 (24.9 – 33.5)
	Fluid spread, 0.5ml	19.5 (13.4 – 28.5)	27.4 (23.6 – 31.8)
	Fluid spread, 1.0ml	22.5 (15.5 – 32.6)	26.2 (22.6 – 30.4)
	Elastogram, fusion 0.25ml	27.0 (18.5 – 39.3)	94.6 (81.5 – 109.9)
	Elastogram, fusion 0.5ml	57.2 (39.2 – 83.4)	129.2 (111.1 – 150.1)
	Elastogram, fusion 1.0ml	47.3 (32.7 - 68.6)	122.9 (106.0 – 142.5)

Using stratified logistic regression, predictors of extra displacement were, in order of importance: strain elastography imaging; consultant anaesthetist assessment; volume of injectate and femoral block (Table 18)

Table 18. Logistic regression model

	Univariate analysis Odd Ratio (95%CI)	**P-value**
Volume	2.19 (1.11 – 4.31)	0.02
Nerve		
Femoral	----------	
Interscalene	0.58 (0.35 – 0.94)	0.03
Consultant	3.81 (2.29 - 6.45)	<0.001
Mode		
B-Mode	----------	
Elastography	5.31 (3.14 – 8.96)	<0.001
Nerve*Volume	1.28 (0.63 – 2.60)	0.49
Volume*Mode	1.03 (0.49 – 2.18)	0.93

5.4.5 Conclusion

This study showed improved perception of distractor tissue changes using fusion elastography compared to B-Mode ultrasound. Perception was volume dependent and better with experts compared to novices and with femoral block. Learning was facilitated over a short period but not to the level of experts.

5.4.5.1 Strengths of study

The principal strength of our study is that our results have demonstrated the utility of what Awh et al proposed in 2001, a framework for visual processing . We showed that a saliency-based approach using white enhancement of strain patterns and differences in volume drew attention to key targets for novices. Novice search and performance was enhanced in the short term, but has potential to speed up learning curves with repeated practice.

I extended my fusion elastography work on soft embalmed cadavers that showed that trainees were more likely to diagnose intraneural injection using fusion elastography. This study proved more difficult because trainees were expected to recognise low volume tissue changes. Therefore, it is not surprising that trainees could only recognise 62% of distractor patterns compared to 80% of intraneural injections as in our previous study. All trainees were able to detect perineural displacement on B-Mode images

secondary to injection of volumes between 0.25ml and 1ml, an observation that agrees with that of Krediet et al 2014 (Krediet et al, 2014).

I identified three distinct distractor patterns that varied in brightness, size and movement to target patterns, and described them as bilateral, rebound and distal. Bilateral patterns occurred in 7 femoral blocks, secondary to forceful needle nerve contact during out-of-plane needle insertion, and sideways spread of injectate. Forceful needle nerve contact and nerve haematoma has been proposed as one cause of chronic nerve damage after regional anaesthesia (Steindfelt et al, 2011). This observation suggests a need for investigation of the role of elastography along with pressure monitoring in the diagnosis of forceful needle verve contact. We hypothesise that rebound phenomena represented movement and reflection of fluid within fascial planes and therefore likely to contribute to clinical block. provides an insight into the hydrodynamics of perineural spread, an aspect of regional blockade that hitherto has not been investigated. An assumption exists in practice that flow of local anaesthetic is unidirectional. Our results suggest otherwise for test doses. We hypothesise that injectate distends tissue planes, but once wavefront pressure is insufficient to open up fascial layers, it returns as a wave to the point of origin. There is a need to investigate this phenomenon further using the range of volumes used. The distal pattern seen is likely to be associated with excessive longitudinal strain secondary to excessive transducer pressure, albeit we would expect that local anaesthetic deposition far from the nerve would be associated with similar tissue changes. My observations on elastography confirm previous work that suggests a potential clinical role detecting test doses. However, elastography should not be regarded as a surrogate for hydrolocation because strain area was greater than hydrolocation area on B-Mode images. Strain reflects relative displacement of all tissues during fluid injection, and tissue displacement depends on tissue elasticity or stiffness.

I used elastography as an experimental tool because it demonstrated white areas of strain and spatial, temporal and dynamic changes using a standard ultrasound transducer. Injections are presented as videos because tissue change using 0.25ml to 1ml is difficult to see on static images. Use of two cadavers may be regarded as a weakness but we had limited availability at the time of the study. The University of

Dundee has now converted to the whole-time use of soft embalmed cadavers and future studies will randomise to different cadavers.

I hypothesise that novices were reliant on cognitive learning, which may help detect single distinctive targets, but that this compromised their performance during multiple-target search tasks because the cognitive effort needed to match targets to expectations was overwhelming (Nakashima et al, 2013). In contrast, experts used an automatic global search strategy gained by long-term exposure to repeated images (Nakashima et al, 2013). These results show that novices had deficiencies in visual search and that improvement in visual attention was salience driven. Visual search is quantifiable using eye tracking, a technology used in other industries to quantify eye gaze fixations and saccades, and thus can create individual learning curves, and investigate the transfer of visual search and image interpretation to decision making (Kundel et al, 1978).

5.4.5.2 Weaknesses of study

Use of two cadavers may be regarded as a weakness but we had limited availability at the time of the study. The University of Dundee has now converted to whole-time use of soft embalmed cadavers and future studies will have the capacity to randomise to different cadavers. We gave limited training to anaesthetists in order to gain a baseline and compare to experienced consultants. Strain elastography is a surrogate for tissue elasticity, assumptions are made interpreting data. The relationship between stress and strain for soft tissue shows an approximately linear slope as only small forces are needed to displace tissue. With greater force, the relationship becomes curvilinear and application of large loads has little impact on strain.

Therefore, conditions that favour accurate and reliable elastography include close proximity of the transducer to the nerve (< 4cm), homogeneous tissue (e. g. liver) and constant application of force across the face of the transducer. However, strain elastography remains operator dependent and cannot be quantified because it represents relative and not absolute displacement.

6 DISCUSSION

6.1 Reappraisal of hypotheses

For discussion of my work I shall re-visit my hypotheses, stated in italics.

- *Theil soft embalmed cadavers would be useful to visualise nerves, muscles and arteries on B-Mode ultrasound images at sites commonly used for UGRA.*
- *The soft embalmed Thiel cadaver has physical properties and functional alignment such that it provides excellent simulation conditions for training ultrasound guided regional anaesthesia.*

My experimental model, the soft embalmed Thiel cadaver, demonstrated good face and content validity. It looked like, felt like and responded to perineural injection in a similar way to that experienced clinically, and was robust enough to tolerate frequent block repetition over several days. Using B-Mode ultrasound, characteristic anatomical features were discernible in the cadaver. For example, the reduced echogenicity of interscalene nerve roots in patients secondary to the high ratio of fascicles to stromal tissue and the mixed echogenicity of the femoral and median nerves were similar in cadavers to that seen when imaging patients. Blood vessels were visible but not compressible.

Simulation

The drainage properties of the soft embalmed Thiel human cadaver provided good conditions for repeated injections. My results showed that elastogram area did not change with sequential 1ml or 5ml injections, even when administered every 5 to 10 minutes, and provides excellent conditions for UGRA simulation. Retention of anatomical integrity is important because it encourages ”suspension of belief” during simulated training, and permits novices to practice repeatability in a safe environment. Moreover, it also allows adoption of learning techniques such as mastery learning and dedicated practice otherwise not used with traditional destructive models such as plastic phantoms(Adhikary et al 2013), tofu, animal tissue, and fresh frozen cadavers(Hocking et al 2011). My study is prescient because the drive to improve safety and quality in healthcare, allied to limitations in anaesthesia training time has encouraged the development of simulation outside the operating room(Flin et al 2010), and as yet UGRA simulated training is limited to low fidelity models and teaching is unstructured.

The results of this study helped inform the University of Dundee to build a new state of the art Thiel facility costing £2.5 million, 40% of which was paid for by local fundraising, http://www.millionforamorgue.com/new-forensic-centre-of-excellence. The facility now handles 80 Thiel embalmed cadavers per year for medical and dental teaching and has successfully hosted the first mastery learning UGRA course for anaesthetists sitting the MSc in regional anaesthesia at the University of East Anglia.

Textured needles were more visible than smooth surfaced needles, that visibility was not dependant on needle gauge and was improved in-plane and out-of-plane to the ultrasound transducer.

My needle study showed that, as with patients textured needles were visualised better in the soft embalmed Thiel cadaver compared to non-textured needles. Futhermore, I showed that the effect of texturing on visibility was better than that of needle size and enabled me to standardise my needle to a single shot textured 21g shaft.

Elastography was able to capture tissue displacement in colour using 1ml volumes of embalming fluid, representative of test doses of local anaesthetics in patients.

Elastography is a relatively cheap ultrasound based technology that captured real-time events in colour. It Identified tissue strain, the relative displacement of both fluid and surrounding tissue. I showed that, as expected, the elastogram and fusion patterns were much larger than equivalent hydrolocation on B-Mode images because the size of the strain pattern varied according to the relative stiffness of surrounding tissue.

However some caution should be exercised when interpreting strain images. Strain elastography remains operator dependent and cannot be quantified because it represents relative and not absolute displacement. Strain elastography is also a surrogate measure of tissue elasticity, defined as $\frac{stress}{strain}$ and mathematical assumptions are made. The relationship between stress and strain for soft tissue shows an approximately linear slope when applying small forces to displace tissue, but with greater force, the relationship becomes curvilinear and application of large loads has little impact on strain. Therefore, conditions that favour accurate and reliable elastography include close proximity of the transducer to the nerve (< 4cm),

homogeneous tissue (e. g. liver) and constant application of force across the face of the transducer.

- *Software conversion of the elastography image had the potential to provide an objective measure of hydrolocation*
- *Strain patterns were readily seen secondary to injection of 5ml embalming fluid*
- *A dose response existed between 0.25ml and 7.5ml to injection of perineural volumes.*
- *Strain elastography differentiated between intraneural injection and extraneural injection*

For the aforementioned reasons, I considered whether application of strain elastography would be more pertinent if strain images were contained within the confines of an anatomical structure whose walls were relatively stiff, resistant to deformation and provide a consistent response to injection. The model that fitted these requirements was intraneural injection. Nerves have a thick, stiff epineurium and relatively compliant interfascicular stromal tissue, and I hypothesized that strain elastography could differentiate between intraneural and extraneural injection.

However, in order to test this hypothesis I had to combine B-Mode and elastogram images before testing on trainees, because interpretation of two screens is almost impossible at the same time. The results showed that novices were more likely to diagnose intraneural injection using fusion elastography because the fusion image, irrespective of volume, overlay of the nerve and any tendency to expand in size was restricted by the stiff epineurium. Fluid dissipated up and down the length of the needle through interfascicular tissue presumably following the path of least resistance. In comparison, extraneural strain images increased with volume and spread inconsistently over muscle.

- *Strain patterns identified additional features during perineural injection otherwise hidden on B-Mode images*

I did not consider extraneural strain patterns as diagnostic markers because their patterns were inconsistent. However, within early studies I noticed that extraneural strain was not a simple response to perineural injection and that many other events

were occurring that were not apparent on B-Mode imaging. Using fusion elastograms trainees and consultants identified bilateral patterns of strain consistent with forceful needle nerve contact, distal dispersion of fluid away from the block site and a rebound phenomenon never previously described.

Taken together my results suggest that elastography is a visual technology that has broad benefits. Table 19 summarises the efficacy of current interventions such as B-Mode ultrasound, PNS and pressure monitoring compared to elastography in detecting detecting intraneural injection, needle nerve contact, perineural fluid displacement and distal flow. Overall elastography appears to supplement other modalities and suggests that its role in gauging the exact position of the needle tip is worthy of further investigation.

Table 19. Summary of efficacy of methods used to identify peripheral nerves, including elastography + least effect, ++++ greatest effect

	Intraneural	**Forceful needle-nerve contact**	**Perineural**	**Extraneural**
B-Mode	++	++	+++	++
Elastography	+++	++	+++	+++
PNS	++	+	++	+
Pressure	+++	+++	+	+

- *Shear wave elastography imaged peripheral nerves in colour*
- *Shear wave elastography quantified the stiffness of nerves and surrounding tissue in cadavers and humans*
- *The coloured ROI mapped by SWE was similar in size to the cross-sectional area of the underlying nerve.*

Shear wave elastography presented the first colour images of nerves, but cannot be considered as a realistic UGRA interventional tool. Time to build the elastogram was

perceptively slow and the coloured shear image did not overlap nerves closely enough nor provide sufficient epineural and subepineural detail to justify clinical application. Nevertheless shear wave elastography proved useful validation of the cadaver. Measurements of interscalene and sciatic stiffness reflected available human data, both with regard to absolute measurements and confirmed the 2 to 3 fold difference between neural and perineural Young's modulus that we had previously noted(Munirama et al 2013). A recent study investigating the stiffness of head and neck glandular tissue and muscle showed that Young's modulus was approximately 20% higher in Thiel embalmed cadavers compared to historical data on volunteers(Joy et al 2015), and fits with our results. High stiffness of the median nerve in the soft embalmed cadaver (consistent with recent work by Kantarci and colleagues(Kantarci et al 2014) and low stiffness in the sciatic nerve reflects the site-specific values measured in our volunteers. High median nerve stiffness in our cadavers was similar to results from a study in volunteers, particularly when matched for age(Eby et al 2015), and probably reflects the deterioration of muscle morphology and increased muscle stiffness in the sixth to seventh decade.

6.2 Future work

6.2.1 Soft embalmed Thiel cadaver

Our experience is that different tissues are preserved with different degrees of flexibility, which may affect the elasticity of individual structures and the spread of fluid between tissue planes. Some cadavers provide excellent views of specific blocks and some cadavers excellent views of other blocks. The reason for this is unknown. The cadavers lack a circulation and are not ventilated routinely. The University of Dundee has now converted to whole-time use of soft embalmed cadavers and future studies will have the capacity to randomise to different cadavers.

6.2.2 Simulation

Our next step is to use the cadaver as an educational tool for the teaching of specialist UGRA trainees in the first instance (Meyer et al 2012). We will need to validate the educational process, learning outcomes and assessment of competency(Neal 2012). Unlike the traditional clinical apprentice model, a stable, high fidelity simulator should offer the opportunity to provide measurable,

consistent training by standardizing teaching, assessment and learning (Burckett-St Laurent et al 2014).

Provision of a high fidelity simulator does not equate with better training effectiveness(Hamstra et al 2014), and we need to test the dynamics of this simulator within a variety of simulation-based scenarios allied to educational need. Ultimately any simulator should be judged on its capacity to enhance personal learning irrespective of its appearance. Nevertheless we anticipate that both the appearance and dynamic response of our simulator can suspend belief sufficiently to enhance the quality of regional anaesthesia training and translate it to patient care(Maran & Glavin 2003). We do not as yet know which trainees benefit from training on the soft embalmed cadaver and studies are needed to match task difficulty and simulator complexity with educational needs and pre-existing skills (Hamstra et al 2014).

6.2.3 Fusion elastography

Real-time detection of intraneural injection remains a challenge in clinical practice because ultrasound equipment and operators lack sufficient confidence and accuracy. Increase in clinical morbidity such as obesity, diabetes and age-related chronic illness will increase the need for UGRA but, as such, will be technically more difficult. We have shown that fusion elastography may be a valuable diagnostic training aid and, indicated that it has the potential for further development as a visible warning signal that may prevent further harm. Moreover, it is the first durable simulator of intraneural injection, and incorporation of this technology allied to haptic feedback would provide a valuable training tool. Development of an accurate and reliable clinical detector of intraneural injection will probably require a computing solution such as machine learning in order to extract and analyse image data. The advantage of using computers is that diagnosis would be instant, and visualised or heard as an alarm, and algorithms would automatically improve with increased use.

6.2.4 Micro-ultrasound

Outwith training, I see application of strain and shear wave elastography to micro-

ultrasound. Clinical ultrasound systems have insufficient resolution to image nerves in detail, and anaesthetists have difficulty interpreting the anatomical relationships between the tip of the needle, connective tissue, epineurium, and intraneural nerve anatomy. No technology is currently available to clinicians that differentiate between subepineural and subperineural tissue during needle insertion. However micro-ultrasound, commonly used for pre-clinical imaging has image resolution suitable for visualising neural anatomy(Foster et al 2011). Micro-ultrasound uses transducer frequencies between 20 MHz and 100 MHz and offers resolution of anatomy between 150 μm and 30 μm respectively. Micro-ultrasound using a single element transducer has been used to identify the epidural space(Chiang et al 2011), used in a needle to aid neurosurgical guidance to targets in fresh porcine and soft embalmed cadaver models(Jiang et al 2016) and has been used in a real-time imaging system to visualise cutaneous nerves in the hand and wrist(Stokvis et al 2009).

Our recent study was the first UGRA study to show that micro-ultrasound imaging of peripheral nerves is feasible, and enabled us to differentiate for the first time between subepineural and subperineural needle insertion using micro-ultrasound images. We visualised rotation and elasticity of fascicles in response to needle tip pressure and mechanical trauma to fascicles in response to forceful needle insertion.

Our results indicate that micro-ultrasound supplements the use of histology and electrophysiology in intraneural injection experiments because it provides visible evidence of subepineural and subperineural morphology and trauma. We readily recognised fascicles as round, hypoechoic areas, and subepineural tissue as bright echogenic tissue residing between fascicles. Our results showed fascicle rotation secondary to subepineural needle insertion but we also observed that nerve fascicles are elastic and return to their original position after removal of the needle. Alarmingly, subperineural needle insertion traumatically split a fascicle into two, and segments failed to revert to pre-injection. Current bioengineering work has developed a 16 element array that can fit onto the end of a Tuohy needle. Researchers using new ultrasound machines from Verasonix, Seattle and Visualsonics, Toronto can program strain and shear wave elastography into ultrasound arrays. I forsee futute microultrasound needles with the capacity to visualise intraneural contents accurately

using 30MHz to 50MHz transducers, strain elastography to visualise intraneural injection or extraneural spread and shear wave elastography to visualise and quantify stiff barriers such as the epineurium and perineurium.

REFERENCES

Abdallah FW, Macfarlane AJ, et al. 2016. The Requisites of Needle-to-Nerve Proximity for Ultrasound-Guided Regional Anesthesia: A Scoping Review of the Evidence. *Reg Anesth Pain Med* 41: 221-8

Abrahams MS, Aziz MF, et al. 2009. Ultrasound guidance compared with electrical neurostimulation for peripheral nerve block: a systematic review and meta-analysis of randomized controlled trials. *Br J Anaesth* 102: 408-17

Adhikary SD, Hadzic A, et al 2013. Simulator for teaching hand-eye coordination during ultrasound-guided regional anaesthesia. *Br J Anaesth* 111: 844-5

Aldrete JA. 2003. Neurologic deficits and arachnoiditis following neuroaxial anesthesia. *Acta Anaesthesiol Scand* 47: 3-12

Auroy Y, Benhamou D, et al. 2002. Major complications of regional anesthesia in France: The SOS Regional Anesthesia Hotline Service. *Anesthesiology* 97: 1274-80

Auroy Y, Narchi P, et al. 1997. Serious complications related to regional anesthesia: results of a prospective survey in France. *Anesthesiology* 87: 479-86

Awh E, Belopolsky AV, et al. 2012. Top-down versus bottom-up attentional control: a failed theoretical dichotomy. *Trends Cogn Sci* 2012; **16**: 437-43

Balthasar A, Desjardins AE, et al. 2012. Optical detection of peripheral nerves: an in vivo human study. *Reg Anesth Pain Med* 37: 277-82

Barr RG, Memo R, et al. 2012. Shear wave ultrasound elastography of the prostate: initial results. *Ultrasound quarterly* 28: 13-20

Barrington MJ. 2012. International registries of regional anesthesia: Are we ready to collaborate in virtual departments of anesthesiology? *Reg Anesth Pain Med* 37: 467-9

Barrington MJ, Kluger R. 2013. Ultrasound guidance reduces the risk of local anesthetic systemic toxicity following peripheral nerve blockade. *Reg Anesth Pain Med* 38: 289-99

Barrington MJ, Snyder GL. 2011. Neurologic complications of regional anesthesia. *Curr Opin Anaesthesiol* 24: 554-60

Bartlett JW, Frost C. 2008. Reliability, repeatability and reproducibility: analysis of measurement errors in continuous variables. *Ultrasound Obstet Gynecol* 31: 466-75

Bercoff J. 2011. Ultrafast Ultrasound Imaging In *Ultrasound Imaging - Medical Applications*, ed. O Minin

Bigeleisen PE. 2006. Nerve puncture and apparent intraneural injection during ultrasound-guided axillary block does not invariably result in neurologic injury. *Anesthesiology* 105: 779-83

Bigeleisen PE, Moayeri N, et al. 2009. Extraneural versus intraneural stimulation thresholds during ultrasound-guided supraclavicular block. *Anesthesiology* 110: 1235-43

Borgeat A, Ekatodramis G. 2001. Nerve injury associated with regional anesthesia. *Curr Top Med Chem* 1: 199-203

Brinkmann S, Tang R, et al. 2013. Single-operator real-time ultrasound-guided spinal injection using SonixGPS: a case series. *Can J Anaesth* 60: 896-901

Brull R, Hadzic A, Reina MA, et al. 2015. Pathophysiology and Etiology of Nerve Injury Following Peripheral Nerve Blockade. *Reg Anesth Pain Med* 40: 479-90

Brull R, McCartney CJ, et al. 2007. Neurological complications after regional anesthesia: contemporary estimates of risk. *Anesth Analg* 104: 965-74

Brynolf M, Sommer M, Desjardins AE, et al. 2011. Optical detection of the brachial plexus for peripheral nerve blocks: an in vivo swine study. *Reg Anesth Pain Med* 36: 350-7

Burckett-St Laurent DA, et al. 2014. A valid and reliable assessment tool for remote simulation-based ultrasound-guided regional anesthesia. *Reg Anesth Pain Med* 39: 496-501

Carstensen B, Simpson J, et al. 2008. Statistical models for assessing agreement in method comparison studies with replicate measurements. *Int J Biostat* 4: Article 16

Cash CJ, Sardesai AM, et al. 2005. Spatial mapping of the brachial plexus using three-dimensional ultrasound. *The British Journal of radiology* 78: 1086-94

Chan VW, Brull R, et al. 2007. An ultrasonographic and histological study of intraneural injection and electrical stimulation in pigs. *Anesth Analg* 104: 1281-4, tables of contents

Chandra A, Hu Q, et al, et al. 2014. Visualising needle nerve trauma using High Frequency Ultrasound *British Jjournal of anaesthesia*

Chiang HK, Zhou Q, et al. 2011. Eyes in the needle: novel epidural needle with embedded high-frequency ultrasound transducer--epidural access in porcine model. *Anesthesiology* 114: 1320-4

Chun MM, Jiang Y. 1998. Contextual cueing: implicit learning and memory of visual context guides spatial attention. *Cogn Psychol* 1998; **36**: 28-71

Claudio R, Hadzic A, et al. 2004. Injection pressures by anesthesiologists during simulated peripheral nerve block. *Reg Anesth Pain Med* 29: 201-5

Clendenen SR, Robards CB, et al 2010. Real-time 3-dimensional ultrasound-assisted infraclavicular brachial plexus catheter placement: implications of a new technology. *Anesthesiol Res Pract* 2010

Cohen JM, Gray AT. 2010. Functional deficits after intraneural injection during interscalene block. *Reg Anesth Pain Med* 35: 397-9

Cox CR, Checketts MR, et al. 1998. Comparison of S(-)-bupivacaine with racemic (RS)-bupivacaine in supraclavicular brachial plexus block. *Br J Anaesth* 80: 594-8

Desjardins AE, Hendriks BH, et al. 2011. Epidural needle with embedded optical fibers for spectroscopic differentiation of tissue: ex vivo feasibility study. *Biomed Opt Express* 2: 1452-61

Ebell M, Information Mastery, FP Essentials AAFP Home Study Edition, No 318, American Academy Of Family Physicians, 2005

Eby SF, Cloud BA, et al. 2015. Shear wave elastography of passive skeletal muscle stiffness: Influences of sex and age throughout adulthood. *Clinical biomechanics* 30: 22-7

Eckstein MP. 2011. Visual search: a retrospective. *J Vis* 2011; **11**: 1-36.

Evans A, Whelehan P, et al. 2012. Differentiating benign from malignant solid breast masses: value of shear wave elastography according to lesion stiffness combined with greyscale ultrasound according to BI-RADS classification. *Br J Cancer* 107: 224-9

Evans A, Whelehan P, et al. 2010. Quantitative shear wave ultrasound elastography: initial experience in solid breast masses. *Breast Cancer Res* 12: R104

Fanelli G, Casati A, et al. 1999. Nerve stimulator and multiple injection technique for upper and lower limb blockade: failure rate, patient acceptance, and neurologic complications. Study Group on Regional Anesthesia. *Anesth Analg* 88: 847-52

Farber SJ, Saheb-Al-Zamani M, et al. 2013. Peripheral nerve injury after local anesthetic injection. *Anesth Analg* 117: 731-9

Feinglass NG, Clendenen SR, et al. 2007. Real-time three-dimensional ultrasound for continuous popliteal blockade: a case report and image description. *Anesth Analg* 105: 272-4

Fenster A, Parraga G, Bax J. 2011. Three-dimensional ultrasound scanning. *Interface Focus* 1: 503-19

Flin R, Patey R, et al, 2010. Anaesthetists' non-technical skills. *Br J Anaesth* 105: 38-44

Foster FS, Hossack J, et al. 2011. Micro-ultrasound for preclinical imaging. *Interface Focus* 1: 576-601

Fredrickson MJ, Kilfoyle DH. 2009. Neurological complication analysis of 1000 ultrasound guided peripheral nerve blocks for elective orthopaedic surgery: a prospective study. *Anaesthesia* 64: 836-44

Gadsden J, Latmore M, et al. 2015. Evaluation of the eZono 4000 with eZGuide for ultrasound-guided procedures. *Expert Rev Med Devices* 12: 251-61

Gelfand HJ, Ouanes JP, et al. 2011. Analgesic efficacy of ultrasound-guided regional anesthesia: a meta-analysis. *J Clin Anesth* 23: 90-6

Gentili F, Hudson AR, et al. 1980. Nerve injection injury with local anesthetic agents: a light and electron microscopic, fluorescent microscopic, and horseradish peroxidase study. *Neurosurgery* 6: 263-72

Guo S, McLeod G, et al. 2012. Echogenic regional anaesthesia needles: a comparison study in Thiel cadavers. *Ultrasound Med Biol* 38: 702-7

Hadzic A, Shah S, et al. 2004. Combination of intraneural injection and high injection pressure leads to fascicular injury and neurologic deficits in dogs. *Reg Anesth Pain Med* 29: 417-23

Hamstra SJ, Brydges R, et al. 2014. Reconsidering fidelity in simulation-based training. *Academic medicine : journal of the Association of American Medical Colleges* 89: 387-92

Hara K, Sakura S, et al. 2014. The role of electrical stimulation in ultrasound-guided subgluteal sciatic nerve block: a retrospective study on how response pattern and minimal evoked current affect the resultant blockade. *J Anesth* 28: 524-31

Hara K, Sakura S, et al. 2012. Incidence and effects of unintentional intraneural injection during ultrasound-guided subgluteal sciatic nerve block. *Reg Anesth Pain Med* 37: 289-93

Hebard S, Hocking G. 2011. Echogenic technology can improve needle visibility during ultrasound-guided regional anesthesia. *Reg Anesth Pain Med* 36: 185-9

Hocking G, Hebard S, et al. 2011. A review of the benefits and pitfalls of phantoms in ultrasound-guided regional anesthesia. *Reg Anesth Pain Med* 36: 162-70

Hogan QH. 2008. Pathophysiology of peripheral nerve injury during regional anesthesia. *Reg Anesth Pain Med* 33: 435-41

Jiang Y, Qiu Z, McPhillips R, et al. 2016. Dual Orientation 16-MHz Single-Element Ultrasound Needle Transducers for Image-Guided Neurosurgical Intervention. *IEEE Trans Ultrason Ferroelectr Freq Control* 63: 233-44

Joy J, McLeod G, et al. 2015. Quantitative assessment of Thiel soft-embalmed human cadavers using shear wave elastography. *Ann Anat* 202: 52-6

Kantarci F, Ustabasioglu FE, et al. 2014. Median nerve stiffness measurement by shear wave elastography: a potential sonographic method in the diagnosis of carpal tunnel syndrome. *European Radiology* 24: 434-40

Kapur E, Vuckovic I, et al. 2007. Neurologic and histologic outcome after intraneural injections of lidocaine in canine sciatic nerves. *Acta Anaesthesiol Scand* 51: 101-7

Karmakar M, Li J, et al. 2012. Three-dimensional/four-dimensional volumetric ultrasound imaging of the sciatic nerve. *Reg Anesth Pain Med* 37: 60-6

Karmakar MK, Li X, et al 2012b. Volumetric three-dimensional ultrasound imaging of the anatomy relevant for thoracic paravertebral block. *Anesth Analg* 115: 1246-50

Kaur B, Vaghadia H, et al. 2013. Real-time thoracic paravertebral block using an ultrasound-guided positioning system. *Br J Anaesth* 110: 852-3

Kirchmair L, Strohle M, et al. 2016. Neurophysiological effects of needle trauma and intraneural injection in a porcine model: a pilot study. *Acta Anaesthesiol Scand* 60: 393-9

Kitagawa N, Oda et al. 2004. Possible mechanism of irreversible nerve injury caused by local anesthetics: detergent properties of local anesthetics and membrane disruption. *Anesthesiology* 100: 962-7

Krediet AC, Moayeri N, et al. 2014. Intraneural or extraneural: diagnostic accuracy of ultrasound assessment for localizing low-volume injection. *Reg Anesth Pain Med* 39: 409-13

Krupinski EA. The role of perception in imaging: past and future. *Semin Nucl Med* 2011; **41**: 392-40

Krupinski EA, Tillack AA, et al. Eye-movement study and human performance using telepathology virtual slides: implications for medical education and differences with experience. *Hum Pathol* 2006; **37**: 1543-56

Kundel HL, Nodine CF, et al Visual scanning, pattern recognition and decision-making in pulmonary nodule detection. *Invest Radiol* 1978; **13**: 175-81

Kuo WC, Kao MC, et al. 2015. Fiber-needle swept-source optical coherence tomography system for the identification of the epidural space in piglets. *Anesthesiology* 122: 585-94

Landis JR, Koch GG, et al 1977. The measurement of observer agreement for categorical data. *Biometrics* 33: 159-74

Liao X, Corner G, et al. 2016. Differentiation between epidural tissues using a novel piezoelectric sensing Tuohy needle. *Br J Anaesth* 116: e939

Lirk P, Haller I, Myers RR, et al. 2006. Mitigation of direct neurotoxic effects of lidocaine and amitriptyline by inhibition of p38 mitogen-activated protein kinase in vitro and in vivo. *Anesthesiology* 104: 1266-73

Liu SS, YaDeau JT, et al. 2011. Incidence of unintentional intraneural injection and postoperative neurological complications with ultrasound-guided interscalene and supraclavicular nerve blocks. *Anaesthesia* 66: 168-74

Lupu CM, Kiehl TR, et al. 2010. Nerve expansion seen on ultrasound predicts histologic but not functional nerve injury after intraneural injection in pigs. *Reg Anesth Pain Med* 35: 132-9

Maran NJ, Glavin RJ. 2003. Low- to high-fidelity simulation - a continuum of medical education? *Medical education* 37 Suppl 1: 22-8

McLeod G, Hales T. 2015. *Local Anaesthetic Agents. In: Smith and Aitkenhead's Textbook of Anaesthesia*. Elsevier.

McVicar J, Niazi AU, et al. 2015. Novice performance of ultrasound-guided needling skills: effect of a needle guidance system. *Reg Anesth Pain Med* 40: 150-3

Melloni L, van Leeuwen S, et al. 2012. Interaction between bottom-up saliency and top-down control: how saliency maps are created in the human brain. *Cereb Cortex* 2012; **22**: 2943-52

Meyer GF, Wong LT, et al 2012. Objective fidelity evaluation in multisensory virtual environments: auditory cue fidelity in flight simulation. *PloS one* 7: e44381

Moayeri N, Bigeleisen PE, et al. 2008. Quantitative architecture of the brachial plexus and surrounding compartments, and their possible significance for plexus blocks. *Anesthesiology* 108: 299-304

Moayeri N, Groen GJ. 2009. Differences in quantitative architecture of sciatic nerve may explain differences in potential vulnerability to nerve injury, onset time, and minimum effective anesthetic volume. *Anesthesiology* 111: 1128-34

Moore T, Zirnsak M. Neural Mechanisms of Selective Visual Attention. *Annu Rev Psychol* 2017; **68**: 47-72

Munirama S, Joy J, et al. 2013. Images in anesthesiology: shear wave elastography: novel technology for ultrasound-guided regional anesthesia. *Anesthesiology* 119: 698

Munirama S, Satapathy AR, et al. 2012. Translation of sonoelastography from Thiel cadaver to patients for peripheral nerve blocks. *Anaesthesia* 67: 721-8

Munirama S, Zealley K, et al. Trainee anaesthetist diagnosis of intraneural injection-a study comparing B-mode ultrasound with the fusion of B-mode and elastography in the soft embalmed Thiel cadaver model. *Br J Anaesth* 2016; **117**: 792-800

Myers RR, Heckman HM. 1989. Effects of local anesthesia on nerve blood flow: studies using lidocaine with and without epinephrine. *Anesthesiology* 71: 757-62

Myles PS, Cui J. 2007. Using the Bland-Altman method to measure agreement with repeated measures. *Br J Anaesth* 99: 309-11

Nakashima R, Kobayashi K, et al. 2013. Visual search of experts in medical image reading: the effect of training, target prevalence, and expert knowledge. *Front Psychol* 2013; **4**: 166

Neal JM. 2012. Education in regional anesthesia: caseloads, simulation, journals, and politics: 2011 Carl Koller Lecture. *Reg Anesth Pain Med* 37: 647-51

Neal JM, Barrington MJ, et al. 2015. The Second ASRA Practice Advisory on Neurologic Complications Associated With Regional Anesthesia and Pain Medicine: Executive Summary 2015. *Reg Anesth Pain Med* 40: 401-30

Neal JM, Brull R, et al. 2010. The ASRA evidence-based medicine assessment of ultrasound-guided regional anesthesia and pain medicine: Executive summary. *Reg Anesth Pain Med* 35: S1-9

Newton DJ, McLeod GA, et al. 2005. Vasoactive characteristics of bupivacaine and levobupivacaine with and without adjuvant epinephrine in peripheral human skin. *Br J Anaesth* 94: 662-7

Newton DJ, McLeod GA, et al. 2007. Mechanisms influencing the vasoactive effects of lidocaine in human skin. *Anaesthesia* 62: 146-50

Newton DJ, Sur EL, et al 2003. Mechanisms contributing to the vaso-active effects of prilocaine in human skin. *Anaesthesia* 58: 6-10

Niazi AU, Chin KJ, et al. 2014. Real-time ultrasound-guided spinal anesthesia using the SonixGPS ultrasound guidance system: a feasibility study. *Acta Anaesthesiol Scand* 58: 875-81

Ophir J, Cespedes I, et al 1991. Elastography: a quantitative method for imaging the elasticity of biological tissues. *Ultrason Imaging* 13: 111-34

Orebaugh SL, McFadden K, et al. 2010. Subepineurial injection in ultrasound-guided interscalene needle tip placement. *Reg Anesth Pain Med* 35: 450-4

Orebaugh SL, Mukalel JJ, et al. 2012. Brachial plexus root injection in a human cadaver model: injectate distribution and effects on the neuraxis. *Reg Anesth Pain Med* 37: 525-9

Palmeri ML, Nightingale KR. 2011. Acoustic radiation force-based elasticity imaging methods. *Interface Focus* 1: 553-64

Partridge BL. 1991. The effects of local anesthetics and epinephrine on rat sciatic nerve blood flow. *Anesthesiology* 75: 243-50

Perez-Castro R, Patel S, et al. 2009. Cytotoxicity of local anesthetics in human neuronal cells. *Anesth Analg* 108: 997-1007

Perlas A, Niazi A, et al. 2006. The sensitivity of motor response to nerve stimulation and paresthesia for nerve localization as evaluated by ultrasound. *Reg Anesth Pain Med* 31: 445-50

Perris TM, Watt JM. 2003. The road to success: a review of 1000 axillary brachial plexus blocks. *Anaesthesia* 58: 1220-4

Pong RP, Gmelch BS, et al. 2009. Does a paresthesia during spinal needle insertion indicate intrathecal needle placement? *Reg Anesth Pain Med* 34: 29-32

Radwan IA, Saito S, et al. 2002. The neurotoxicity of local anesthetics on growing neurons: a comparative study of lidocaine, bupivacaine, mepivacaine, and ropivacaine. *Anesth Analg* 94: 319-24

Rathmell JP, Desjardins AE, et al. 2010. Identification of the epidural space with optical spectroscopy: an in vivo swine study. *Anesthesiology* 113: 1406-18

Reiss W, Kurapati S, et al 2010. Nerve injury complicating ultrasound/electrostimulation-guided supraclavicular brachial plexus block. *Reg Anesth Pain Med* 35: 400-1

Robards C, Hadzic A, et al. 2009. Intraneural injection with low-current stimulation during popliteal sciatic nerve block. *Anesth Analg* 109: 673-7

Rodriguez J, Taboada M, et al. 2008. Intraneural catheterization of the sciatic nerve in humans: a pilot study. *Reg Anesth Pain Med* 33: 285-90

Sadiq M. 2015. http://www.activeneedle.com/services/.

Sala Blanch X, Lopez AM, et al. 2009. Intraneural injection during nerve stimulator-guided sciatic nerve block at the popliteal fossa. *Br J Anaesth* 102: 855-61

Sala-Blanch X, Lopez AM, 2011. No clinical or electrophysiologic evidence of nerve injury after intraneural injection during sciatic popliteal block. *Anesthesiology* 115: 589-95

Sala-Blanch X, Ribalta T, et al. 2009. Structural injury to the human sciatic nerve after intraneural needle insertion. *Reg Anesth Pain Med* 34: 201-5

Sauter AR, Dodgson MS, et al. 2009. Current threshold for nerve stimulation depends on electrical impedance of the tissue: a study of ultrasound-guided electrical nerve stimulation of the median nerve. *Anesth Analg* 108: 1338-43

Sauter AR, Dodgson MS, et al. 2007. Ultrasound controlled nerve stimulation in the elbow region: high currents and short distances needed to obtain motor responses. *Acta Anaesthesiol Scand* 51: 942-8

Schafhalter-Zoppoth I, et al. 2004. Ultrasound visibility of needles used for regional nerve block: an in vitro study. . *Regional Anesthesia and Pain Medicine* 29: 480-88

Scolaro L, Lorenser D, et al. 2012. High-sensitivity anastigmatic imaging needle for optical coherence tomography. *Optics letters* 37: 5247-9

Selander D, Dhuner KG, et al. 1977. Peripheral nerve injury due to injection needles used for regional anesthesia. An experimental study of the acute effects of needle point trauma. *Acta Anaesthesiol Scand* 21: 182-8

Selander D, Edshage S, et al. 1979. Paresthesiae or no paresthesiae? Nerve lesions after axillary blocks. *Acta Anaesthesiol Scand* 23: 27-33

Selander D, Sjostrand J. 1978. Longitudinal spread of intraneurally injected local anesthetics. An experimental study of the initial neural distribution following intraneural injections. *Acta Anaesthesiol Scand* 22: 622-34

Simons DJ, Ambinder MS. Change blindness: Theory and consequences. *Current Directions in Psychological Science* 2005; **14**: 44-8

Sim YT, Vinnicombe S, et al. 2015. Value of shear-wave elastography in the diagnosis of symptomatic invasive lobular breast cancer. *Clin Radiol* 70: 604-9

Sinha SK, Abrams JH, et al. 2007. Ultrasound-guided interscalene needle placement produces successful anesthesia regardless of motor stimulation above or below 0.5 mA. *Anesth Analg* 105: 848-52

Sites BD, Spence BC, et al. 2007. Characterizing novice behavior associated with learning ultrasound-guided peripheral regional anesthesia. *Reg Anesth Pain Med* 32: 107-15

Sites BD, Taenzer AH, et al. 2012. Incidence of local anesthetic systemic toxicity and postoperative neurologic symptoms associated with 12,668 ultrasound-guided nerve blocks: an analysis from a prospective clinical registry. *Reg Anesth Pain Med* 37: 478-82

Soto-Astorga RP, et al. 2013. Epidural catheter with integrated light guides for spectroscopic tissue characterization. *Biomed Opt Express* 4: 2619-28

Steinfeldt T, Nimphius W, et al. 2010. Nerve injury by needle nerve perforation in regional anaesthesia: does size matter? *Br J Anaesth* 104: 245-53

Steinfeldt T, Poeschl S, et al. 2011a. Forced needle advancement during needle-nerve contact in a porcine model: histological outcome. *Anesth Analg* 113: 417-20

Steinfeldt T, Werner T, et al. 2011. Histological analysis after peripheral nerve puncture with pencil-point or Tuohy needletip. *Anesth Analg* 112: 465-70

Stokvis A, Van Neck JW, et al. 2009. High-resolution ultrasonography of the cutaneous nerve branches in the hand and wrist. *The Journal of hand surgery, European volume* 34: 766-71

Sugimoto Y, Takayama S, et al. 2002. An experimental study on the perineurial window. *Journal of Peripheral Nervous System* 7: 104-11

Tang Q, Liang C-P, et al. 2014. *Real-time Epidural Anesthesia Guidance Using Optical Coherence Tomography Needle Probe.* Presented at CLEO: Applications and Technology, San Jose, California United States

Tang Q, Liang CP, et al. 2015. Real-time epidural anesthesia guidance using optical coherence tomography needle probe. *Quant Imaging Med Surg* 5: 118-24

Tielens LK, Damen RB, et al. 2014. Ultrasound-guided needle handling using a guidance positioning system in a phantom. *Anaesthesia* 69: 24-31

Treece G, Lindop J, et al. 2011. Real-time quasi-static ultrasound elastography. *Interface Focus* 1: 540-52

Treue S. 2003. Visual attention: the where, what, how and why of saliency. *Curr Opin Neurobiol* 2003; **13**: 428-32

Tsai TP, Vuckovic I, et al. 2008. Intensity of the stimulating current may not be a reliable indicator of intraneural needle placement. *Reg Anesth Pain Med* 33: 207-10

Tsui BC, Pillay JJ, et al. 2008. Electrical impedance to distinguish intraneural from extraneural needle placement in porcine nerves during direct exposure and ultrasound guidance. *Anesthesiology* 109: 479-83

Umbarje K, Tang R, et al. 2013. Out-of-plane brachial plexus block with a novel SonixGPS(TM) needle tracking system. *Anaesthesia* 68: 433-4

Urmey WF. 2006. Using the nerve stimulator for peripheral or plexus nerve blocks. *Minerva Anestesiol* 72: 467-71

Urmey WF, Stanton J. 2002. Inability to consistently elicit a motor response following sensory paresthesia during interscalene block administration. *Anesthesiology* 96: 552-4

Van der Gijp A, Ravesloot CJ, et al. How visual search relates to visual diagnostic performance: a narrative systematic review of eye-tracking research in radiology. *Adv Health Sci Educ Theory Pract* 2017; **22**: 765-87

Verlinde M, Hollmann MW, et al. 2016. Local Anesthetic-Induced Neurotoxicity. *Int J Mol Sci* 17: 339

Voelckel WG, Klima G, et al. 2005. Signs of inflammation after sciatic nerve block in pigs. *Anesth Analg* 101: 1844-6

Walker KJ, McGrattan K, et al. 2009. Ultrasound guidance for peripheral nerve blockade. *Cochrane Database Syst Rev*: CD006459

Watts SA, Sharma DJ. 2007. Long-term neurological complications associated with surgery and peripheral nerve blockade: outcomes after 1065 consecutive blocks. *Anaesth Intensive Care* 35: 24-31

Wells PN, Liang HD. 2011. Medical ultrasound: imaging of soft tissue strain and elasticity. *J R Soc Interface* 8: 1521-49

Wiesmann T, Borntrager A, et al. 2014. Minimal current intensity to elicit an evoked motor response cannot discern between needle-nerve contact and intraneural needle insertion. *Anesth Analg* 118: 681-6

Yang S, Abrahams MS, et al. 2011. Local anesthetic Schwann cell toxicity is time and concentration dependent. *Reg Anesth Pain Med* 36: 444-51